Alma Mater Studiorum – Università di Bologna

DOTTORATO DI RICERCA IN

Meccanica dei materiali e processi tecnologici

Ciclo XXII

Settore/i scientifico-disciplinare/i di afferenza: ING-IND/18

TITOLO TESI

Neutronic Analysis for ITER CXRS Diagnostic Upper Port-Plug

Presentata da: **PETER BOURAUEL**

Coordinatore Dottorato

Prof. Ing. Tullio Trombetti

Relatore

Prof. Ing. Domiziano Mostacci
Prof. Dr. Rahim Nabbi

Esame finale anno 2010

ABSTRACT

The Research Center Jülich (FZJ), Germany is involved in the construction of the experimental nuclear fusion reactor ITER. The Institute of Plasma Physics will design together with international partners the so called CXRS Upper Port Plug (CXRS UPP), a technical component, that will view directly into the fusion plasma and guide its light to the outside of the reactor chamber by a system of mirrors – much like a periscope - to a set of spectrometers, where the light is analyzed and crucial plasma parameters like density profile and plasma composition are determined.

As the CXRS UPP will be positioned directly in the shielding, facing the hot plasma where also high numbers of high energy neutrons will be created it is clear that a detailed neutronic analysis has to be made. All structures inside the reactor have to conform to ITER regulations and to limits by the construction itself. These computations have been done with the Monte Carlo Code MCNP and the activation code FISPACT.

There were some challenges associated to these tasks. One point is the high complexity of the geometry not only for ITER but also for the Port Plug. As modelling in MCNP is not possible by a GUI but is happening manually by including mathematical surfaces and cell descriptions in a ASCII input file, ways had to be found to simplify the workflow when modelling, especially as model modifications had to be made in short time due to the nature of the design process. This has been done by introducing a dynamic model, where MCNP models can be defind by simply providing the border conditions. Solutions also have been found for converting the output text files into some useful mode of visualization by processing of MCNP FMESH Tallies.

The most important work was the development of a software tool, that combines the computer code MCNP with the activation code FISPACT and that is able to deliver the original zero-dimensional activation data as two-dimensional maps or three-dimensional distributions and is also capable to compile the activation-output to a new MCNP gamma source for determination of activation gamma dose data. This can be done not only for the ITER problems but for any MCNP input as the tool has been written in a general form.

The methods and tools have been compared with models and data from other groups and have been used to deliver critical values needed for the construction of the ITER CXRS PP, for example the neutron and gamma flux, neutron and gamma heating during operation, radiation damage, helium production, activation, isotope vectors, activation heat production and dose rate distributions for critical volumes. It is shown, that the used model of the CXRS Port Plug is meeting the critical design limits demanded by ITER regulations.

Acknowledgement

Any significant work cannot be completed without cooperation and support. I would like to use this opportunity to thank everybody who has given me valuable support.

I thank Prof. R. Nabbi for providing me with the opportunity to work under his supervision on such an interesting and sophisticated scientific work. I also want to thank him for his continuous guidance and encouragement for correcting, improving and completing this thesis.

Also I wish to thank Dr. W. Biel from IEF-4 for his guidance and support throughout all phases of the thesis work. I have to thank also Prof. Wolf and Prof. Reiter, who gave me the opportunity to work for the IEF-4.

Especially I want to thank Prof. D. Mostacci from the University of Bologna, Italy, for his guidance and enduring support. Also at the University of Bologna I wish to thank Prof. T. Trombetti for his support.

In the IEF-4 I wish to thank also Dr. Neubauer, Dr. Krasikov and Dr. Sadakov, who provided information and data for the modelling of the Port Plug.

In the IEF-6 I have to thank especially Frederic Simons, who did all of the coding work for the MOPAR visualization tool. My collegues Judith Coenen, Oliver Schitthelm und Klaus Biss gave me forther help throughout the project.

At FZ Karlsruhe I wish to thank Dr. Fischer and Dr. Serikov, who provided important information about the MCNP models and methods common in fusion neutronics.

Furthermore I wish to thank Dr. Hogenbirk from NRG Petten and Dr. Pampin and Andrew Davis from UKAEA for exchange of experiences and data, supporting the validation of the introduced methods.

In addition I want express thanks to the staff of ZFR, IEF-4 and IEF-6 at the Research Center Jülich for providing infrastructure and computer systems for performing the computer simulations.

I also would like to thank Prof. U. Scherer from the FH Aachen/Jülich for his encouragement and help in the first phase of the thesis work.

Finally I want to dedicate this thesis paper to my father P. Gerhard Bourauel, who encouraged me in undertaking a career in engineering and science, but sadly died shortly after the start of this thesis work.

Table of Contents

Index of Figures

Index of Tables

Nomenclature

Symbols

h	height	[cm]
n	number of neutrons generated	[1/s]
r	radius	[cm]
t	thickness	[cm]
N	number of neutrons, atoms	[-]
R	relative error	[-]
V	volume	[cm³]
Φ	neutron flux	[1/cm²s]
P	power	[kW]
E	energy	[kWh], [eV]
T	temperature	[°C], [°K], [eV]
n	plasma density	[1/m³]
τ	energy confinement time	[s]
m	mass	[kg]
Q	Plasma amplification	[-]
B	magnetic field	[T]
H	heat load	[W/cm²],[W/cm³]
I	electric current	[A]
U	electric voltage	[V]
v	velocity	[m/s]
C	concentration	[%], [appm]
S	standard deviation	[-]
x	population	[-]
σ	cross section	[barn]
A	activity	[Bq]
D	Dose	[Sv], [Gy]
D/t	Dose Rate	[Sv/h]
t	time	[s],[a],[y], [fpy]
f	fluence	[MWa],[MWa/m²]
d	radiation damage	[dpa]

Indices

E	Energy confinement
eff	effective
epi	epithermal
therm	thermal
fast	fast
stat	statistical

Abbreviations

ACTL	Activation Library
ADL	Activation Data Library
ALARA	As Low As Reasonably Achievable
ALARP	As Low As Reasonably Practicable
appm	atomic parts per million
ASCII	American Standard Code for Information Interchange
BSM	Blanket Shield Module
CAD	Computer Aided Design
CC	Correction Coils
CS	Central Solenoid
CXRS	Charge eXchange Recombination Spectroscopy
CXRS	Charge eXchange Recombination Spectrometer
D1S	Direct One-Step
DA	Domestic Agencies
DD	Deuterium-Deuterium
DE	Dose Energy
DEMO	DEMOnstration Power Plant
DNB	Diagnostic Neutral Beam
DT	Deuterium-Tritium
EAF	European Activation File
EAST	Experimental Advanced Superconducting Tokamak
EASY	European Activation System
ECRH	Electron Cyclotron Resonance Heating
ENDF	Evaluated Nuclear Data File
ENDL	Evaluated Nuclear Data Library
FEM	Finite Element Method
FENDL	Fusion Evaluated Nuclear Data Library
FNG	Frascati Neutron Generator
fpy	fusion power year
FzJ	Forschungszentrum Jülich
FzK	Forschungszentrum Karlsruhe
GUI	Graphical User Interface
HFR	High Flux Reactor
HHFC	High Heat Flux Components
IAEA	International Atomic Energy Agency
IFMIF	International Fusion Material Irradiation Facility
IO	Iter Organization
JENDL	Japanese Evaluated Nuclear Data Library
JET	Joint European Torus
JUMP	Juelich Multi Processor
JUROPA	Jülich Research on Petaflop Architectures
LANL	Los Alamos National Laboratory
LLNL	Lawrence Livermore National Laboratory
MC	Monte Carlo
MCNP	Monte Carlo n-Particle Transport Code
MHD	Magnetohydrodynamic
MOPAR	MCNP Output Parser and Reckoner
MPH	(ITER) Material Properties Handbook
MTR	Material Test Fission Reactors
NAR	(ITER) Nuclear Analysis Report
NEA	Nuclear Energy Agency (France)
NRG	Nuclear Research and consultancy Group
NRT	Norgett-Ribinson-Torrens model

OECD	Organisation for Economic Co-operation and Development
PDE	Partial Differential Equation
PDF	Propability Density Function
PF	Poloidal Field
PP	Port Plug
PP	Port Plug
R2S	Rigorous Two-Step
RSICC	Radiation Safety Information Computational Center
TEXTOR	Tokamak EXperiment for Technology Oriented Research
TF	Toroidal Field
TFTR	Tokamak Fusion Test Reactor
UKAEA	United Kingdom Atomic Energy Authority
UP3	Upper Port #3
UPP	Upper Port Plug
VV	Vacuum Vessel
ZAID	nuclide identification number

1. Introduction

The Research Center Jülich is (FZJ) involved in the construction of the experimental nuclear fusion reactor ITER, an international enterprise to show that is technically and economically feasible to build thermonuclear reactors for energy generation. The Institute of Plasma Physics will design together with international partners the so called CXRS Upper Port Plug (CXRS UPP), a technical component, that will view directly into the fusion plasma and guide its light to the outside of the reactor chamber by a system of mirrors – much like a periscope - to a set of spectrometers, where the light is analyzed and crucial plasma parameters like density profile and plasma composition are determined.

As the CXRS UPP will be positioned directly in the shielding, facing the hot plasma where also high numbers of high energy neutrons will be created it is clear that a detailed neutronic analysis has to be made. All structures inside the reactor have to conform to ITER regulations, for example there are maximum numbers on certain parameters as helium production in welded parts or maximum nuclear heating in certain materials. Also it is important, that no other parts of ITER are endangered, as structures inside the shielding can lead to higher neutron fluxes outside. Especially the insulations of the magnetic coils are sensitive to neutron and gamma radiation, so there are limits again given by ITER regulations.

Of course there are limits not only due to regulations but also by the construction itself. Especially the first mirror in the CXRS Port Plug is facing directly the plasma and is subject to high neutron fluxes as well as high neutron and gamma heating. So it is important to determine the exact amount of these quantities, so that construction is optimized for these loads. Values for neutron flux, neutron and gamma heating and also material damage should be determined for any point in the geometry. Also it is important to make an activation analysis of the component to determine the activation, activation heating and the composition and masses of activation products and its radiation dose rates at certain times of ITER operation, especially after shut down, when workers are supposed to have access to some areas of the reactor interior.

Because of availability and good experiences these calculations should be done with the Monte Carlo Code MCNP and the activation code FISPACT. MCNP is capable of using three-dimensional models with a high amount of detail and it can be run on the Jülich JUMP and JUROPA supercomputers in parallel mode to reduce the computation time. FISPACT is an activation code, especially developed by UKAEA for fusion problems.

There are some challenges associated to these tasks. One point is the high complexity of the geometry not only for ITER but also for the Port Plug. As modelling in MCNP is not possible by a GUI but is happening manually by including mathematical surfaces and cell descriptions in a ASCII input file, ways had to be found to simplify the workflow when modelling,

especially as model modifications had to be made in short time due to the nature of the design process.

As MCNP is capable of determining a lot of data in one model, some ways had to be found to prepare these data for easy analysis and interpretation. Usually MCNP and FISPACT are giving computed data in the format of output text files. Solutions had to be made to compile these text files into some useful mode of visualization.

Another challenge was the workflow of using MCNP simulation results as inputs for the FISPACT code. While MCNP is able to give data for three-dimensional models, FISPACT is working zero-dimensional. When using FISPACT for complex structures, several runs have to be made to get distributions. There are in fact codes to forward MCNP results for single cells to FISPACT, so that activation data can be achieved for single MCNP cells, but there are disadvantages with respect to spatial resolution and also visualization capabilities when using this method, so an alternative method should be developed to get activation data for all points of a model in any resolution.

These newly to developed methods should be made in a general form, so that any geometry not only the CXRS Port Plug can be simulated with them. Finally the methods should be applied to the Port Plug and the results had to be compared to that of other groups for verification purposes.

2. Nuclear fusion principles & ITER description

2.1. Nuclear Fusion

More than ninety percent of the world's energy consumption is won from fossil energy sources: mostly by coal, petrol and gas. Limited resources and questions about the climate change demand a discussion about the origin of the energy in the future. The problem will get more critical by the increasing world population and the higher need for energy [COENEN 09].

All over the world energy research is looking for alternatives to the fossil energy sources. There is a broad spectrum of possibilities for the future and the rising contributions by regenerative energy sources like wind power and solar electric power are first steps on the road.

Nuclear fusion is the vision of realising the application of the sun's energy here on earth. Its promise is a save and almost unlimited source of energy. From the nuclear fusion of one gram of deuterium and tritium it is possible to get 26,000 kWh of energy what is equal to the energy won from 11 tons of coal. In the long term, nuclear fusion is the only option. Humanity will suffer if researchers don't solve its problems. [SEIFE 08]

As the tritium is won from lithium by breeding inside the reactor, and the lithium is processed from stones, it is possible to deliver the energy needed for a family in one year by two litres of water and half a pound of stones. The world's energy consumption could be covered by the natural resources of deuterium and lithium for ten thousands of years.

Furthermore a fusion reactor would be inherent safe. No chain reaction is possible as the amount of fusion fuel in a reactor at any given time is very low and also no climate endangering gases like carbon dioxide are emitted.

In a fusion reactor light nuclei are more plentiful than fissile nuclei, and thus there would be much less radioactive waste from a fusion reactor than from a fission reactor. Furthermore, any radioactivity would decay away rapidly and there would be no need to store the waste for geological periods of time. [LILLEY 01] [HULME 69]

Aim of the world's fusion research projects is the development of the plasma physical basics and also to get the technical knowledge of designing a workable fusion reactor.

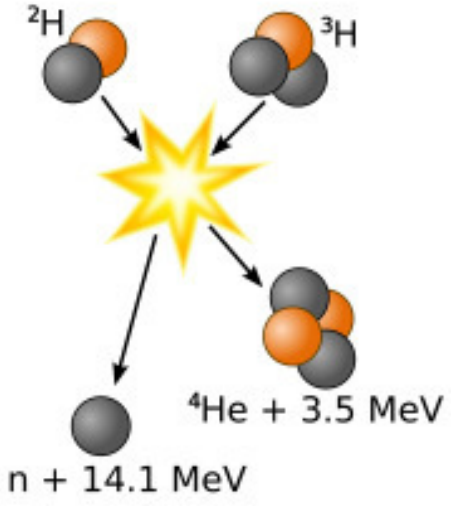

Figure 1: nuclear Fusion of Deuterium and tritium

Nuclear fusion gets its energy from the same origin than nuclear fission: the binding energy of the nuclear core. If two light atoms are fused to one heavier core, a part of the binding energy is transferred to kinetic energy. Figure 1 shows the mechanism for deuterium and tritium, which are transformed by fusion to a helium atom and a neutron. The excess energy amounts to 17.6 MeV from which the most part is carried away by the neutron. While the helium is supposed to give its energy to other nuclei for sustaining the fusion reaction, the neutron carries its energy to the outside where it can be used by thermal conversion to electric energy. [BRÖCKER 97]

There are several fusion reactions suitable for energy generation, the most important are shown in Figure 2. From the ones shown, the deuterium-tritium reaction has the highest reaction rate at temperatures of about hundred million degrees Celsius, which are reachable today.

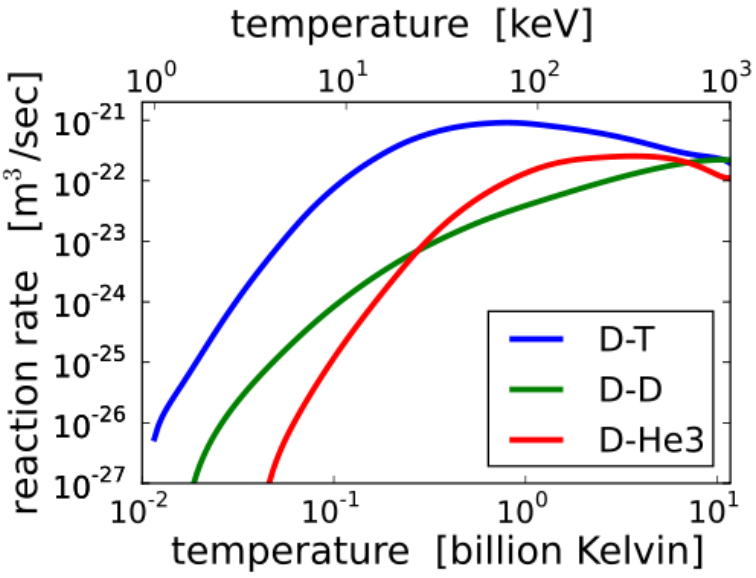

Figure 2: Reaction Rates of different fusion fuels dependent on the temperature

To get fusion reactions, the atoms must have a certain kinetic energy as they have to overcome the Coulomb barrier, which has the effect of a repulsing force up to a certain distance from the core. Once the Coulomb force is surmounted, the strong nuclear force will gravitate the atoms to each other and fusion will occur. The needed initial kinetic energy will be reached by heating the fusion fuel to a plasma inside a toroidal vacuum chamber, called a tokamak. Some hundred million degrees Celsius are realizable today by holding the plasma with magnetic fields to prevent cooling by contact with the wall.

The technology of heating the fuel in a plasma is called magnetic confinement fusion. There are other options researched today, like the inertial confinement fusion or the Z-pinch method, but these are not of relevance for this work. [GLASSTONE 64]

The energy released by the fusion reaction is shared between the alpha particle, with 20% of the total energy, and the neutron, with 80%. As the neutral neutron will leave the plasma immediately, only the energy of the alpha particle will contribute to the heating of the plasma. To get rid of the need for external heating, the temperature of the plasma must be high enough for the rate of the alpha particles to sustain the fusion reaction in the reactor by themselves. [KAMMASH 75] [RAEDER 81]

The condition for this ignition in magnetic confinement is calculated by setting the alpha particle heating equal to the rate at which energy is lost from the plasma. The ignition condition has the same form as the Lawson criterion [LAWSON 57]. The product of density and confinement time must be larger than some specified value, which depends on the plasma temperature and has a minimum value in DT at about 30 keV. The condition for ignition is

$n\tau_E > 1.7E+20\ m^{-3}s$

where τ_E is the energy confinement time that gives the rate at which energy is lost from a plasma. In a steady state working reactor, τ_E is a measure for the quality of the magnetic confinement. [MCCRACKEN 05]

As the fusion cross sections and some other parameters depend on temperature, it turns out that the most suitable temperature range is between 10 and 20 keV. The ignition condition can also be written in a form called ‘triple product’, which includes the temperature:

$nT\tau_E > 3E+21\ m^{-3}skeV$

For magnetic confinement fusion, an energy confinement time of about 5 seconds and a plasma pressure of about 1 bar is one combination that could meet this condition.

The earliest magnetic-confinement devices were developed in the UK in the late 1940s. These were toroidal pinches, which attempted to confine plasma with a strong, purely poloidal

magnetic field produced by a toroidal plasma current, but this arrangement proved seriously unstable. [McCracken 05]

The second approach to toroidal confinement is the stellarator, invented at Princeton in the early 1950s. Here a strong toroidal magnetic field is produced by an external toroidal solenoid. But here it is necessary to twist the magnetic field as it passes around the torus, what results in complicated coil shapes. Advances in physics and engineering are resulting in further experiments like the W7-X machine at Greifswald.

The most successful toroidal confinement scheme is the tokamak, developed in Moscow in the 1960s. The tokamak can be thought of either as a toroidal pinch with very strong stabilizing toroidal field or as using the poloidal field of a current in the plasma to add the twist to a toroidal field. ITER will be a tokamak type fusion reactor. [McCracken 05]

2.2. ITER

ITER – once the abbreviation for International Thermonuclear Experimental Reactor, today simply the Latin translation of 'the way' is the international research and engineering proposal for an experimental project that will help to make the transition from today's studies of plasma physics to future electricity-producing fusion power plants. It will build on research done with todays devices such as DIII-D, EAST, TFTR, JET, TEXTOR, and will be considerably larger than any of them. A simplified 3D CAD sketch of ITER with the most important components designated can be seen in Figure 3.

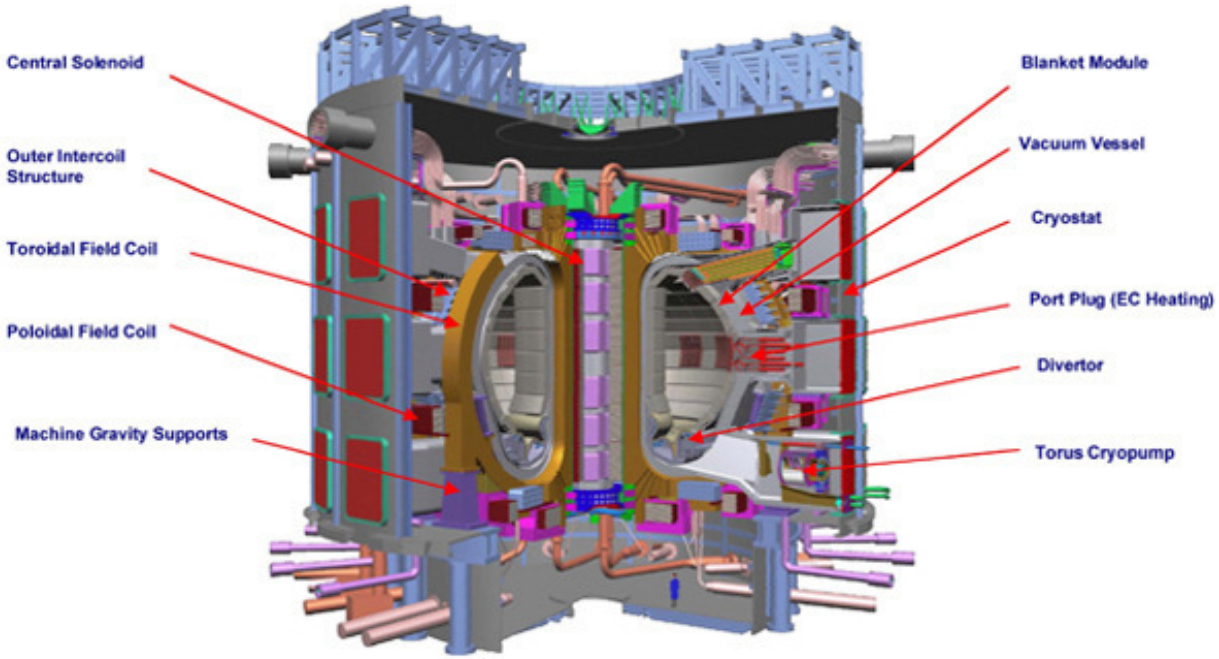

Figure 3: CAD model of ITER

Fusion scientists are convinced that the main goal will be achieved: the generation of a burning fusion plasma, which will be showing the availability of a controllable nuclear fusion. While the physical laws of the plasma conditions are known to a sufficient degree, there are still a number of unsolved technical and engineering problems. This is mainly because there are demands to a full scale nuclear fusion power plant, which are playing no role in today's experimental machines.

While fusion plasmas are only of short duration in existing tokamaks, there must be a constant burning in an economically working fusion plant. This will result in enormous challenges to the machines structures and components to withstand these loads. Even while ITER is "only" generating an eight minute fusion plasma, it will do so at power outputs in a power plant scale and is an ideal test bed for materials and techniques needed for full scale power plant construction.

Apperture Radius	10,7 m
Apperture Height	30 m
Plasma Radius	6,2 m
Plasma Volume	837 m^3
Plasma Mass	0.5 g
Magnetic Field	5.3 tesla
Heating Power	73 MW
Fusion Power	500 MW
Temperature	1E+8 K
Pulse Duration	400 s

Table 1: ITER base parameters

The main operational parameters of ITER are shown in Table 1. The fuel for ITER will be a deuterium-tritium mixture to react to helium with the reaction

$$D + T \rightarrow He^4 + n$$

In future fusion devices it is planned to generate the radioactive tritium by nuclear breeding reactions. For this there will be a certain amount of lithium6 in a so called breeder blanked near the first wall of the plasma. The fusion neutrons will the react with the lithium atoms to tritium in the reaction

$$Li^6 + n \rightarrow T + He^4$$

and

$$Li^7 + n \rightarrow T + He^4 + n$$

In ITER the tritium will be produced external. But the techniques of the breeding components will be tested in special modules near the first wall.

Originally planned due to an international initiative by the statesmen Gorbatschow, Reagan and Tanaka in 1986, it was supposed to have a fusion power of 1500 MW. After a change in the US research politics, the USA receded from the program. The other partners EU, Russia and Japan reacted by downscaling ITER to a output power of 500 MW.

ITER will be produced largely through in-kind contributions from the ITER members. The responsibilities for the management of in-kind procurement activities is assigned by each member to entities called domestic agencies (DA). During the same period that ITER Organization (IO) was established at the Cadarache site, the domestic agencies were set up. Today the ITER site has been cleared and work has started on the basic infrastructure. Also, construction of major components has started in the DAs. [HOLTKAMP 09]

The machines main goal is a burning fusion plasma of eight minute duration and an energy amplification of at least Q=10. These parameters will allow new physical examinations, like alpha-heating mechanism and analyzing instabilities that will limit the operational borders in certain plasma density and plasma pressure boundaries.

With some operational schemes it should be possible to extend the burning time of the plasma to 30 minutes by implementing a plasma flow operation with a combination of induction and high frequency energy input. This operation mode is important, as it will simulate a constant operation of a fusion reactor.

During its lifetime, ITER will be operated in successive phases. First phase is the H-Phase. In this non-nuclear phase only hydrogen or helium plasmas will be ignited, mainly for commissioning of the tokamak-system in a non-nuclear environment, where no remote handling procedures are needed. Second phase is the D-Phase, where deuterium plasmas are used. As the characteristics of deuterium plasmas are similar to that of DT-plasmas, this phase is ideal for simulating the procedures and operations of the DT-phase. During the DT-phase, the fusion power and burn pulse length will be gradually increased until the operational goals are reached.

ITER is a long pulse tokamak with elongated plasma and single null poloidal divertor. The major components of the tokamak, as depicted in Figure 4, are the superconducting toroidal and poloidal vacuum vessel. The magnet system comprises toroidal field (TF) coils, a central solenoid (CS), external poloidal field (PF) coils and correction coils (CC). The TF coil windings are enclosed in strong cases used also to support the external PF coils.

ITER has one of the largest and the most complex high vacuum system ever. Reliable vacuum is the key to the success of the ITER project. Due to the extensive nature of the ITER vacuum there are very few ITER systems which will not have an important vacuum interface. [ITER 08]

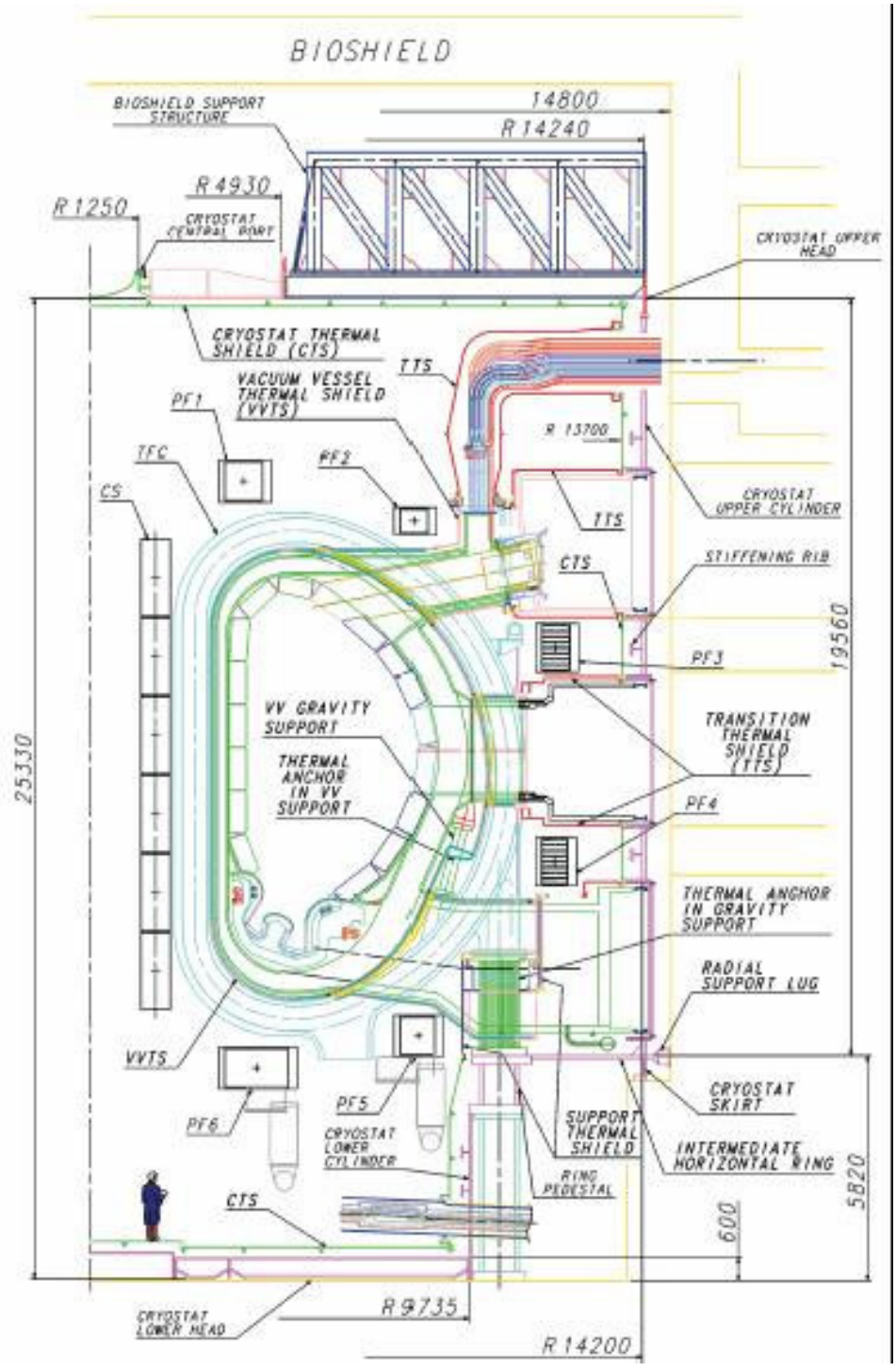

Figure 4: cut through the cryostat ITER with important structures designated

The vacuum vessel is a double-walled structure, made of a stainless steel welded ribbed shell, with internal shield plates and ferromagnetic inserts to reduce toroidal field ripple and is also supported by the toroidal field coils. The magnets together with the vacuum vessel are

supported by gravity supports. Inside the vacuum vessel, the internal components including blanket modules, divertor cassettes and port plugs absorb the radiated heat as well as most of the neutrons from the plasma and protect the vessel and magnet coils from excessive nuclear radiation.

The 421 blanket modules have a single-curvature facets separate first wall attached to the vessel through 3 cm diameter access holes in the first wall. The plasma facing components are beryllium armour attached to a copper substrate, mounted on a water-cooled stainless steel support. The outboard modules may later be replaced with tritium-breeding modules.

The 54-cassette single null divertor has carbon targets and tungsten high heat flux components, mounted on a copper substrate bolted to rails on the vessel floor. These targets can accommodate heat loads of more than 20 MW/m² for 20s, but the normal peak heat load will be 5 to 10 MW/m².

Equatorial and upper port plugs are used for heating antennae and neutral beam ducts and diagnostics. Divertor ports are housing torus cryopumps, diagnostics, cleaning systems and are also used for remote replacement of the divertor cassettes.

The heat deposited in the components of ITER is rejected to the environment by means of the tokamak cooling water system designed to exclude releases of tritium and activated corrosion products. The entire tokamak is enclosed in a cryostat, essentially a cylinder 24 m high and 28 m diameter, with thermal shields between the hot components and the cryogenically cooled superconducting magnets. [ITER 01] [THOMAS 07]

The ITER design status is far from closed. Results from running experiments and design studies as well as changes in the demands to the physics experiments are resulting in constant modifications of the ITER specifications. The maximum operating density, auxiliary heating power and the criteria to achieve a certain mode of confinement defines the operating space for the baseline 15 MA, 5.3 T scenarios. The baseline heating power is 73 MW and could be further increased if necessary.

In the last years several further changes have been made to the original design. The core parameters were reaffirmed and many detailed issues were addressed to ensure that ITER would meet its mission requirements. The poloidal field coil was modified to ensure that the plasma can be adequately controlled. Stabilization of a vertical disruption event was addressed by including in-vessel coils and the vacuum vessel was changed as a result of recognizing the implications of prior results on JET and associated modelling. [HAWRYLUK 09]

2.3. ITER Diagnostics and CXRS Upper Port Plug

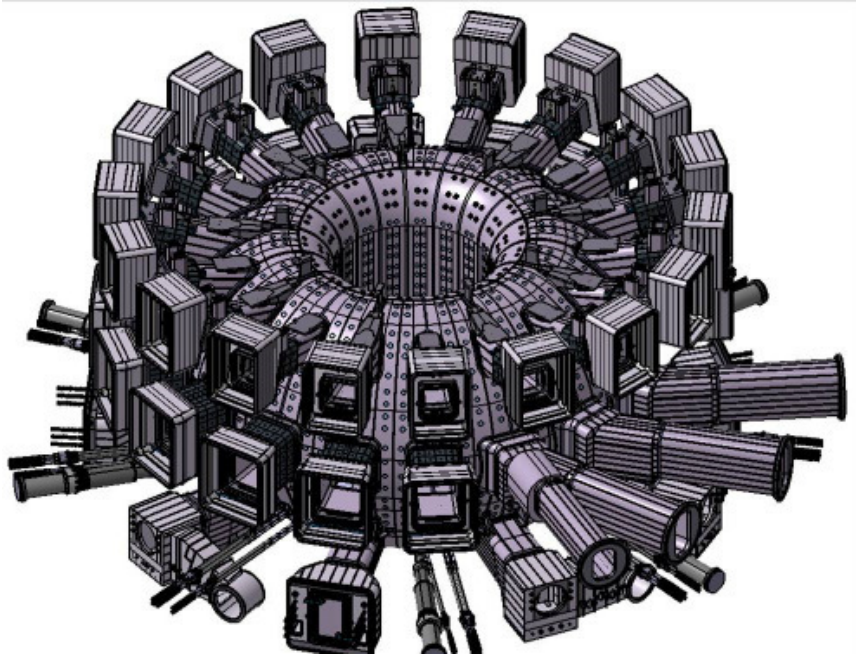

Figure 5: ITER Vacuum Vessel with locations of the ports

The implementation of diagnostics on ITER will be a major challenge, as the environment will be much harsher than in existing reactor experiments. For example the levels of neutral particle flux, neutron flux and fluence will be respectively about 5, 10 and 10,000 times higher than in today's machines. [COSTLEY 01]

ITER diagnostic equipment is integrated in six equatorial and 12 upper ports, five lower ports, and at many other locations in the vacuum vessel, as seen in Figure 5. The integration has to satisfy multiple requirements and constraints and at the same time must deliver the required performance. [WURDEN 97]

To control and evaluate plasmas on ITER it will be necessary to measure the plasma current in the range of 1 – 20 MA with an accuracy of 1%; the plasma shape and position to a few cms; the loop voltage to within a few mV, the plasma energy to < 10%, and the amplitude of MHD modes to typically 10%. The measurements are required with a time resolution of < 10 ms and for pulse lengths of up to 3,600 s.

Another important parameter to be measured on ITER will be the fusion power and related parameters such as the neutron flux and emissivity, neutron fluence and ion temperature. For the control and evaluation of ITER performance these are required to an accuracy of 10% with good temporal and spatial resolution. [COSTLEY 01]

The CXRS (Charge Exchange Recombination Spectroscopy) upper port viewer for ITER is an active diagnostic measuring light from the interaction of the charged plasma particles with the ions of a neutral beam (DNB). [SADAKOV 09]

Parameters to be measured are temperature profile, Helium ash density profile, Impurity density profile, plasma rotation, alpha particle confinement. The system will be installed at the upper port for measurements in the plasma core region. The CXRS system consists of the following subsystems: Collecting and re-imaging optics, fibre optic channels, spectrometers, detectors and data-acquisition. A CAD drawing of the CXRS Port Plug is shown in Figure 6. [KONING 09]

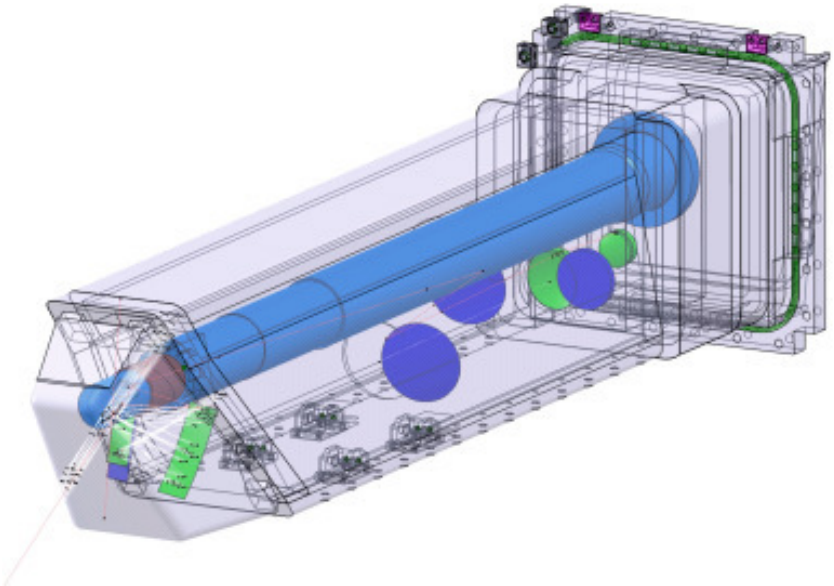

Figure 6: CAD model of the CXRS Port Plug

Light emitted from the ITER plasma is collected by the front optics system. The light is guided through a labyrinth and imaged on the entrance surface of a bundle of fibre optic waveguides. Through the fibre optic waveguides the light is guided to a set of spectrometers of different types.

The instrument will be installed in a port plug in diagnostic upper port #3 (UP3). The upper port plugs are installed in the ITER Vacuum Vessel (VV) and include a plasma-viewing first wall blanket shield module. Required mirror diameters are in the order of 35 cm which fits within the available cross-section of the port plug.

The measurement requirements of this system are summarized in Table 2. To achieve these, a 3.6 MW, 100 keV hydrogen diagnostic neutral beam (DNB) is foreseen. [JASPERS 08]

Parameter	Range	Time resolution	Space resolution	Accuracy
Helium density	1-20%	100 ms	a/10	10%
Ion temperature	0.5 - 40 keV	100 ms	a/10	10%
Poloidal plasma rotation	1-50 km/s	10 ms	a/30	5 km/s - 30 %
Toroidal plasma rotation	1-200 km/s	10 ms	a/30	5 km/s - 30 %
Impurity concentration Z<10	0.5 - 20 %	100 ms	a/10	20%
Impurity concentration Z>10	0.01-0.3 %	100 ms	a/10	20%

Table 2: CXRS measurement specifications

However, design issues are seriously increased due to the following facts: The high amount of radiation in the front of the port plug precludes the use of transmissive elements, so that at the front opening only reflective optics can be used.

The first mirror is exposed to a high neutron and heat load and is in an environment where deposition of carbon is likely. Both leads to a high degradation rate of the first mirror and therefore protective measures are required to ensure the lifetime of the first mirror. Also the first mirror is exposed to large heat transients at the beginning of operation that may create a change in curvature of the mirror surface.

The mirror material is one of the most important parameters to determine the rate of degradation. Presently the most likely option is to use a mirror made of mono-crystalline molybdenum.

Furthermore, the mirror shall be placed in a retractable tube in order to be replaced after a while and a shutter will enable protection when CXRS is not functional between the shots. The shutter and the exchange construction are both mechanical moving systems. They should be simple in order to guarantee functionality.

The shutter is a movable element located in a harsh nuclear, vacuum and electromagnetic environment: volumetric heat up to 3 W/cm³, surface heat up to 1 W/cm². Poloidal magnetic field variation rate in the gap between plasma and FW reaches up to 120 T/s.

Figure 7 shows the position of the CXRS port plug inside the ITER reactor and the principle layout of the instrument. In order to separate the mechanical systems from the optical labyrinth, the periscope has been divided in a mechanical and an optical layer.

The mechanical layer resides in the upper part of the periscope and consists of mirror #1, the shutter mechanism and the replacement system. The optical layer resides in the lower part of the periscope and consists of all optical elements except for mirror #1.

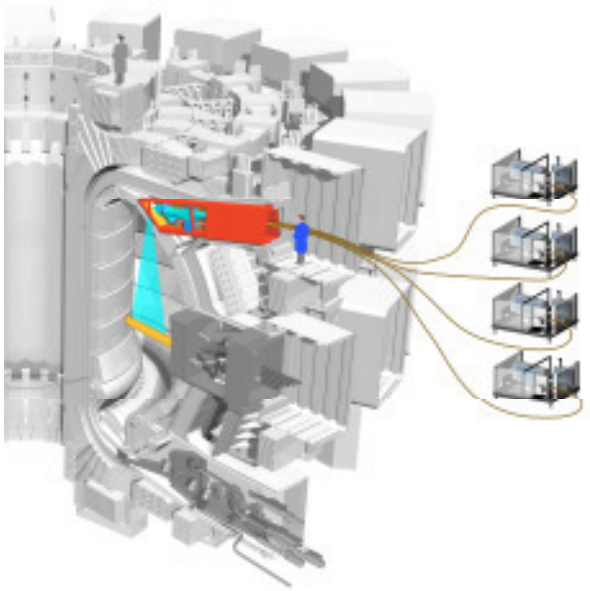

Figure 7: Position of the CXRS Port Plug inside ITER

The BSM is different from the standard blanket concepts, because it needs to have apertures and is attached to the port plug and not to the vessel.

The main shell encloses and supports the "shielding cassette" which, in turn, encloses and supports the retractable tube. The shell has a closed cross section which maximizes the stiffness and allows local round access hatches for adjustment and replacement of the secondary mirrors. In the reference design the shell also carries the blanket shield module, but this might be reconsidered.

The shielding cassette forms optical channel, holds the retractable tube and the secondary mirrors. It also has an endoscope channel for the inspection of the 1st mirror and calibration. The cassette holds main water pipes at the rear flange and delivers the cooling water to all other components of the plug including the main shell.

The rear flange is congested with allocation of tube's flange, optical channel, main water pipes and smaller pipes connecting the tube with the cassette, and a docking area for remote handling cask for tube replacement. Secondary mirror holders are located at side or bottom surfaces. Round hatches for the mirrors at the bottom surface of the shell is the preferred option.

Behind the Port Plug, a fibre bundle transports the light over tens of meters to the spectrometer room. For the spectrometer and the detection systems several options are yet under study to arrive at a system measuring simultaneously four wavelength bands. [JASPERS 08]

Possible technical solutions for the CXRS plug were developed. The major efforts have been spend on the resolution of three critical problems. The first problem is the uncertain and likely short lifetime of mirror one. A relocation of the mirror to a bigger distance from the front wall would be suggested. Second task is the development of a robust and efficient shutter in the

harsh environment. Specific design utilizes elastic bearings and pneumatic actuators. A further problem is the BSM to Plug Plug attachment. A robust design should have good margins for eddy current and halo loads. [SADAKOV 09]

Nuclear analysis is required for the licensing of the Port Plug. Of interest are the neutron and gamma fluxes throughout the Port Plug geometry and especially the neutron flux and nuclear heating at the mirrors. The effect of port plug leakage on neighbour relevant ITER systems must be studied. [WALKER 03]

The computations needed and ITER limits are discussed in detail in 3.6.

3. Theoretical basis and standard methods

3.1. Nuclear fusion neutronics

In a fission reactor, approximately one neutron gets released for each 80 MeV of fission energy, and the average energy of fission neutrons is about 2 MeV. In a deuterium-tritium based fusion reactor, one neutron is released per 17.6 MeV of fusion energy, and the fusion neutrons have initially a kinetic energy of about 14.1 MeV. [WASASTJERNA 07] [STEPHENSON 58]

With other words, the sole number of neutrons released per energy unit is higher by about a factor of four and the energy of the single neutrons is higher by about a factor of seven. In contrast to fission reactors, neutrons are not needed for sustaining a chain reaction, but neutrons are needed nonetheless for breeding the tritium and carrying the energy from the plasma to the wall, where the neutron kinetic energy is transferred into thermal energy for conversion into electricity.

But the thermal energy, deposited by the neutrons in the material will also be responsible for stresses in the structure. Furthermore the neutrons will generate gamma radiation by collisions with other nuclei, which also will be carrying heat to other regions. Both of them, neutrons and gammas will also be responsible for radiation damage, when colliding with atoms, knocking them out of their metal lattice. All these processes have to be calculated and analyzed by neutron simulation codes to help the engineers in designing the structures, shielding, cooling systems.

Further neutrons will be getting absorbed by atoms of the structures and activate the material, transferring it to another isotope or element by transmutation. Optical elements will degrade by these processes; other materials will get radioactive, emitting gamma radiation even after shut down of the machine. Activation will also produce hydrogen and helium, what can be fatal for welded parts. Also these processes have to be computed and analyzed with activation codes to design the reactor in a way that radiation limits can be guaranteed. [CHENG 00], [ERIKSSON 03]

In principle, shielding calculations, like other neutronics calculations, can be performed using either deterministic or Monte Carlo methods. However, deterministic methods have difficulties in coping with the geometrically-complex mixture of shielding materials and voids typical of ITER and presumably other fusion reactors. Typically they use one or the other of two opposite methods of representing the angular dependence of the flux. The SN method and the method of characteristics use a limited number of discrete flight directions. The PL method expands the flux in terms of Legendre polynomials of the angular variables. The former method is plagued by ray effects when applied in voids, and the latter introduces a spurious angular spreading. [WASASTJERNA 07]

Discrete ordinates codes (Sn) used in fusion to date were only 1D oder 2D and even greater geometrical simplifications led to the need for confirmation of the results using MC methods. A 3D discrete ordinate tool based on direct CAD input exists nowadays which, whilst preserving geometrical detail, provides fast evaluation capability and practical post-processing tools. This tool, the Attila 3D Sn code, is actually studied in fusion applications with respect to its performance, functionality and results.

Different evaluations still show a series of issues regarding the functionality and methodology. For example preparations of appropriate CAD inputs proved to be very challenging, but good agreement with MC methods were also achieved. [PAMPIN 07]

Several approaches have been made in the past to combine the advantages of the deterministic and the Monte Carlo codes and use the MC advantages for the interior of the reactor and to compute the shielding problem with deterministic codes. This can be achieved by coupling of different codes like MCNP5/MCNPX with ANISN, DORT or TORT. [HANSLIK 06], [CHEN 05]

Computations to determine the neutron and gamma flux and the accompanying dose rates within the ITER building but outside the cryostat, where low numbers are expected, have been done with these coupling methods. [EGGLESTON 98]

In this work we relied on the Monte Carlo method, which is capable of handle material filled cells as well as large voids in three-dimensional geometries. Reliability of the results is mostly dependent on the number of particle trajectories calculated. In large and complex structures like ITER it can sometimes be hard to get good statistics, as discussed later, but variance reduction methods can help in saving computation time.

3.2. Fundamentals of the Monte Carlo Method

The Monte Carlo method provides approximate solutions to a variety of mathematical and physical problems by performing statistical sampling experiments on a computer. A classic use is the evaluation of definitive multidimensional integrals by random sampling which is extensively utilized in the field of particle transport. [FISHMAN 95]

In this connection Monte Carlo may be considered as a means of repeatedly applying interaction probability data to individual particles selected randomly until a sufficient number of particles have been observed to allow conclusions to be drawn concerning the macroscopic multicollision behaviour of the total population of particles within a material region.

The rise in calculating capacity of recent supercomputers has made MC Methods very common today. MC is also used in other applications like illumination computations which produce photorealistic images of virtual 3D-Models (ray tracing). They are useful in studying systems with a large number of coupled degrees of freedom, such as liquids, disordered materials, and

strongly coupled solids. They are also used for modelling phenomena with significant uncertainty in inputs, such as the calculation of risk in operational research. [BRIESMEISTER 03]

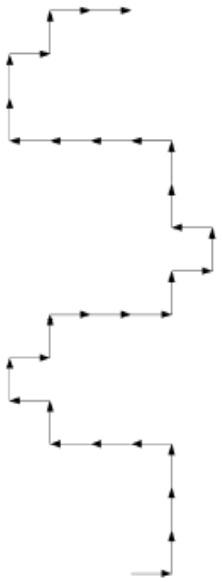

Figure 8: Principle of Random Walk

To understand the principle of stochastic methods, it is important to know about the elementary concepts of probability, namely, that the probability of one of several possible events occurring will be approximately equal to the ratio of the number of times the desired event occurs to the total number of events observed in an unbiased manner. As the number of observations increases, this ratio should more closely approximate the true probability.

Much of the information available on the physics of individual nuclear interactions is obtained experimentally by observing the fate of large numbers of particles. So, MC may be considered as a means of repeatedly applying interaction probability data to individual particles selected randomly until a sufficient number of particles have been observed to allow conclusions to be drawn concerning the macroscopic behaviour of the total population of particles.

Although Monte Carlo may be considered a means of solving the Boltzmann transport equation, it is more properly a modelling of the physical principles from which the Boltzmann equation was developed. [SCHAEFFER 73]

Simply stated, the Monte Carlo approach requires the construction of case histories of the travel of individual particles through the geometry and then analyzes these histories to derive relevant data, such as flux density and dose rate. One particle history includes birth of a particle at its source, its random walk (Figure 8) through the transporting medium as it undergoes various interactions, and its death, which terminates the history. A death can occur when the particle becomes absorbed, leaves the geometric region of interest, or loses significance to other factors (e.g., low energy). [SCHAEFFER 73]

Single particle histories inside any given 3D geometry are simulated like shown in Figure 9. In this example a random neutron incident takes place inside a block of fissionable material. The neutron enters the material coming from an (simulated) void and collides at event 1. The neutron is scattered in the direction shown, which is selected randomly from the physical scattering distribution. A photon is also produced and is temporarily stored for later analysis. Fission occurs at event 2; the incoming neutron is terminated while two new, outgoing neutrons and one photon are generated. One photon and one neutron are again temporarily stored for later analysis.

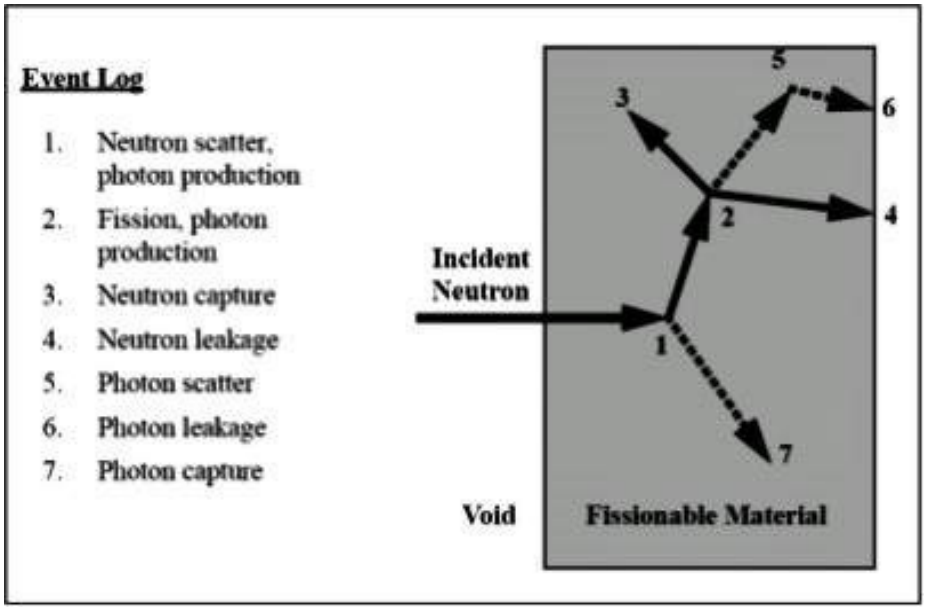

Figure 9: Neutron Path in Monte Carlo Simulation [BRIESMEISTER 03]

The first fission neutron is captured at event 3 and terminated. The second, stored neutron is now retrieved and, by random sampling, leaks out of the material cell at event 4. The photon that was created in the fission process has a collision at event 5 and leaks out at event 6. The photon from the first collision is now retrieved. It undergoes capturing at event 7. This was now one complete neutron history. More of such histories, millions of them, are followed to make a better distribution 0. A more detailed description on the background of this process is described in the following lines.

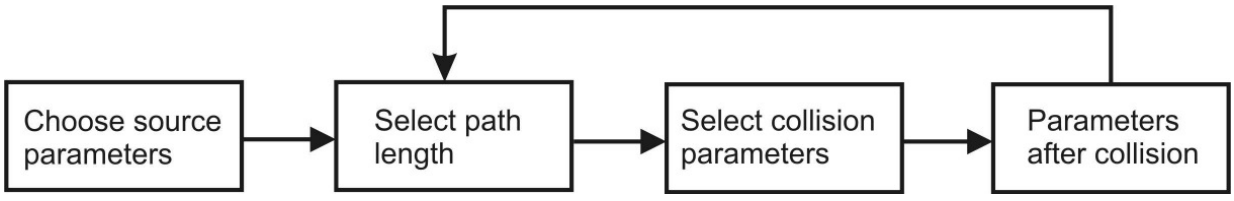

Figure 10: Neutron History in Monte Carlo Simulation

If the problem geometry is accordingly modelled, the major steps involved in generating a particle history are shown in Figure 10. The loop is continued until the particle parameters fall outside certain limits, such as geometrical bounds or minimum energy .The first three

operations displayed in the picture involve the selection of parameters at random from a probability distribution of all possible values of these parameters. The steps in making a random selection from such probability distributions are based on the use of numbers randomly positioned between 0 and 1.

All physical processes, including the emission of radiation and their subsequent transport through material, are probabilistic. It's not possible to predict with certainty the destiny of an individual particle in a process. But it's possible to characterize effectively these stochastic processes by describing the average behaviour of many elements or by estimating with a known degree of confidence the behaviour of one single element.

Inherent in the Monte Carlo procedure is the concept of the probability density function (PDF). This function describes the relative frequency of occurrence of its random variable x out of its domain (all possible values for x) constituting the event space (all possible events in the process). The random numbers needed may be taken from tables called into the machine memory or they may be generated by a subroutine of the MC computer program.

The first step in starting a particle history is the choosing of the source parameters. The source parameters include the energy, the spatial point of origin and the direction of motion. These parameters can be independent or may be interrelated with each other. The source energy is usually chosen from a given energy distribution. Same is true for the spatial distribution. Usually the user is giving coordinates as a starting point for the histories.

If a whole region in the model is designed for starting particles, the starting points will be chosen randomly within the coordinate limits of this region. If the sources are emitting particles isotropically, the program is simply picking unit vectors terminating uniformly on the surface of a unit sphere. The probability function (PDF) would then be the integral over a spherical surface area.

In certain calculations it may be desirable to prejudice the selection of one or more source parameters to favour those most likely to contribute to the quantity of interest. This can be done by selecting a larger number of the important source particles and assigning each particle a weighting number to adjust for the bias that was introduced.

The next step, if particle generation is complete, would be the determination of the particle path length from the source to the point of interaction. The path length together with the parameters of initial direction defines the point where an interaction occurs. If now the path length of the particle L is larger than the geometrical limits of the system A, the particle history will be terminated. Otherwise a collision or interaction is assumed to have occurred at the selected point and the collision parameters will be calculated.

If a collision has been detected it is necessary to determine, which of the possible nuclear species (if the material consists of multiple elements or isotopes) was involved and which

interactions of that species took place. For that the interaction cross sections must be available to the computer for each nuclide over the energy range of interest. These cross sections are usually stored in external databases, but more on this subject is mentioned, when the MCNP program is described in the next chapter.

For neutrons the possible reactions and therefore the necessary cross sections would be usually elastic scatter, absorption, fission, (n,n'), (n,2n) and (n,3n). The occurring reaction is then simply chosen by the computer program by selecting randomly according to the probability of that reaction. Secondary neutrons would be included by tracking them after the history of the incident neutron is terminated.

The next task is the determination of the parameters of the particles that survive an interaction. These parameters include the type, number, energy, and direction of the surviving incident particle and of any secondaries created. Depending on the type of data needed it may be useful to determine the energy stored in the material during the collision.

After the particle termination, that could be the result of absorption or due to low energy or the leaving of the system boundaries, the scoring takes place. The scoring is the output of a Monte Carlo simulation that can include the following results:

- Flux density as a function of position, direction and energy deposition
- The penetrating dose or flux density
- The energy and angular distribution of the penetrating particles
- The distribution of penetrating particles relative to the number of collisions encountered before penetrating
- The distribution in time of arriving particles

Many other possible data are thinkable for collection.

The Monte Carlo technique has been proven useful in special cases, such as complex geometries where other methods encounter difficulties and in some cell calculations. Moreover, when there is considerable detail in the variations of the neutron cross section with energy, the MC method eliminates the necessity for making subsidiary calculations, e.g., of resonance flux. [BELL 70]

In 1930 physicist Enrico Fermi used MC methods to calculate the properties of the newly-discovered neutron and these methods were central to the simulations required for the Manhattan Project. Extensive use was made after 1945, when the first electronic computers were built. At that time MC methods began to be studied in depth and became popular in the fields of physics and operations research. [NORDLUND 06]

3.3. The MCNP computer code

MCNP (Monte Carlo n-Particle Transport Code) is widely used for this type of nuclear calculations. Furthermore in the ITER project, the MCNP code has been chosen as a standard, as it is versatile, accurate and well-tested program. [WASASTJERNA 07]

MCNP was originally developed by the Monte Carlo Group, currently the Radiation Transport Group, at the LANL (Los Alamos National Laboratory). MCNP is constantly improved and maintained and there is limited consulting and support for users. MCNP is distributed to users through the Radiation Shielding Information Center (RSICC) at Oak Ridge, USA and the OECD/NEA data bank in Paris, France.

MCNP (Version 4B) consists of approximately 40,000 lines of FORTRAN and 1000 lines of C source code. Worldwide, there are about 1000 active users.

MCNP takes advantage of parallel computer architectures. It has been made as system independent as possible to enhance its portability, and has been written to comply with the ANSI FORTRAN 77 standard. With one source code, MCNP is maintained on many platforms including UNIX, LINUX and Microsoft Windows.

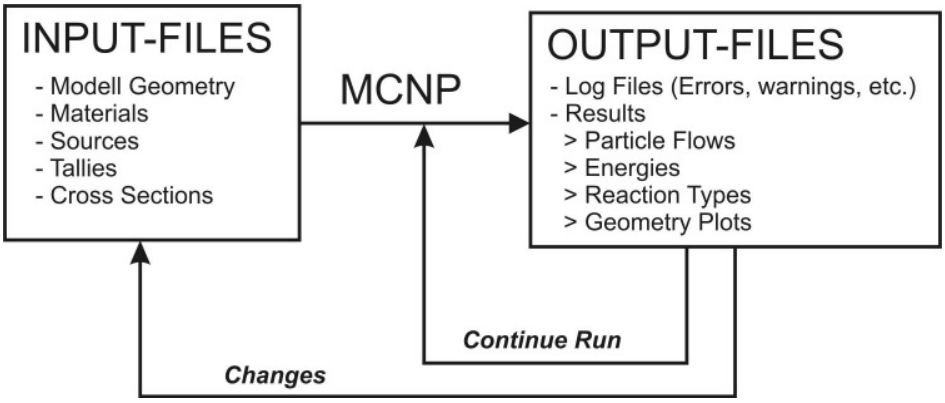

Figure 11: Working Flow of MCNP

Figure 11 shows the typical work flow of a MCNP run. The user first has to create one or more input files that specify the problem to be calculated. The input includes definitions of the geometry, the properties of the materials used, and links to the files with the cross sections, particle sources information and many other things.

For the calculation of the reactions, MCNP uses external cross section files. These are continuous-energy nuclear and atomic data libraries. The primary sources are evaluations from the Evaluated Nuclear Data File (ENDF) system, the Evaluated Nuclear Data Library (ENDL) and the Activation Library (ACTL) compilations from LLNL (Lawrence Livermore National Laboratories), USA.

Nuclear data tables exist for neutron interactions, neutron-induced photons, photon interactions, neutron dosimetry or activation, and thermal particle scattering. Photon and electron data are atomic rather than nuclear. Over 500 neutron interaction tables are available for approximately 100 different isotopes and elements.

When the MCNP program is started, it begins with checking the input files. If no errors are found the particle histories are started. In fissionable materials MCNP can determine all the starting points alone, from which neutron paths can be randomly started. Also it determines the k_{eff} factor of the geometry, when fissile material is abundant. The histories of the particles together with all other desired data are written from the program into output files. The user then can analyze the data and modify the input if necessary or the last run can be continued if the accuracy of the output has to be raised. MCNP geometrical nodalization

The largest part of the MCNP input file is mostly the definition of the problem geometry. MCNP geometry works with different 3-dimensional cells, consisting of a defined material.

A cell is defined in MCNP by a composition of different surfaces in spaces. If the user wants to create a cell with the shape of a cube, he has to give the parameters of the six surfaces, which are the borders of the cube. More complex geometries are composed out of additions and/or intersections of simple geometrical objects.

For new users this way of dealing with geometries is somewhat difficult but with some training this works very well. MCNP is supporting the user by the possibility to plot 2D pictures of the geometry on the screen what is a help for the debugging of the input.

To get overviews of more complex geometries it can help to get three dimensional pictures of the input file. This is possible with an external tool with the name SABRINA. [VAN RIPER 06] The program has been used several times in this work for visualization of complex models. Furthermore it is possible to insert particle paths into the geometry. There are also some other more complex methods for scanning the model with the help of the MCNP source routine in order to visualize the material cells. [SNOJ 09]

The cells have to be assigned now to specific materials. The composition of the material is given by a nuclide identification number, the so called ZAID, and the weight fraction or nuclide fraction of it in the material. The ZAID links to the external data file with the cross sections of the nuclide. The user has to take care, that the given data files are accessible in the MCNP directory.

When all material and nuclear data files have been chosen, the user has to define the quantities of interest. They are called “tallies” and can be whatever one wants to know. One tally could be the number of neutrons, at certain energies, that entered certain cells or surfaces. Another tally could be the amount of energy delivered by photons within a certain volume inside the geometry or the number of certain collision reactions inside a given cell.

Usually the last lines of an input file are filled with some commands for the processing of the calculations and the neutron/gamma source definition.

Results of the MCNP calculations are given in output files that include the values for the tallies and corresponding statistical uncertainties as well as exhausting log data of the Monte-Carlo run and parsing of the input.

Monte Carlo results represent an average of the contributions from many histories sampled during the course of the problem. An important quantity equal in stature to the Monte Carlo answer itself is the statistical error or uncertainty associated with the result.

The quantity S is the estimated standard deviation of the population of x based on the values of x_i that were actually sampled. The estimated variance of x is given by

$$S_{\bar{x}}^2 = \frac{S^2}{N}$$

All standard MCNP tallies are normalized to be per starting particle history and are printed in the output file together with the relative error, which is defined as

$$R \equiv S_{\bar{x}} / \bar{x}$$

The relative error is a convenient number because it represents statistical precision as a fractional result to the estimated mean. The range of R values is between zero and unity.

n	1	4	16	25	100	400
R	1.00	0.50	0.25	0.20	0.10	0.05

Table 3: Estimated Error vs. Number of identical tallies [BRIESMEISTER 03]

Table 3 shows a number of R values against the number of identical tallies. A relative error of 0.5 is equal to four counts. To reduce the relative error to lower than 0.1, what is somewhat a minimum condition for reliable results, at least 100 counts in the tally have to be measured.

Range of R	Quality of the Tally
0.5 to 1	Garbage
0.2 to 0.5	Factor of a few
0.1 to 0.2	Questionable
<0.1	Generally reliable except point detectors
<0.05	Generally reliable for point detectors

Table 4: Interpretation of the relative error [BRIESMEISTER 03]

Table 4 presents the recommended interpretation of the relative error associated with a MCNP tally. Results with errors higher then 0.5 are in general not usable. Errors around 0.4 to 0.5 give at least some information about the order of magnitude of the results. Errors higher then 0.2 can

be misleading by a factor of a few. Goal for precise values should at least have a relative error lower then 0.1. These guidelines were determined empirically.

The precision of a Monte Carlo result is affected by four user controlled choices: [BRIESMEISTER 03]

- forward vs. adjoint calculation
- tally type
- variance reduction techniques
- number of histories run

Within a smaller tally region, the number of particles crossing the region also will be lower. In really small volumes, like the cells for the mirrors of the Port Plug in the huge ITER geometry, it can be hard to get good tally precision. To overcome this problem, variance reduction techniques are available within MCNP.

The most important methods to increase the efficiency of deep-penetration Monte-Carlo calculations are the biasing and splitting/roulette (S/R) techniques. [NOACK 91]

Another common variance reduction technique is ‘weight windows’. Weight windows depend on the importance functions and allow the Monte Carlo code to concentrate on ‘important’ particles, which eventually contribute to the tally. Although variance reduction techniques are sometimes necessary and may be quite successful, they may also be difficult to properly employ. For instance, the user must often further subdivide the cells for sufficient resolution of the importance function. This additional refinement requires extra time and work to properly implement. [VAN RIPER 97]

To overcome that problem, utilities for automated variance reduction, have been independently developed and tested. [WAGNER 02]

Some of them have been implemented into the MCNP computer code, for example the ‘weight windows generator’. Further information about the variance reduction methods used can be found in 4.1.

It is important to note that S_x is proportional to $1/\sqrt{N}$, which is a drawback to the Monte Carlo methods as four times the original number of particles has to be computed to halve the estimated variance. Running more particles is often very costly in computer time but in complex geometries like ITER it is sometimes the only choice of getting reliable results. Thus the adoption of supercomputer resources is largely desirable for fusion neutronic problems.

3.4. MCNP Nuclear Data and cross section libraries

The MCNP package is incomplete without the associated nuclear data tables. For most materials there are many cross-section sets available because of multiple sources of evaluated data and different parameters used in processing the data. An evaluated nuclear data set is produced by analysing experimentally measured cross sections and combining these data with the predictions of nuclear model calculations in an attempt to extract the most accurate cross-section information.

In recent years the primary evaluated neutron interaction data for MCNP has been the ENDF/B system. Recently evaluated neutron interaction data tables are also extracted from two other sources: ENDL and supplemental evaluations performed in the Applied Nuclear Science Group at Los Alamos.

Data on the MCNP neutron interaction tables include cross sections and much more. Cross sections for all reactions given in the evaluated data are specified. Depending on the number of resolved resonances for each isotope, the energy grid may contain as few as 250 points or as many as 22,500 points.

Other information, including the total absorption cross section, the total photon production cross section and the average heating number (for energy deposition calculations), is also tabulated on the same energy grid. Angular distributions of scattered neutrons are included in the neutron interaction tables for all nonabsorption reactions. Other miscellaneous information on the neutron interaction tables includes the atomic weight ratio of the target nucleus, the Q-values of each reaction, and $\bar{\nu}$ data (the average number of neutrons per fission) for fissionable isotopes.

For fusion applications a special database has been compiled. The FENDL/A-2 ‘important reactions sublibrary’ contains pointwise cross section data for the 390 most important reactions for activation studies within the ITER design. The goal for the library was to be as complete as possible (i.e., containing at least all target nuclides with $t_{1/2}$>0.5 days and all reactions energetically possible for En<20 MeV. To achieve this in reasonable time, all reaction data from the European Activation File (EAF-4.1) in pointwise format were selected to complement the FENDL library.

For the assembly of the database all data were extracted from the latest versions of candidate libraries or individual data sources, as EAF-4.1, ADL-3, FENDL/A-1.1, VONACH, CRP, ADL-3/I and JENDL/A-3.2. [PASHCHENKO 98]

A list of the important reactions, with assigned priority to the ITER design, that are significant in producing activation both at short and long cooling times was compiled. The library was then merged with the EAF-4.1 library and formally tested at UKAEA Culham with the FISPACT code and was made available to the IAEA Nuclear Data Section.

Complementary to the activation cross section is the ENDF-6 formatted decay data library. The library is taken directly from the decay data used in the European Activation System (EASY). FENDL/D2.0 contains decay properties (decay type, decay energy, half-life) for 1867 nuclides and isomers.

In 2004 an updated version of the FENDL-2 has been made available, and these data are freely available from IAEA-NDS upon request. A new feature of this FENDL-2.1 package is the availability of the ACEDOP package, which allows Doppler broadening of the cross sections in the MCNP ace file.

The evaluated nuclear data files selected for FENDL/E-2.1 were then processed using the NJOY-99.90 modular code system to the FENDL/MC-2.1 library, which is formatted in ACE-format and thus suitable for use by the MCNP family. [ALDAMA 04]

Several calculations for benchmarks and verifications have been carried out with the FENDL database also compared with other databases. Differences are very small and usability of the database should be verified for calculations for ITER but further work is needed for updating FENDL for fusion systems beyond ITER [SAWAN 09].

A continuous effort is required to further develop and improve fusion nuclear data both for transport and activation calculations. This includes benchmark experiments required for testing and qualifying the data evaluations through computational analyses. In addition there is a further need to provide co-variance data for the assessment of qualified uncertainty estimates in design calculations. [FISCHER 02].

3.5. FISPACT

FISPACT is an inventory code that has been developed for neutron induced activation calculations for materials in fusion devices. It is a powerful code that can answer the basic questions about the numbers of atoms and the activity in a material following neutron irradiation, and can also give details of the pathways by which these nuclides are formed. It can treat trace amounts of actinides that are able to fission, and includes the effects of sequential charged particle reactions.

FISPACT was developed from the FISPIN inventory code that was designed for fission reactor calculations and dealt in greater detail with inventories arising from the irradiated fuel in a reactor. FISPACT is complementary to FISPIN and has been designed for activation calculations; however, it can be used with any type of neutron spectrum and is not restricted to only fusion applications. [FORREST 05]

FISPACT is used by many groups throughout Europe and has been adopted by the ITER project as the reference activation code. It is available for UNIX workstations and IBM compatible personal computers running a Windows operating system.

FISPACT uses external libraries of reaction cross sections and decay data for all relevant nuclides to calculate an inventory of nuclides produced as a result of the irradiation of a starting material with a flux of neutrons. The actual output quantities include the amount (number of atoms and grams), the activity (Bq), α-, β- and γ-energies (kW), γ dose-rate (Sv h^{-1}), the potential ingestion and inhalation doses (Sv), the legal transport limit, the clearance index and the half-life for each nuclide. Amounts and heat outputs are also given for the elements and the γ-ray spectrum for the material is listed as well as various summed quantities, such as total activity and total dose-rate.

The core task of FISPACT is the solution of a set of differential equations that describe the amounts of atoms of various nuclides present following the irradiation of a given material in a neutron field. The set of differential equations is given in the following equation:

$$\frac{dN_i}{dt} = -N_i\left(\lambda_i + \sigma_i\phi\right) + \sum_{j\neq i} N_i\left(\lambda_{ij} + \sigma_{ij}\phi\right) + \sum_k N_k\sigma_k^f\phi Y_{ik}$$

It is necessary to use an efficient method of solution to the equation. The method used in FISPACT is the Sidell-method, what is an extension of the first order Taylor series, which uses an exponential function of the step length.

At the end of each time interval the dominant nuclides (in terms of activity, heat, γ dose-rate, potential biological hazards and clearance index) and the pathway data for the production of these nuclides can be shown. The uncertainties in eight total radiological quantities can be calculated and output. As options, data files can be produced for subsequent use by other programs to plot graphs of the total responses as functions of elapsed time and selected blocks of output may be written to external data files. [FORREST 05]

FISPACT requires connection to several data libraries before it can be used to calculate inventories. While any libraries in the correct format could be used, the development of FISPACT over the last few years has run in parallel with the development of the European Activation File and this library is the recommended source of cross section data.

The user will give details of the material to be irradiated by neutrons, the times of irradiation and cooling and, most importantly, details of the neutron spectrum that is to be used. The spectrum must be available either in one of the standard energy structures used by FISPACT or in an arbitrary energy structure in which case the user must supply details of the energy boundaries.

The standard energy structures are WIMS, GAM-II, XMAS, VITAMIN-J, VITAMIN-J+, TRIPOLI, and TRIPOLI+. Cross section data in these seven energy structures are available for the EAF cross section library. One of the seven group format libraries is used to form the 1-group ‘effective’ cross sections that FISPACT requires by ‘collapsing’ the library with the neutron spectrum.

The FISPACT input file constructed by a user consists of a series of code words that fall into two categories. The first series ('preliminary') are concerned with library specifications and the second ('main') give details of the materials and irradiation history. A separate file containing a list of file names and the various data streams (units) to which the input and output files are connected is also required. [FORREST 05]

An important part of library processing is the 'collapsing' of the cross section library with a neutron spectrum to a one-group-structure file. The user must construct a file (generic name 'fluxes') containing the spectrum data. Figure 12 shows the input files needed and the output files generated by this step.

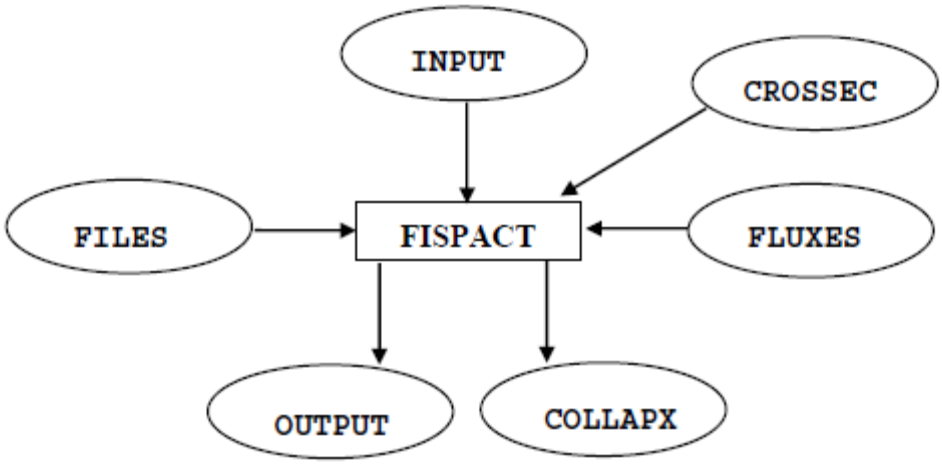

Figure 12: Files used by FISPACT to produce a collapsed library [FORREST 05]

When the collapsed cross section file has been generated, FISPACT can be started with the generic input file that includes the problem parameters. Figure 13 shows the input files needed and the output files generated by this step.

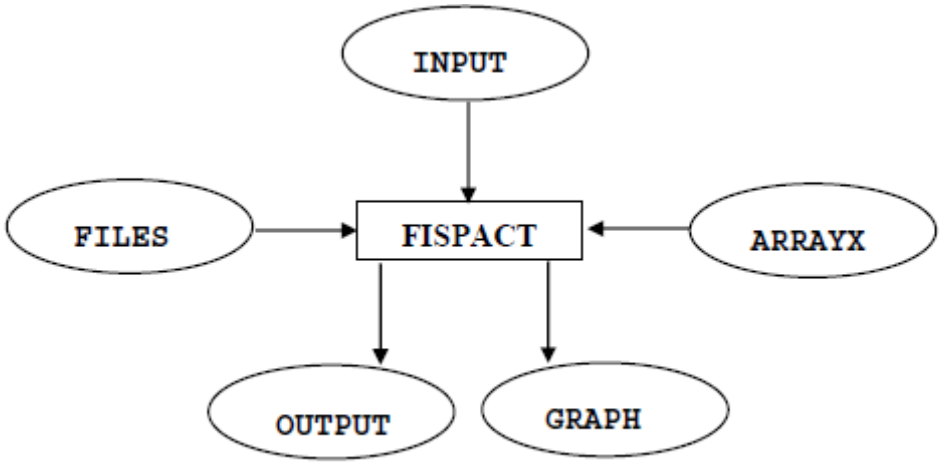

Figure 13: Files used by FISPACT for a standard run [FORREST 05]

3.6. Nuclear conditions, limits and standard methods in ITER

The nuclear design requirements for ITER are determined from the operational phases that are envisioned. The entire operation phase will last about twenty years and will involve a few thousand hours of D-T operation with the tritium supplied from external sources.

Radiation transport calculations for prediction and confirmation of expected neutronic parameters are an essential part of the reactor design process. Development and optimisation of the design of tokamak components and other plant systems must be carried out in a logical progression based on initial results obtained with one- and two-dimensional scoping and parametric analyses followed by three-dimensional radiation transport calculations. The latter better characterise the radiation streaming through ports, diagnostic systems, other penetrations, and the overall geometric complexity of the tokamak system. For meaningful and self-consistent nuclear analyses to be done, quality assurance and even improvement of the calculational tools and nuclear data are essential. [IIDA 06]

A set of critical parameters arise from design requirements that must be simultaneously controlled to minimise radiation damage and nuclear heating in materials and structures, such as

- damage and gas production rates in in-vessel components
- local nuclear responses in superconducting magnets
- integral nuclear heating in the Toroidal Field Coils (TFC) and intercoil structures
- neutron fluxes and residual radiation doses at maintenance locations
- radiation conditions behind the cryostat
- performance of diagnostic equipment

For the calculation of nuclear analysis the operating parameters are important as they have to be considered as input values for MCNP as well as for FISPACT activation calculations. These reference operating parameters, shown in Table 5, are specified in the NAR: [IIDA 06]

Fusion power	500	[MW]
Total average neutron fluence at first wall	0.3	[MWa/m²]
Integrated full power operation time	4600	[h]
Peak burn duty cycle	25	[%]
Nominal number of 400s equivalent pulses	30000	[-]

Table 5: ITER main operating parameters

The burn duration for the reference design is 400s. However, 3000s burn time and 12000s minimum repetition time is foreseen in the assessed non-inductive operation scenario II. For the preliminary analyses done for this work, only the reference parameters have been used.

For activation calculations with FISPACT, the pulses are homogenized throughout a ten year operation scenario what leads to a neutron flux multiplied with a factor of 0.0525. This is equal to about half a fpy (fusion power year). Many results are given in [per fpy] what is often a common unit in fusion calculations. Most nuclear responses scale linearly with the reactor fusion power, including the shutdown dose rate. [SERIKOV 08]

There is also maximum heat loads defined to structures cooled at cryogenic temperature. These are summarized in Table 6. Specifications of heat loads to these structures are considered as the nominal value for the heat removal systems and as a maximum allowable for the thermal and nuclear shielding systems. Limits on integral nuclear heating in the poloidal field (PF) coils using NbTi superconductor and in the Nb_3Sn central solenoid are not specified.

Maximum nuclear heating to TF Coils	14	[kW]
radiated power to magnet and cold structures from Thermal Shields:		
normal conditions	5.6	[kW]
baking conditions	12.1	[kW]

Table 6: Heat loads specifications for ITER magnet system

One of the main functions of the vessel and in-vessel components is that to provide sufficient nuclear shielding to protect the superconducting coils. Guidelines are existing for assessing the structural design and requirements relating radiation effects for ITER magnets and their support structures in the range of 4 to 77 K. It is assumed, that neutron fluences up to 5E+22 n/m² do not cause any change of structural stability in any of the material properties except for copper. There is also a peak dose rate arising from gamma radiation and fast neutrons specified. Limits are summarized in Table 7. [IIDA 06]

Peak gamma- and neutron-radiation dose to coil insulator	10	[MGy]
Total neutron flux to coil insulator	5.00E+21	[n/m²]

Table 7: Radiation limits to ITER magnets

More on the radiation limits to the ITER magnets and insulations can be found in the respective chapters, where the results of the nuclear analysis are discussed.

Personnel access in the pit and behind the biological shield will be prohibited during reactor operation. However, worker access at the TFC and inside the cryostat, for this work especially inside the Port Cells, may be necessary after shut down.

Because of that, the radiation shield, including the BSM, the vacuum vessel and other in-vessel and out-vessel structures shall provide sufficient nuclear shielding not only to protect the coils but also to reduce the activation and residual dose rates inside the cryostat at port areas. The reduction of the residual dose rate should be as low as reasonably achievable. Latest research reported that one or two orders of magnitude of additional neutron attenuation could be necessary. [IIDA 06]

The ALARA principle is used in the case of determining the maximum dose rates and dictates, that *the residual risk shall be as low as reasonably practicable*.

The ALARA target threshold for dose rate is less than 100 µSv/h at a time 1E+6 s (~12 days) after shutdown during and at the end of the DT operation period. The accessibility of all areas of the ITER plant and personnel access limitations are defined depending on the anticipated radiological hazard and conditions during maintenance as displayed in Table 8.

	Access Limitation	**Total Dose Rate**	**Area Contamination Characteristics**
A	Free (unlimited) access for all site personnel	< 0.5 µSv/h	No surface, airborne and cross-contamination
B	Supervised areas. Allowing limited access for non-radiation workers and unlimited one for radiation workers	< 10 µSv/h	No loose contamination tolerated
C	Controlled and limited access areas for all workers. Appropriate radiation protection and exposure planning	< 1 mSv/h	Identified and controlled contamination levels maintained by ALARA
D	Controlled/Restricted areas, entry by exception with a high level of approval.	> 1mSv/h, exceeding those allowable in Zone C	Permanent contamination levels (or exceeding those allowable in Zone C)

Table 8: Area Classification and Radiation Access Conditions [IIDA 06]

Areas with limited access requirements dedicated for specific maintenance, such as the NB cell and the areas inside the bioshield of the port maintenance areas shall meet the requirements for Access Zone C, 1E+6 seconds after shutdown, and should be limited to 100 µSv/h. This value is also the ALARA guideline for allowing radiation workers hands-on access. Areas where the guideline of 100 µSv/h is not meet shall be reviewed for acceptability on an individual basis. [IIDA 06]

ITER wants to assure that main components can be replaced or removed and repaired. This will only be possible if welds and also hydraulic connections are protected by shielding to allow rewelding.

Weldability of irradiated stainless steel is determined mainly by the production of helium. Welding experiments show micro and macro cracks in the irradiated material. From literature it is known, that these intergranular cracks are induced by helium bubbles, which are located at the grain boundaries. These helium bubbles grow by thermal and stress induced diffusion during the welding process. [BLOM 04]

The reweldability limits are specified as followed: [IIDA 06]

limit	welding type
< 1 appm	thick plate welding
< 3 appm	thin plate or tube welding

Table 9: Helium limits for different type weldings [IIDA 06]

A prominent issue in neutronics calculations for ITER is the calculation of dose rates with reactor shut down. The ITER limits say that it must be possible to carry out hands-on maintenance at the port cell 10E+6 seconds (about 11.6 days) after reactor shut down. Assuming a maximum annual dose of 20 mSv and 200 hours of work per year, this means that the dose rate must be lower than 100 μSv/h. This has turned out to be the most difficult requirement to fulfil for the port shielding, much more than limiting the heating in the superconducting coils to an acceptable level. [WASASTJERNA 07] [LAMARSH 01]

A shutdown dose rate calculation is a three-stage computation. At stage one a neutron simulation must be made to determine the neutron flux and its spectrum. This is done with MCNP. Next step would be to calculate the activation of the components with FISPACT and as third step, the resulting gamma flux is given back to MCNP as a gamma source for calculating the gamma flux distribution, which resembles the shutdown dose rate.

There are two methods ready to compute this problem. The Research Center Karlsruhe (FzK) developed the Rigorous Two-Step (R2S) method. The described method is made automatically for all cells in the geometry. A disadvantage of this method is its dependence on the MCNP cells, as it is averaging the flux over the cells, what can lead to problems when the cells are too big of size or a huge amount of time can be needed to modify the geometry in a way that the method can be used. Advantage is, that it allows a full activation calculation and to use different geometries in the single MCNP runs. [CHEN 02]

Another method is to compute the neutron flux and the resulting activation gammas as a single computation. Here the photons will be born at the same positions, where the neutrons collide, without discretization errors. This method is called the Direct One-Step (D1S) method. It requires modifications in the MCNP code and the data libraries, as MCNP usually is intended to compute only prompt gammas and some kind of time-dependence must be included. Factors in this computation simulate the irradiation history. [PETRIZZI 06]

The D1S method is easy to use, once the mentioned factors have been computed and the data libraries are working, what sometimes leads to problems. It requires the activation to be directly proportional to the neutron flux, so multi-step reactions or depletion effects cannot be taken into account. [WASASTJERNA 07]

In this work a third method has been developed, that is similar in many parts to the R2S method, but works independent of the MCNP input cell definition and is relying on the use of FMESH elements. Here the geometry is automatically segmented in arbitrarily chosen three-

dimensional lattices. For each of these elements an activation calculation is done and can be converted back to a MCNP gamma source file. Advantage is a high grade of discretization and the equidistant positioning of the elements allow for easy visualization of the activation results. The complete method is described in detail in 4.4.

Numerous preliminary calculations for different ITER components and also for ITER as a whole have been done. One-dimensional radiation transport calculations with discrete ordinate (Sn) codes were initially performed to guide and optimise the design of the blanket and of the vacuum vessel. These calculations were conducted with the code ANISIN [ENGLE 67], the activation code ACT-4 [SEKI 86] and special nuclear fusion optimized databases.

In order to verify analytic tools (MCNP, FISPACT) and the nuclear data (FISPACT), a series of benchmark experiments were conducted in the framework of neutronic R&D tasks. The experiments employed mock-ups of stainless steel and water mixture, which is the major material of radiation shielding in the ITER machine.

Nuclear heating and fast neutron flux are predicted for Experiment T426 at FNG with an accuracy of 30%. As far as actual geometry can be exactly simulated by using MCNP, complexity of geometry does not reduce accuracy of the calculation results. Generally calculated nuclear heating and threshold reactions (Helium production) have smaller values than experimental values.

The dose rate measurements with a Geiger-Mueller counter are well predicted by R2S method within the total uncertainty on the comparison. The D1S method is also in good agreement with measurements and gives slightly lower than the R2S method.

Also other experimental campaigns show sufficient agreement with calculated simulation results. [IIDA 06]

3.7. Materials and their neutronic effects in ITER

Materials used for the components near the 1st wall and especially the BSM are subject to high neutron and also gamma irradiation and also to high thermal loads. Primary demands to fusion materials are not only rigidity, strength and resistance to corrosion, but also a low activation behaviour.

Low energy charged particles originating from the plasma are mainly captured by the divertor, but a limited number of them are intruding into the first wall and lead to sputtering of the surface, but the effect is limited to the first few centimetres.

Alpha particles from the fusion reaction can be implanted into the layers close to the surface of the first wall and will be responsible for the build-up of small helium gas bubbles, what leads to high secondary tensions depending on the thermal-, physical- and mechanical properties of the chosen material.

The 14 MeV neutrons originating from the plasma have a high mean free path and will lead to effects far away from the 1st wall. Their interactions are based on elastic and inelastic scattering reactions with the atoms in the metal lattices, where they emit a part of their kinetic energy. Both processes lead to singular defects like gaps and interstitial atoms and also to secondary effects that change the properties of the materials. [EHRLICH 03] [LINTNER 62]

The first measured effect by radiation is the 'primary damage parameter', what is equal to the atomic displacements per lattice atom and commonly measured in dpa/s and is proportional to the neutron fluence as can be seen in Figure 14. [NABBI 01]

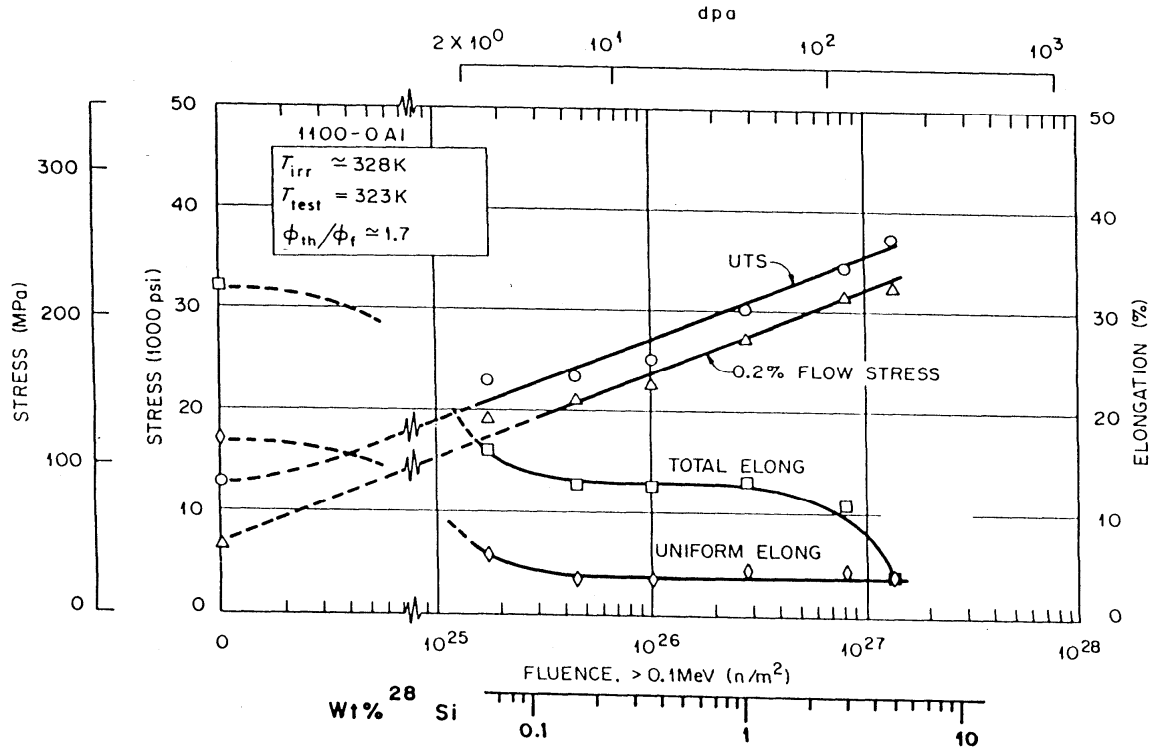

Figure 14: Radiation damage in aluminium in dependence of the fluence

The cross section for processes of neutron displacement damage is generally in the range of 1 to 10 barns. Damage depends on the neutron fluence. In carbon, beryllium and ceramic materials 1 dpa is produced by a neutron dose of about 1E+25 1/m². Volumetric damage leads to the formation of dislocations what results from direct knock-on of atoms from their sites. Knock-on atoms of sufficiently energy may produce further displacements by cascades. 1 dpa typically leads to 1% volume change. This in turn, leads to a significant drop in thermal conductivity, even by 70% from the original value. [RUBEL]

More on the calculation of the radiation damage parameter for the ITER CXRS Port Plug can be found in 5.2.

In activation reactions free neutrons are captured by an atom, causing a nuclear reaction that transforms the atom into another isotope. This new isotope, often unstable, can decay into another element, changing the chemical material composition of the structure. Activation not only leads to higher radioactivity, further increasing the number of lattice defects, but also has effects on the mechanical properties by modification of the chemical properties.

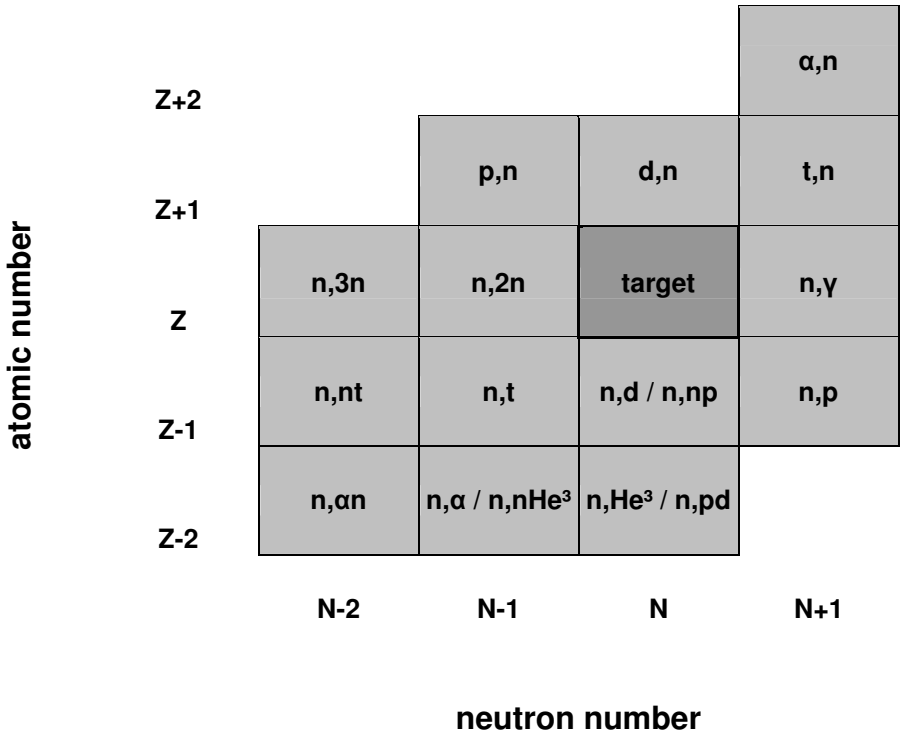

Table 10: Possible transmutation reactions for neutron energy < 15 MeV

With higher neutron energy the number of possible reactions is increasing, what leads to higher build-up of hydrogen and helium by implantation due to (n,p) and (n,α) reactions. Thus the levels of helium and hydrogen generated by transmutations are more than an order of magnitude higher, than in nuclear fission power plants. Table 10 shows a list of possible nuclear reactions for neutrons with energies up to 15 MeV according to [EHRLICH 03]

There are two aspects that are important to analyze low activation materials: From the viewpoint of security and operability materials are preferred, where the 'gamma contact dose' and nuclear heating is low enough immediately after shutdown or after a few days for working at the structures. Here are structural materials like SiC fibre enforced SiC materials the best choice.

In the course of this work some calculations for different materials have been made with the activation code FISPACT. Figure 15 shows a diagram with the activity after reactor shut down of some of the common elements used in ITER. Tantalum and tungsten have the most

activation shortly after shutdown but are dropping fast after 100 days. After three years ytterbium is the most activated material. Low activation is guaranteed by carbon and silicium, so SiC materials are first choice.

On the other hand from the viewpoint of waste management it is important to have low values after more or less longer decay times, what is reached by high purity EUROFER steels and also by vanadium alloys with chrome and titanium admixtures. EUROFER is also reference structural material for DEMO components like blankets, which are currently developed and will be tested in ITER and are also one of the most interesting materials for advanced fission reactor types. [FARKAS 05]

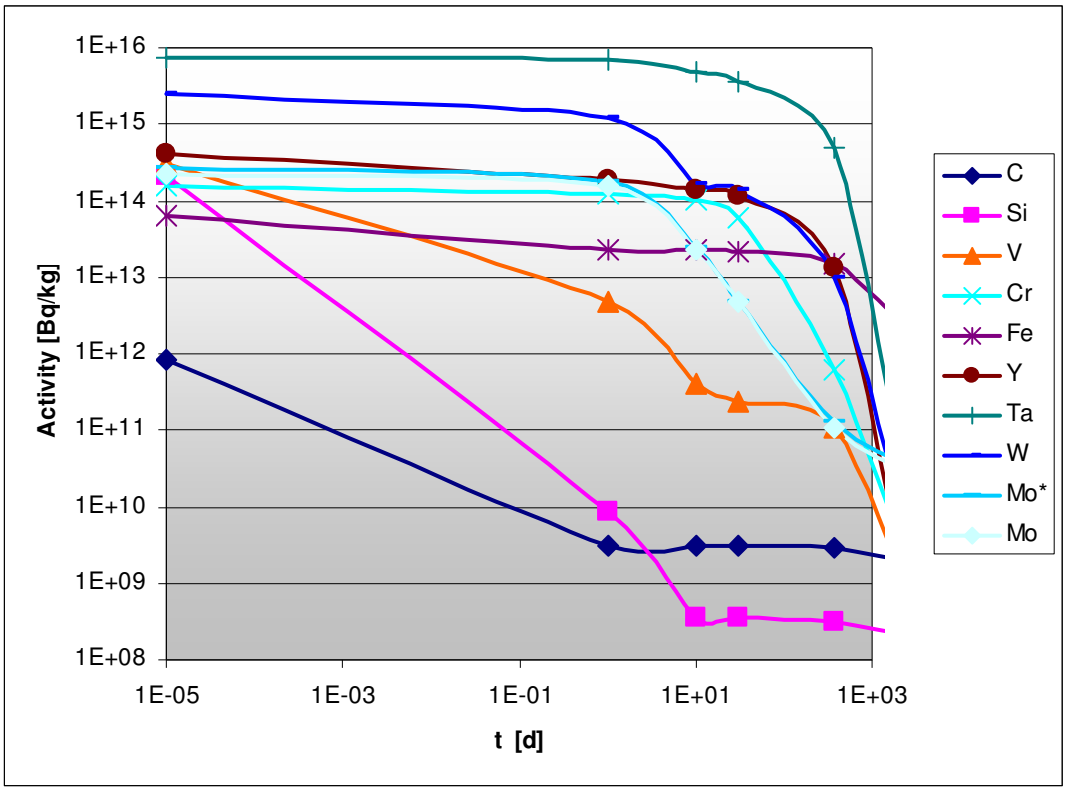

Figure 15: Activity of some elements positioned near the first wall after ITER shutdown

For thermal loads of up to 10 MW/m² tungsten or molybdenum materials would be applicable because of their high melting point, but high activation levels of these materials would lead to other problems.

For standard structural components, not at the first wall, ferritic-martensitic CrMoV steel-alloys are preferred, that proved successful in fission reactors at temperatures up to 600 C and material damages of up to 150 dpa in high radiation environments. [EHRLICH 03]

When looking at steels, a main factor contributing to the activation levels are the impurities especially of the rare earth metals, like silver and niobium. They have to reduced as much as possible.

Effects of irradiation on materials can be calculated in activation codes like FISPACT but verification of the structures should also be made in testing facilities. For this purpose the International Materials Irradiation Facility (IFMIF) is presently organised as an international cooperation. For verification and validation of materials to be used in fusion devices such as DEMO, the decision to build a fusion relevant neutron source with large enough flux in a reasonably sized volume to allow accelerated irradiation of a large number of samples is fundamental.

But as IFMIF is still in an early planning stadium, the best-suited irradiation devices for fusion studies are material test fission reactors (MTR) like the High Flux Reactor (HFR) in Petten, NL and the BR2 in Mol, Belgium. Russian reactors like the BOR60 are being used for achieving high irradiation doses of up to 80 dpa in steels within less than 4 calendar years. [LÄSSER 05]

Reasons for material selection for ITER components, structures and magnets, including permissible variation of main alloying elements and impurities, are given in several documents. [KALININ 01]

All element number densities in materials as based alloying elements as anticipated specified impurities provided by the material manufacturer are in the range of permissible variations or recommended values. A group of elements are materials with the specification of content limitation due to ITER specific requirements. These are, for example, Boron limitation to provide re-weldability of stainless steel, cobalt and niobium limitations in 316 type stainless steel (SS) to satisfy safety requirements. [IIDA 06]

Helium can be generated by (n,α) reactions from B10 what is included to 20% in natural boron with a cross section for thermal neutrons of 3840 barn. Main effects are expected in steel located close to water pipes due to the moderation of neutrons by water. Thus, to minimise the production of helium in stainless steel, it is recommended that the boron content in steel is limited to

- 0.002 wt% or 20 ppm in steel for the first wall
- 0.001 wt% or 10 ppm in steel for the vacuum vessel cooling tubes

Helium production in the borated steel 304B7 used in the vacuum vessel is not a constrain. A 2 wt% boron content is specified for this non-structural material. [IIDA 06]

Assessments of the radiological hazard resulting from alloying elements and impurities content in stainless steel showed that the main contribution to activation comes from ^{54}Mn, ^{56}Mn, ^{55}Fe, ^{57}Co, ^{58}Co, ^{60}Co, ^{57}Ni, ^{51}Cr and ^{94}Nb that originate from transmutation reactions of neutrons with the elements in the initial SS composition (Fe, Ni, Mn, Cr, Co, Nb). All elements, except Co and Nb, are main alloying elements and cannot be markedly changed without having an impact on the stainless steel properties.

Cobalt content is limited because irradiation will lead to increased decay heat and residual dose rate. Cobalt will also be main component of activated corrosion products in the cooling water and will have impacts on occupational dose and accidents like loss-of-coolant.

Irradiation of niobium will lead to long living daughter radioisotopes and thus will have an impact on the mass of radioactive waste after shutdown. So there are strict limits to cobalt and niobium contents in stainless steels in ITER. [IIDA 06]

In addition to the constraints from heat load requirements, the selection of plasma facing materials in ITER is based on a compromise amongst a series of physics and operational requirements, namely (a) minimum effect of impurity contamination on plasma performance and operation, (b) maximum operational flexibility at the start of operation and (c) minimum fuel retention for operation in the D-T phase. This compromise is met by a choice of three plasma facing materials at the beginning of operations (Be, C and W). It is planned to reduce the choices to two (Be and W) before D-T operations in order to avoid long-tern tritium retention in carbon co-deposits during the burning plasma phase. [HAWRYLUK 09]

The cooling water in ITER will be activated by high energy neutrons via the $^{16}O(n,p)^{16}N$ and $^{17}O(n,p)^{17}N$ reactions, as it flows through the cooling channels located in the plasma facing components of the blanket and the divertor. The N-decay photons can result in radiation problems in cryogenically cooled components for a short time after activation.

Material compositions in the ITER MCNP models have been mainly taken from the ITER Material Properties Handbook (MPH). [ETO 06]

A certain problem has been in the last time the decision for a definitive steel-water mixture for the neutronic simulations. As modelling cannot be so detailed, that any water coolant loop is modelled, it is common method to homogenize the cooled structures to a steel-water mixture. Water has different reaction properties with neutrons, so the used ratio will have crucial effects for regional heating, neutron- and gamma flux. Several sources are present for these ratios and different values have been used by different groups. Table 11 shows some of these values.

component	steel	steel [%]	water [%]	source
BSM	NA	84	16	NAR p57
BSM	SS316ln	80	20	ITER Feat MCNP model
BSM	SS316ln	70	30	ITER Alite MCNP model
BSM	NA	80	20	Shatalov et al
BSM	NA	80	20	Serikov 08
filler shield elements	NA	50	50	NAR p58
shield	astm-a887-89 borated	60	40	ITER Feat MCNP model
shield	SS304B4/SS316ln/et al	60	40	ITER Alite MCNP model
shield	NA	80	20	Shatalov et al
shield	NA	80	20	Serikov 08
shield	NA	60	40	Serikov 08

Table 11: Steel to water ratios of different sources

For the calculations of this thesis the generic values of the ITER Feat MCNP model have been used, as these are the mostly used ratios to ensure comparability.

UKAEA did some systematical parametric studies to investigate the effects of homogenization and steel to water ratio. A mere 10% vol water reduces the flux after 100 cm by one order of magnitude compared to plain steel, whereas 30% achieves nearly two orders of magnitude reduction at the same distance. Optimum water fractions range from 70% at the front to 30% at the back. A large water fraction close to the neutron source and a gradual decrease as neutrons travel deeper into the shield maximizes the performance. [PAMPIN 07]

But higher masses of cooling water will lead to higher activation of the water and lead to problems elsewhere in the machine as depicted above. The presence of boron further enhances attenuation. Especially effective is the use of water and borated steel.

Another problem is the homogenization itself. Simulations showed better shielding performances for homogenized structures than heterogeneous ones. Especially regions with low density can lead to streaming situations and the appropriate modeling of homogenized structures must be carefully ensured. Otherwise the application of homogenized models to analyze neutron transport through a truly heterogeneous system can lead to miss-calculation and under-prediction of the total flux passing the component, as well as the energy spectrum and spatial profile of the flux. [PAMPIN 07]

A list of the some of the main materials chosen for the ITER components can be found in Table 12 according to ITER documents. [BARABASCH 09]

Component	Main Material Grades	Form	Approximate mass [t]	Responsible DA	Comments
Cryostat	Steel 304 & 304L	Plates, forgings, bars	3300	IN	
Vacuum Vessel					
Main vessel and port extensions	316L(N)-IG	plates, forgings, bars, pipes	3100	EU, KO, RF	Some amount of bronze, PTFE, Cu
In-wall shielding	Borated Steels 304B4 and 304B7	plates	1500	IN	
	Ferritic steel	plates	280		
	Fasteners XM-19	bolting	30		
Connecting duct	Steel type 304, 304L	plates, forging	300	RF, KO	
Divertor	Carbon Fibre Composites	blocks	3	EU, JA, RF	
	Tungsten	plates	50		
	Copper alloy (CuCrZr)	plates and pipes	12		
	A1 Bronze	forging, rods	30		Some amount of steel 660, alloy 718, Cu
	Steel Type 316L(N)-IG	plates, forgings	400		
First Wall Blanket	Beryllium	tiles	13		Some amount of Ti-6Al-4V, Alloy 718, bronze
	Copper alloy (CuCrZr)	plates	130	EU, JA, KO, CN, RF, US	
	Steel Type 316L(N)-IG	forgings, pipes	1600		
Thermal shield	Steel 304L	plates, pipes	820	KO	Some amount of Ti-6Al-4V, Alloy 718, 316LN, steel 660, insulation
Vacuum Vessel Pressure Suppression Tank	ASTM A-516 Gr.55	plates, forging	220	IN	

Table 12: List of materials foreseen for the ITER components

4. Models and Methods

4.1. ITER MCNP Model

The MCNP Model of the ITER CXRS port plug is a complete 3-dimensional full-scale model with a high level of geometric fidelity representing a detailed geometrical nodalization like depicted in Figure 16. In order to simulate the neutron movements as exactly as possible the port plug has been modelled with the surrounding zones in detail consisting of a whole 20° sector of the reactor.

The MCNP Feat model, consisting of 2400 geometrical cells, was provided by the ITER Team Garching. Side surfaces are reflecting for simulating all of the 360° torus. Cells, encompassing the neutron source, are located in the middle of the torus with a mathematical approximation of the real plasma neutron generation rate.

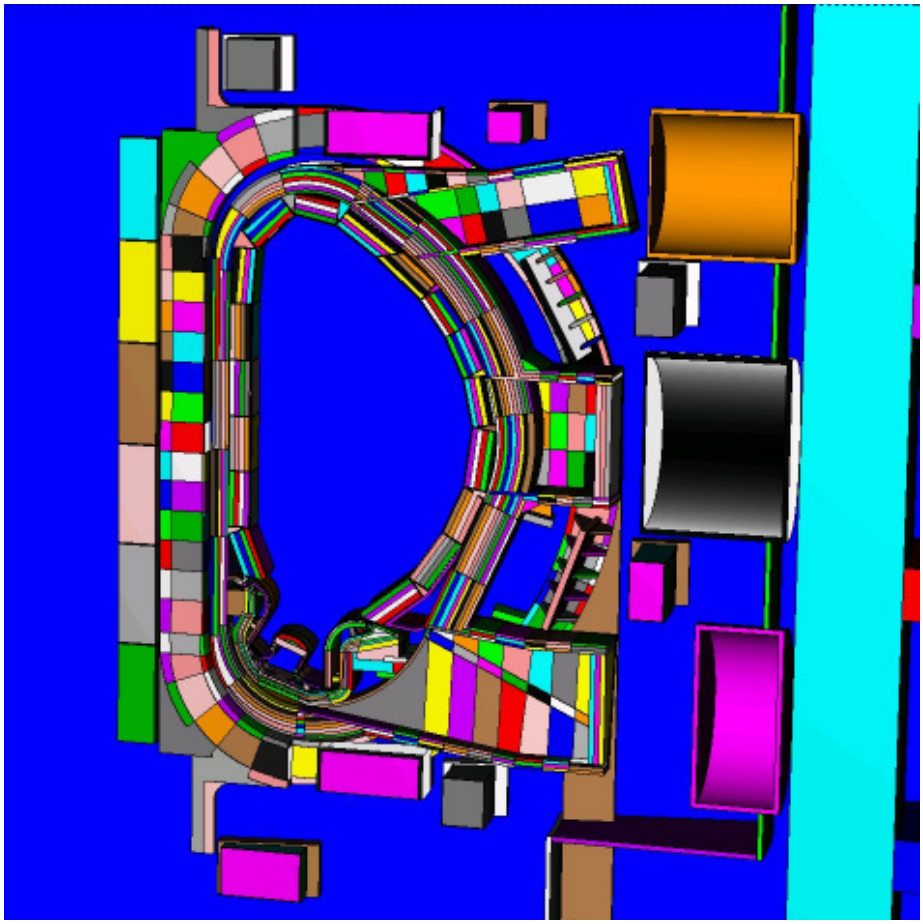

Figure 16: ITER Feat MCNP model

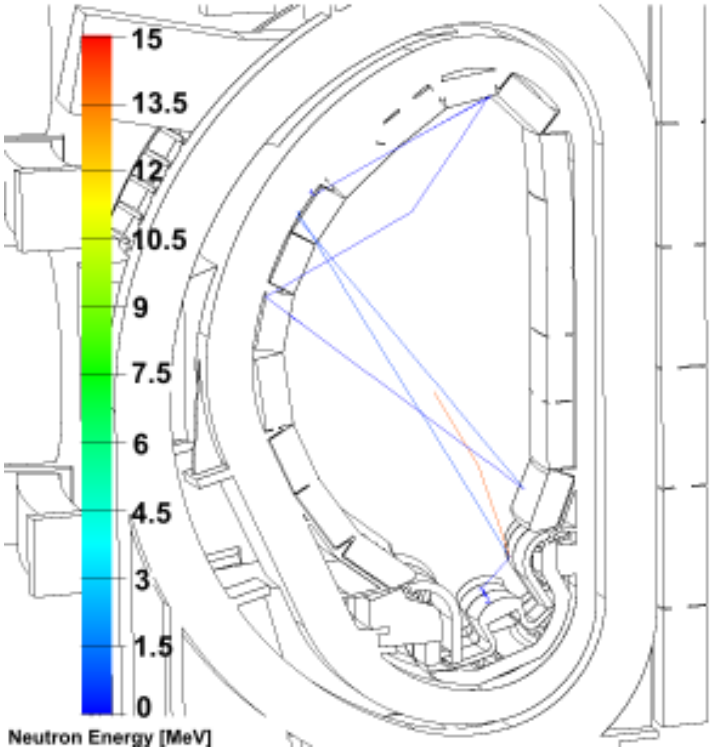

Figure 17: Analyzing single neutron trajectories with MCNP and SABRINA

Several neutron source models have been used in the past. Originally, a simplified DT-neutron distribution in the plasma was implemented in the general ITER models. The source region was divided into five layers (MCNP cells) with the scrape-off layer separating them from the first wall, like shown in Figure 18.

The corresponding DT-source neutron parameters (e.g., coordinates, direction cosines for isotropic angular distribution and neutron energy from the Gaussian fusion spectrum) were sampled by determining the plasma region in which the neutrons were born uniformly in one of the five source layers. The probabilities assigned to these layers correspond to the DT reaction rate, and varying from 0.5 in the innermost cell, to 0.01 in the outermost cell. [IIDA 06]

It was intended to model the neutron source in a tokamak more accurately than the standard MCNP source description allows. In a tokamak geometry, this would require modelling the plasma as a number of discrete cells, each with a constant source density. This step-like representation was considered somewhat unsatisfactory and an alternative method was developed at the UKAEA to represent the source in r-θ-z geometry. A mesh (r,z) of points is used and each point is assigned an appropriate source intensity, calculated by an auxiliary program on the basis of the plasma density and temperature. [WASASTJERNA 07]

For the work of this thesis mainly the old source description that was introduced into the standard MCNP input file was used because recompilation of the MCNP code with a modification of the FORTRAN source module is necessary when using the UKAEA source model, what leads to problems with some own MCNP code modifications described below. As

the important positions for neutron analysis were positioned somewhat behind the first wall, no problems could be reported when using the original ITER Feat source description.

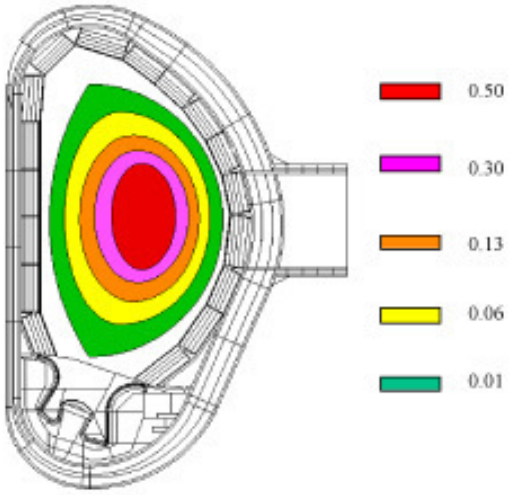

Figure 18: Plasma Region approximated by 5 Cells with uniform source in each layer [IIDA 06]

The vacuum vessel has been modelled according to its layout by three layers. There are two robust outer shells 6 cm thick both made of pure SS 316 L(N) IG. The thickness of the filler region between the two shells varies along the poloidal direction and has been described and a homogenized material mixture of borated steel 60% and 40% water. The overall thickness of the vacuum vessel at the equator is 33.7 cm in the inboard and 75 cm in the outboard. [IIDA 06]

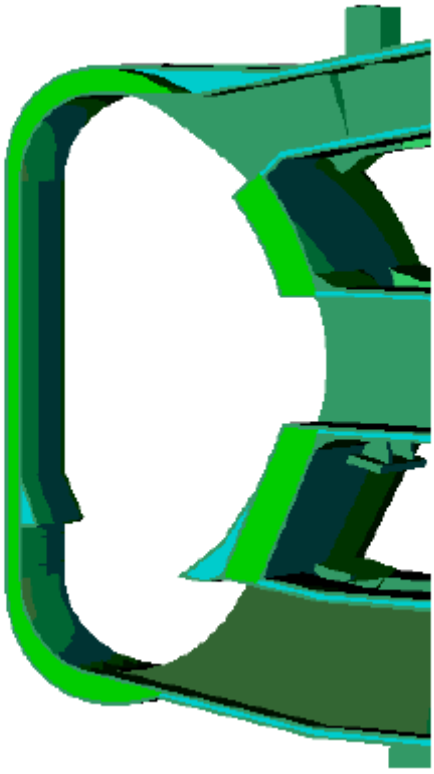

Figure 19: Vacuum Vessel in the ITER Feat model [IIDA 06]

The divertor model has a complex geometry and is made of two different components that have different purposes: the plasma-facing components, called High Heat Flux Components (HHFCs) which remove heat deposited by the plasma and an underlying robust cassette body. For the ITER Feat MCNP geometry, a detailed model has been made with very few approximations introduced. Fine cell subdivisions have been done in order to have a detailed poloidal and radial distribution of the nuclear heating. The cassette itself has been modelled with its two steel layers. [IIDA 06]

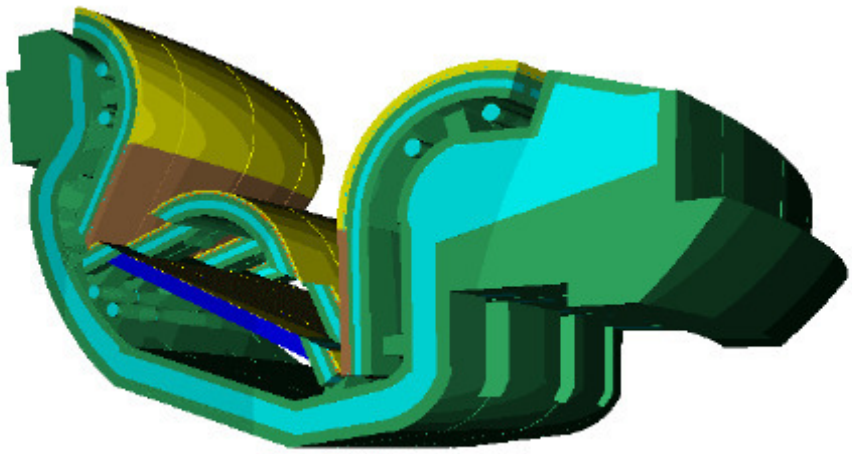

Figure 20: Divertor in the ITER Feat model [IIDA 06]

For the calculations of this work, the original material composition of the provided ITER Feat MCNP model has been adopted. A comprehensive list of the material composition can be found in the appendix.

When calculating neutron flux and heating in cells near the front wall, where the overall flux is high, a sufficient amount of neutron trajectories are entering these cells and are contributing to the statistics of the result, so that error is low within a reasonable amount of computation time. However, many regions of the Port Plug and ITER are in well shielded regions what results in very poor statistics even after long computation time.

To deal with that problem, variance reduction methods have been used. The method of choice in this work was the splitting/russian roulette technology. Cells have been associated an importance number. When entering a cell with higher importance, a particle path will be split in two with reduced weighting factors. By this way neutrons can be guided to regions with low statistics. Equally, by associating low importance numbers in regions that are not of interest for solution of the problem, lesser neutron trajectories are calculated and lesser time has been wasted on these regions. Importance factors of the ITER model has been adjusted in a trial and error process to find adequate numbers for the cells.

Other variance reduction techniques have been tried for the model, for example the automatic weight window generator, where importance factors and weight windows are automatically optimized for a certain tally, but as a high number of tallies have been used and FMESH tallies are covering regions all over the ITER model, the method wasn't of any help. By the way, before the weight window generator can be used, the problem must be run with manually adjusted importance or weight windows.

Due to the stochastic nature of the weight window generator it is important, that these first values are already somewhat effective or no increase in the effectivity is reached by the generator. This alone can lead to a high amount of work, especially in complex models with thousands of cells like ITER, with no guarantee for making any improvements by the weight window generator.

Furthermore a common problem often encountered with automatic variance reduction in shielding calculations with MCNP is that the program crashes. It keeps running indefinitely without producing any output and the program must be killed manually. There are grounds for suspecting that it may be due to excessive splitting, when a too high number of trajectories is split to often and these split trajectories are split again at another position, making the histories so long, that these can't ended anymore. This also is called the long history problem. [WASASTJERNA 07]

4.2. Dynamic CXRS PP Model

Neutronics design calculations require as basic input a suitable geometry model of the ITER device. The Monte Carlo Code technique enables the use of full and detailed 3D geometry models in the neutronics calculation. The modelling of a complex geometry with a Monte Carlo Code is, however, an extensive and time-consuming task. On the other hand, CAD geometry models of ITER are available for design purposes. Unfortunately they cannot be used by Monte Carlo Codes as they are based on different geometry representations.

Suitable algorithms must be and are being developed to convert CAD geometries into the semi-algebraic representation for use with a Monte Carlo Code. Development work for an interface program has been conducted at FZK, Karlsruhe and other groups, following different approaches. [IIDA 06]

The ASIPP approach from Hefei (China) is based on the use of the commercial ACIS CAD-Kernel and has been programmed on the Windows computing platform. The MCAM code has been developed as a translational code and has bi-directional conversion abilities. [ZENG 06]

The FzK approach, called McCad integrates a CAD kernel, a C++ GUI application framework and a conversion algorithm. The CAD kernel provides core data structures, algorithms, and data exchange interfaces for neutral CAD files such as IGES and STEP. [TSIGE-TAMIRAT 07]

A special case is a method currently developed by the Fusion Technology Institute of the University of Wisconsin. Here MCNP is modified in a way, that it can read directly the CAD geometry file. [WANG 05]

Further CAD-MCNP activities are done by the company Raytheon with their TOPACT translation code and by a group in Japan. [SATO 06]

Unfortunately the mentioned methods have not been available for the work of this thesis, so other methods to deal with the complex geometries and frequent design modifications had to be used.

The geometry of the CXRS Port Plug was modelled separately and coupled with the ITER model. Due to the complex geometry and continuous modifications of the design, an efficient and flexible method had to be deployed to alter the model with the design process accordingly.

For this purpose an algorithm was developed, allowing the calculation of geometrical configuration of the mirror system in accordance to the actual location, size and orientation. The program produces new cards for the angles and coordinate of the surfaces for inclusion into the MCNP input file without changing the structure of the input file.

The algorithm was included into the Microsoft Excel environment that also is used as Graphical User Interface (GUI). A screenshot of the input sheet is shown in Figure 21. The user simply provides the positions and the sizes of the mirrors and all other variables will be calculated by mathematical relations.

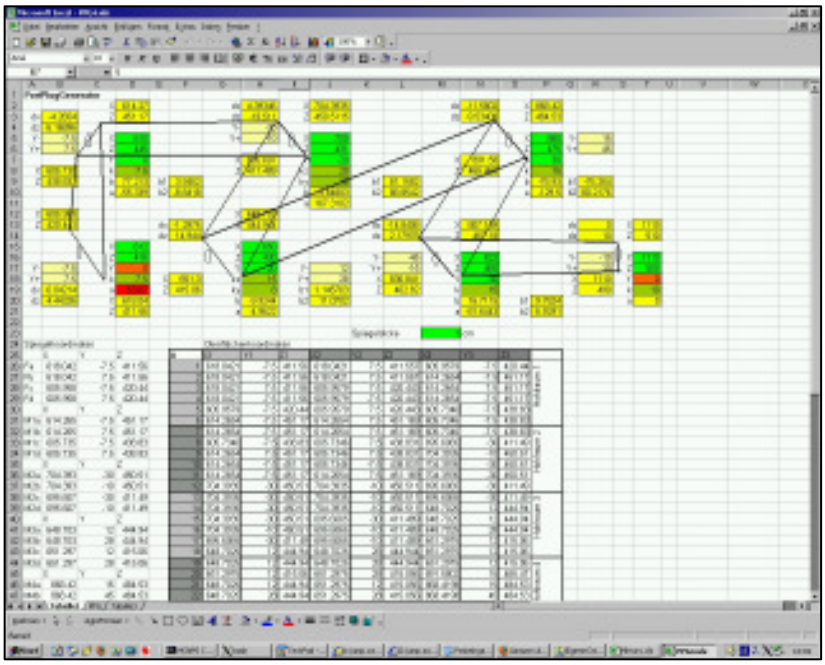

Figure 21: Dynamic CXRS model input sheet

The main source for mathematical surfaces that had to be included into the MCNP model were the walls of the mirror labyrinth. These are defined by the limiting points of the mirror borders. The lines, defining the mirror borders on the other hand, are related to the position and the angle of the mirrors, while the angle of the mirrors are defined by the optical paths between the mirrors. Therefore the only variables to be given by the user are the positions and diameters of the mirrors to define the interior of the Port Plug, if no retractable tube is included.

The retractable tube is modelled by several cylinders that are filled with either a void or a steel material of reduced density to depict a variable distribution of the structures inside the tube. Diameters of the cylinders can be changed quickly either in the input sheet or in the final MCNP model description with a text editor.

The model description given by the dynamic modeller is a simple text file that can be included into the ITER Feat model very simply and the model code is in a structure that allows fast modifications by manual manipulation with any text editor.

A picture of the CXRS Port Plug model with its most important structures plotted with MCNP is given together with a SABRINA plot of the ITER Feat model in Figure 22. [BOURAUEL 09]

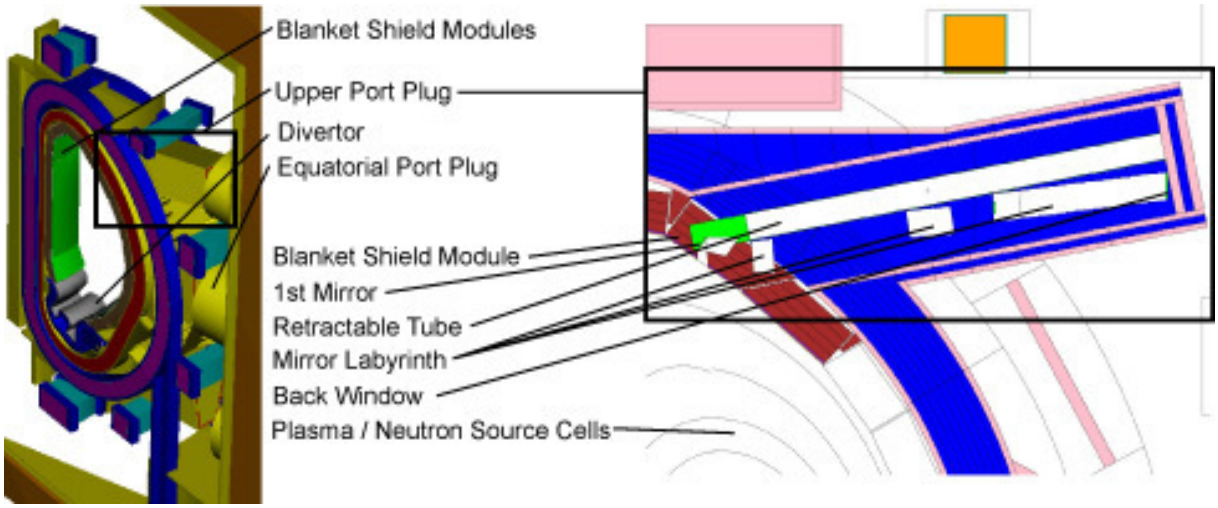

Figure 22: MCNP model of the CXRS Port Plug in ITER Feat model

4.3. Visualization & Processing with MOPAR and MCNPAct

4.3.1. FMESH definition for visualization and data sampling

The MCNP Standard Tallies are sampling data for specific cells or parts of the model. But for the understanding of the physics and the behaviour of complex geometries it is important to have data at any point of the model. For this purpose, extensive use of the FMESH-Feature of the MCNP5 code has been made.

The use of FMESH is not only applied for the generation of 2D and 3D-distributions but is also the base for the MCNP-FISPACT interface described later. So it is appropriate to discuss this feature and the methods of its use in this chapter.

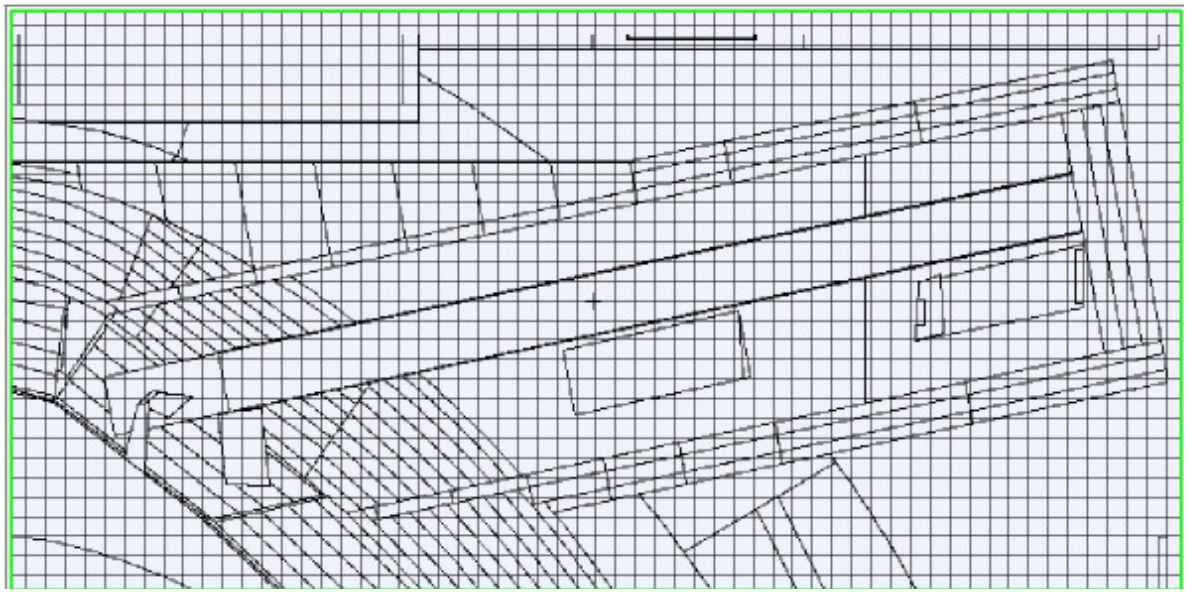

Figure 23: ITER CXRS PP MCNP model super positioned with a FMESH tally

The FMESH card allows the user to define a mesh tally superimposed over the problem geometry. Results are written to a separate output file. By default, the mesh tally calculates the track length estimate of the particle flux, averaged over a mesh cell, in units of particles/cm² [BRIESMEISTER 05].

With multiplier cards it is possible to get results for other data, like neutron heating, gamma heating and material damage.

The general form of the multiplicator card is

FMn C m r1 r2

C is a multiplicative constant and m is the material number of the cell. r1 and r2 are reaction channel identifiers.

For the neutron heating the following multiplication card has been used:

FM1 -1 0 1 -4

C = -1 sets the automatically the density of the material the actual particle is travelling. When m = 0 the reaction cross sections for the material in which the particle is travelling are used and 1 and -4 are the identifier numbers of the total cross section and the average heating number respectively.
For the photon heating the following multiplication card has been used:

FM1 -1 0 -5 -6

Here -5 and -6 are the reaction identifiers for the total cross section and the photon heating number.

Multiplier Cards have been chosen according to the MCNP5 manual. [BRIESMEISTER 05]

The FMESH grid is independent of the geometry and can be in a rectangular shape or in a cylindrical shape, but in this work only rectangular, Cartesian meshes have been used. The user can define freely the origin, dimension and number of steps in 3 dimensions. If only a 2D mesh is needed, for example for a flux map, only one step is chosen in the third dimension.

As data can be provided by FMESH as discrete, equidistant values, it is possible to use these 2D matrices as base for a map with a resolution of one value per pixel. Indeed it is possible to get higher resolution by interpolating between these values or pixels, if the problem physics allows.

```
mcnp   version 5     ld=10212005  probid =  10/29/08 12:40:51
 c CONTINUE
 Number of histories used for normalizing tallies =     132000000.00

 Mesh Tally Number 414
 This is a neutron mesh tally.

 Tally bin boundaries:
    X direction:    590.00    591.00    592.00    593.00    594.00    595.00    596.00
    Y direction:    -11.00     -1.00
    Z direction:    420.00    421.00    422.00    423.00    424.00    425.00    426.00
    Energy bin boundaries: 0.00E+00 1.00E+36

Energy Bin:  0.00E+00 - 1.00E+36 MeV

  Y bin:     -11.00   -    -1.00

     Tally Results:  X (across) by Z (down)
              590.50      591.50      592.50      593.50      594.50      595.50
       420.50 1.88796E+14 1.88979E+14 1.85431E+14 1.86010E+14 1.89052E+14 1.89530E+14
       421.50 1.87393E+14 1.87818E+14 1.83810E+14 1.87807E+14 1.85565E+14 1.88142E+14
       422.50 1.84808E+14 1.88279E+14 1.84824E+14 1.85751E+14 1.86035E+14 1.85200E+14
       423.50 1.86801E+14 1.87023E+14 1.87264E+14 1.83499E+14 1.84975E+14 1.87437E+14
       424.50 1.88985E+14 1.88226E+14 1.84911E+14 1.86483E+14 1.86471E+14 1.87379E+14
       425.50 1.86458E+14 1.88118E+14 1.87919E+14 1.85092E+14 1.86840E+14 1.85522E+14
       426.50 1.88461E+14 1.87511E+14 1.88459E+14 1.85060E+14 1.87860E+14 1.87942E+14
       427.50 1.88668E+14 1.85467E+14 1.88428E+14 1.86679E+14 1.87000E+14 1.86750E+14
```

Figure 24: Section of unformatted MCNP FMESH output

The results of FMESH tallies are written by MCNP into separate output files. These ASCII output files in text format are providing the values in table like forms. Each tally table is coming with several specific header lines. The beginning of a typical FMESH output file is shown in Figure 24.

For further processing with external visualization tools the files have to be converted into adequate formats. A computer code for easy handling of FMESH outputs has been programmed in the course of this work and is described in the next chapter.

4.3.2. FMESH Processing with MOPAR

MOPAR is a software tool for parsing, modifying and previewing the results of MCNP-FMESH files. MOPAR is the abbreviation for MCNP Output Parser And Reckoner. This program is completely written in the programming language Java and so, it is able to run on multiple computer operating systems like Microsoft Windows, GNU/Linux and Mac OSX. Figure 25 shows the GUI of the MOPAR computer code running on a Microsoft Windows operated computer, displaying a FMESH output of the neutron flux inside the ITER CXRS Port Plug.

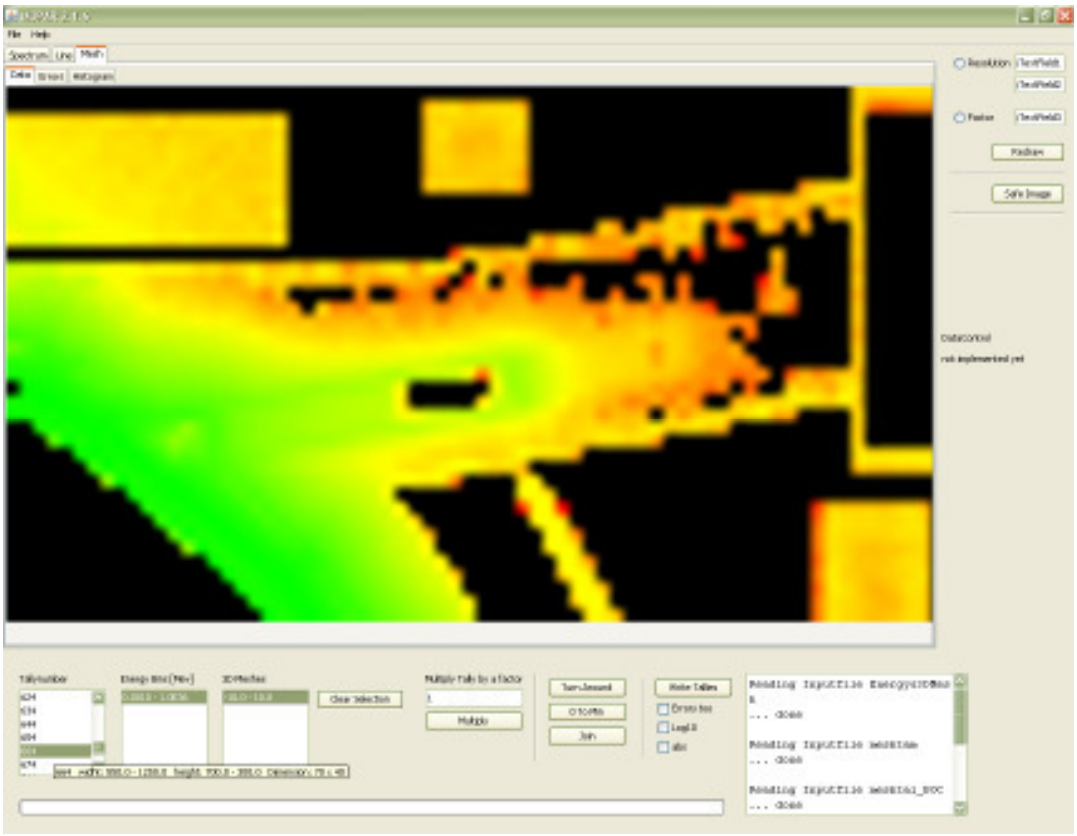

Figure 25: GUI of MOPAR with FMESH preview screenshot

With MOPAR, the user is able to visualize the results of the FMESH output files and their errors. For this purpose MOPAR can produce 2D-colour plots with a green-red gradient where red colours mean higher values. The user is thus able to spot points or regions in his simulated geometry before converting the files to a generic format.

The code shows errors in a white-red distribution. Black areas symbolize the absence of values and therefore the absence of errors too. Another graphical approach for the visualization of errors is the histogram feature as displayed in Figure 26, that shows the error distribution across the whole FMESH chart. With this two methods it is possible to determine, if the number of simulated particles was high enough or if there are local regions where the errors are too high and the importance factors in MCNP have to be adjusted.

The user can iterate through the mesh in slices and also the single energy bins. If the user is satisfied with the results, the values can be written down and saved as generic formatted tables. MOPAR writes for each MESH it's own file. It is also possible to write down the logarithmic values to base 10 into the files and or the absolute value if negative values occur in the MESH.

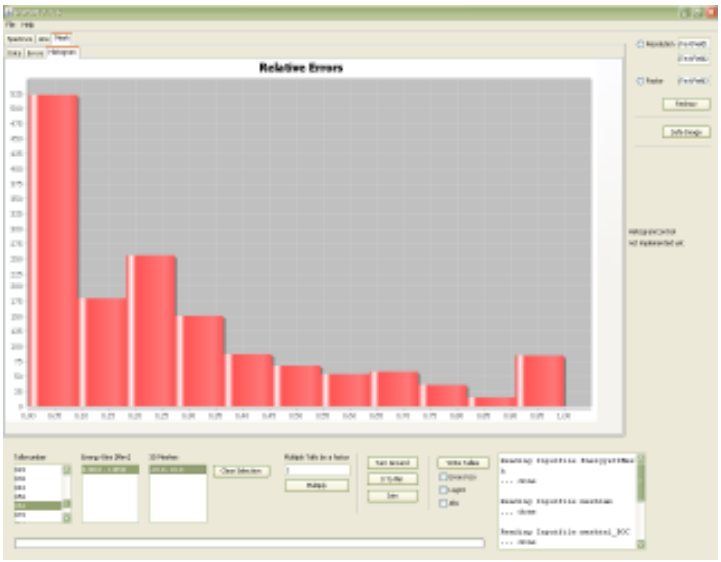

Figure 26: GUI of MOPAR with histogram of statistical errors

Another feature is to view the energy spectrum of a specific point in the MESH geometry. If the user enters coordinates within the geometry, MOPAR displays the energy spectrum on a logarithmic scale of that point. Multiple points can be added and deleted and can be written down in a csv formatted file, that enables the user to analyze the values in external programs. Figure 27 shows a üicture of the GUI with visualization of two spectra at different parts of the Port Plug.

Additional features of the tool include raising all values to a user-defined limit and to add, substitute, multiply or divide MESHES by a given value or with the values of another MESH.

The internal structure of MOPAR consists of MESH objects, each containing two two-dimensional arrays of floating-point values. One for the data values and one for their accompanying statistical errors. These MESH objects are arranged in another two-dimensional array. The first dimension describes the segmentation of the MESH by energy. The second dimension describes the z-axis of the MESH-geometry. By this way the structure of one MCNP-mesh tally is mapped.

An internal list is used for storing several mesh tallies. Each applied function to single tallies or meshes is encapsulated in a 'Task'-object and is also added to a list. This specific list will be processed by work threads.

To create the spectrum distribution of a given point MOPAR first does a range check of the coordinates and then includes the next MESH-cell that fits to the coordinates. Then the code it collects the values for each energy bin and creates a chart with the distribution. For each chart included in MOPAR the open source library JFreeChart is used.

Figure 27: GUI of MOPAR with spectrum analysis of FMESH grid

In principle it would be possible to read these converted tally files with calculation programs like Microsoft Excel, but for an adequate and professional visualization of the data it is better to use sophisticated visualization programs.

For the work done in this thesis paper, mostly the visualization program ‘3DField’ has been used for visualization of the FMESH tallies and their derived tables. With this code it is possible to read the tally files and to plot the distributions in various diagrams. Furthermore it is possible to superimpose the diagrams with MCNP geometry plots for better understanding of the graphics like shown in Figure 28, where the results of a FMESH tally, that includes the area of the Port Plug, are displayed together with the associated geometry of the model as a 2D distribution.

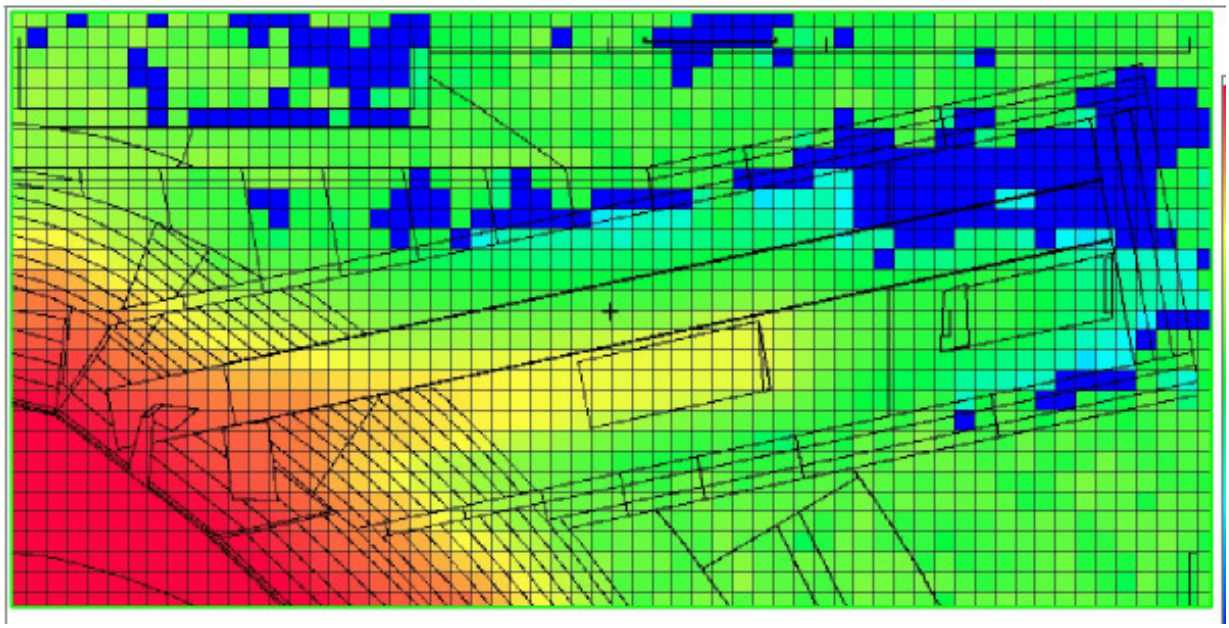

Figure 28: FMESH tally results with geometry plot visualized with 3DField after processing with MOPAR

As 3DField is also capable of transferring appropriate data tables to 3D structures, it is also possible to plot isofluency surfaces like shown in Figure 29. In that picture, quantities of equal flux in the CXRS Port Plug have been linked to a three dimensional surface. It is clearly seen in this diagram, that a high number of neutrons is reaching into the Port Plug at the positions of the mirror labyrinth and also into the volume of the retractable tube to the right of the picture.

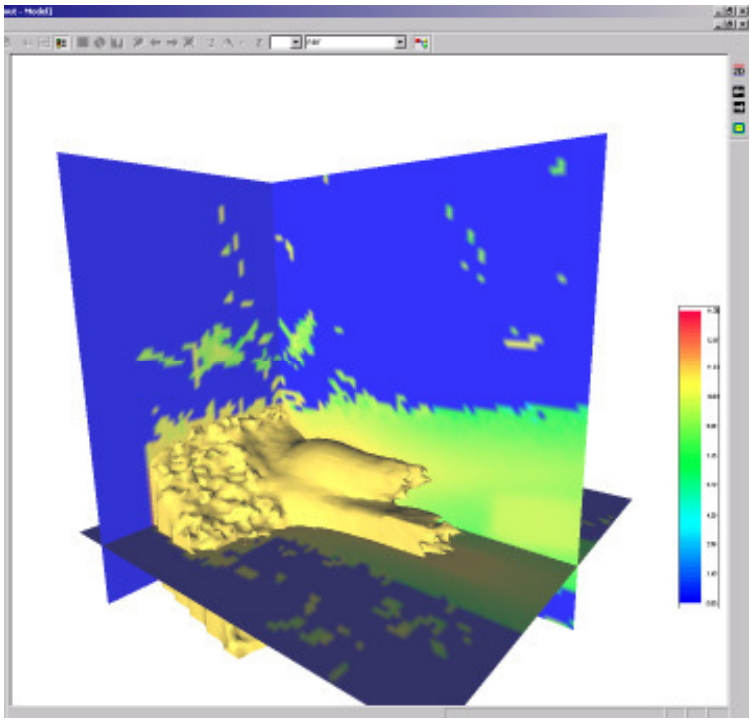

Figure 29: Visualization of processed 3D Neutron Flux Data visualized with 3DField

4.4. MCNPAct: MCNP-FISPACT Interface

4.4.1. Overview

As described earlier, the activation code FISPACT is a zero-dimensional code, what means that no geometrical resolution can be defined. An activation calculation can only be done for one discrete volume, for example a mirror or another component of the CXRS Port Plug. If a more complex geometry or structure has to be calculated it is mandatory to make single activation calculations for all MCNP cells, it is consisting of. The R2S method with its code makes use of this way to automatize the activation calculation. The flowchart of this way can be seen in Figure 30.

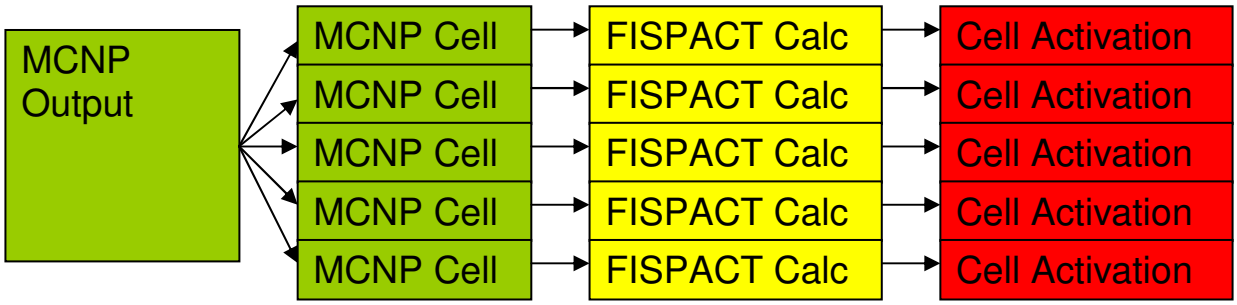

Figure 30: Cell based way of getting activation analysis for a complex MCNP model

Disadvantage of this method is the limitation of the resolution to the number of cells in the model. If there are huge cells in the geometry, the results will be homogenized over the cell or the user has to further segment the cell manually within the MCNP input. Visualization capabilities are also limited, as can be seen in Figure 31, where numbers are printed inside an MCNP plot of the geometry. [FISCHER 03]

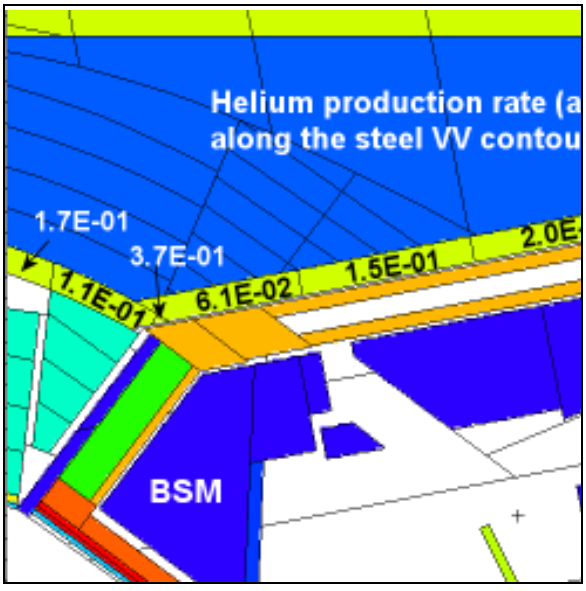

Figure 31: Visualization of Helium production in ECRH PP as part of activation analysis (FZK)

For this work a new method, called MCNPAct, was supposed to be developed. The goal was an automatic code, easy to use with a graphical user interface and it should be able to work independently of any manual segmentations of the MCNP input and have better capabilities for visualization.

MCNPAct makes full use of the MCNP FMESH Tally. The FMESH option generates a 3D grid over the desired part of the geometry, with the number of steps fully adjustable in each dimension as described in 4.3. For every single element of that grid the neutron flux will be computed during the MCNP run and results are grouped in a matrix that is adequate for graphical visualization either with the MCNP plotter or an external program like 3Dfield after changing the output files to a more general format.

MCNPAct is using this technique to generate a FISPACT input file for every single element of an FMESH matrix and to compile the corresponding output files back to matrices for such data as activity, gamma dose, decay heating for the sum and for single isotopes at the desired time steps and furthermore provides a gamma source of the irradiated geometry that can directly used back in MCNP for gamma transport and dose rate calculations. The flowchart of this way can be seen in Figure 32.

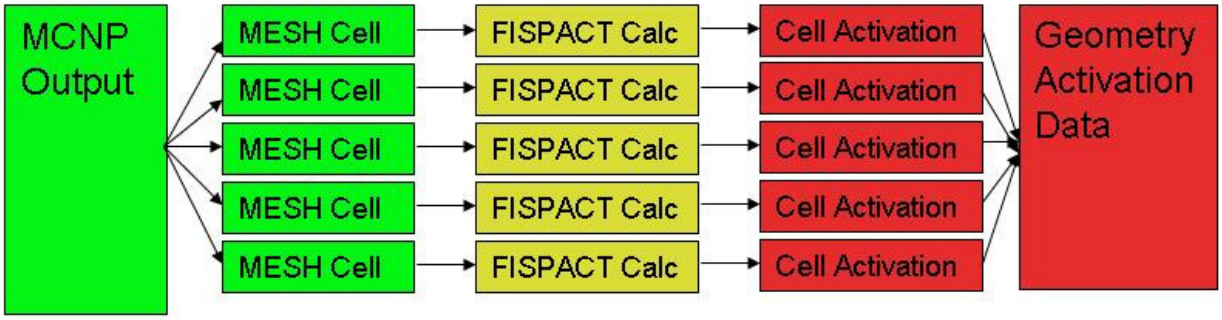

Figure 32: MESH based way of getting activation analysis for a complex MCNP model

The way of generating the FISPACT input is not straight forward, as MCNP cannot provide data for the mass and material composition of FMESH elements. They have to be calculated separately and will be computed automatically by sampling the MCNP geometry. For this purpose the PTRAC option in MCNP is used.

Flow charts, showing the method of the program and the sampling process with the PTRAC card are shown in Figure 34 to Figure 36.

During a simulation run a PTRAC card generates an external file that includes the coordinates of all events inside the model and this can be used to display the paths of single particles inside the geometry. For the sampling a filter option is included in a way that only source events are logged. A new source description is introduced, so that neutrons are generated inside the

volume to be sampled inside the geometry with a random probability. Furthermore the VOID option of MCNP is used, that replaces all materials in the geometry with vacuum, e.g. removes simplay all materials from the list, and by that way no time is spent with scattering of particles in material.

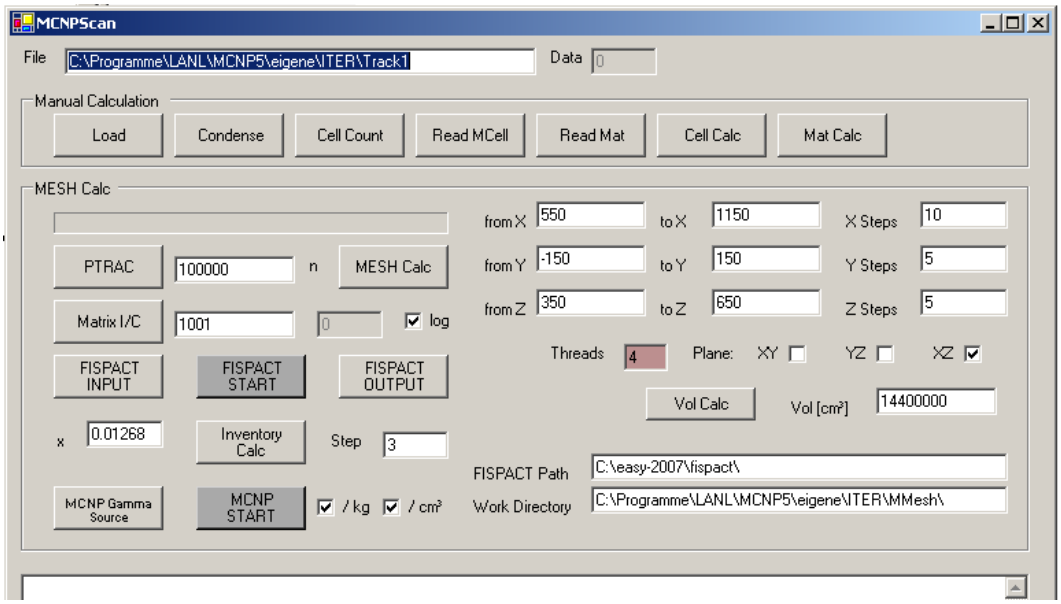

Figure 33: Graphical User Interface of MCNPAct

The log file of this PTRAC run includes then the coordinates of random points in the geometry and the number of the corresponding cells. From the number of points inside certain cells it is possible to determine the volume of the cell itself when the overall volume is known. This operation is done for each element of an FMESH Tally.

Then the MCNP Input file is analyzed to get densities and material composition for the cells that have been sampled inside an FMESH element and so the mass and composition of the whole element will be calculated. A FISPACT input is then generated for each element with its specific material composition and mass and the neutron flux is read out of the FMESH output file.

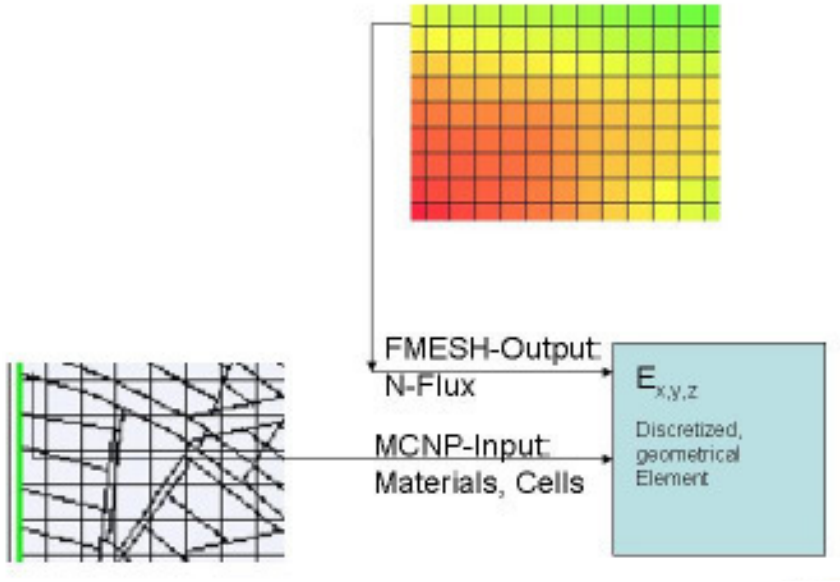

Figure 34: MCNPAct: Combination of MESH data with geometry input data to discrete element files

As a by-product it is possible to simply calculate the volume of any cell in the geometry by running the sampling without segmentation of the geometry. Furthermore it is possible to plot 'material maps' of the input, where the distribution of specific isotopes is mapped over the geometry.

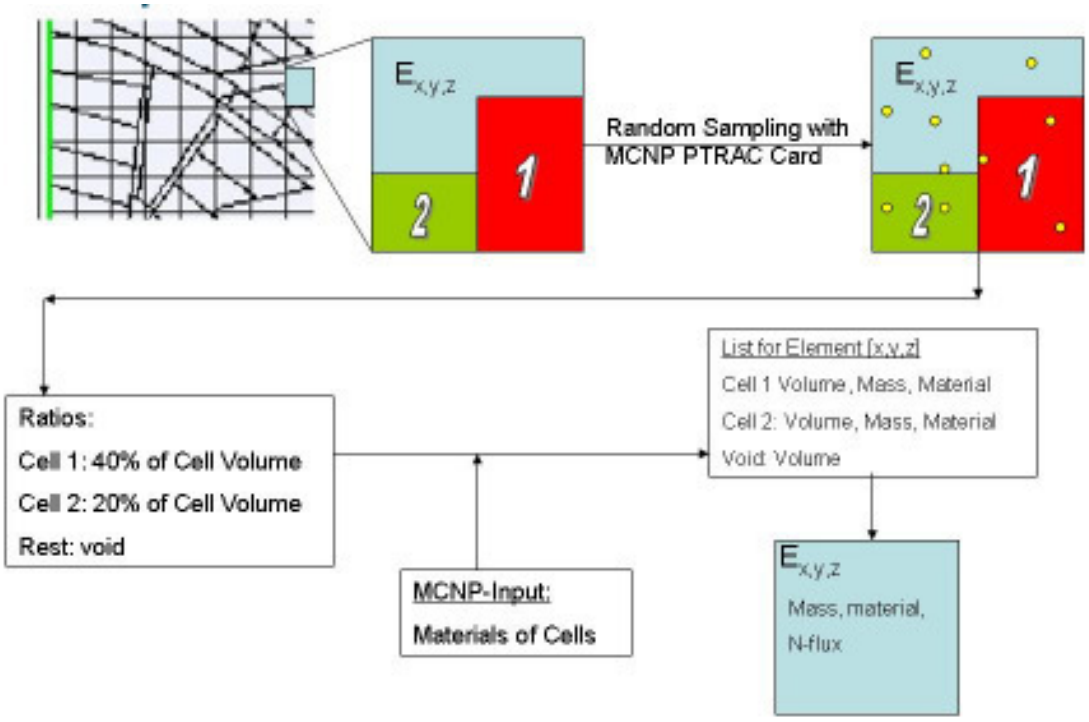

Figure 35: MCNPAct: Determining the element material composition by random sampling (example)

When finally all FISPACT inputs are generated, the activation program is run with the single input files. Output files will be renamed according to their position in the geometry. Finally the output files are analyzed and their results are compiled into single files with matrices for activation, decay heat, gamma dose for the sum of nuclides and also for every single nuclide if needed. These files can simply be opened by visualization programs like 3Dfield or even EXCEL to display results as maps for the whole of the geometry.

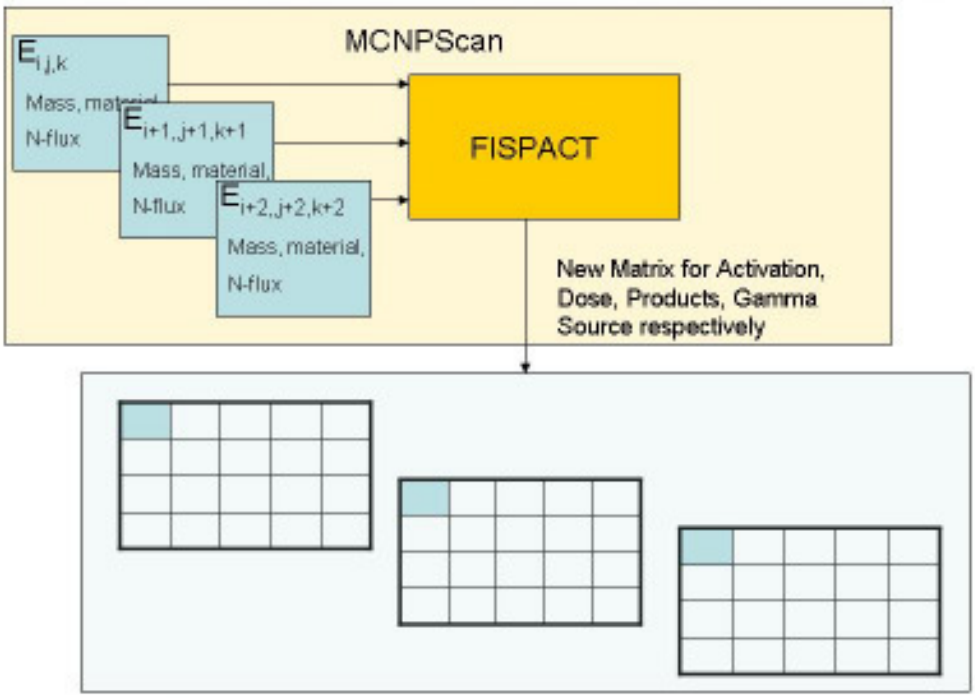

Figure 36: FISPACT computations and compilation of FISPACT output files to new matrix files

Furthermore the gamma spectrum is read from the FISPACT output files and is then compiled into a new gamma source for the calculation of the gamma transport due to activation.

The program has been developed in VisualBasic.NET with the Microsoft Development Environment and it has been given the name MCNPAct as the fundamental basis of the code is the active scanning of the MCNP geometry for activation calculation purposes. In the last version the program consists of more than 4,000 densely packed lines of code. It has a GUI (Graphical User Interface) to give maximum comfort to the user, so that he is able to work intuitively with the code, as shown in Figure 33.

The program is event controlled, so that a click on one of the buttons triggers the start of the corresponding program module with the boundary conditions the user defined in the text fields of the GUI. Necessary MCNP and FISPACT runs are controlled and started by the code itself.

The whole process of the activation calculations with MCNPAct consists of several different modules that usually are executed in a serial order. But the user has the ability to execute single modules, to face changes e.g. when a new MESH tally file has been generated it is not

necessary to rescan the geometry – the user will then begin at step 4, where the FISPACT input is generated.

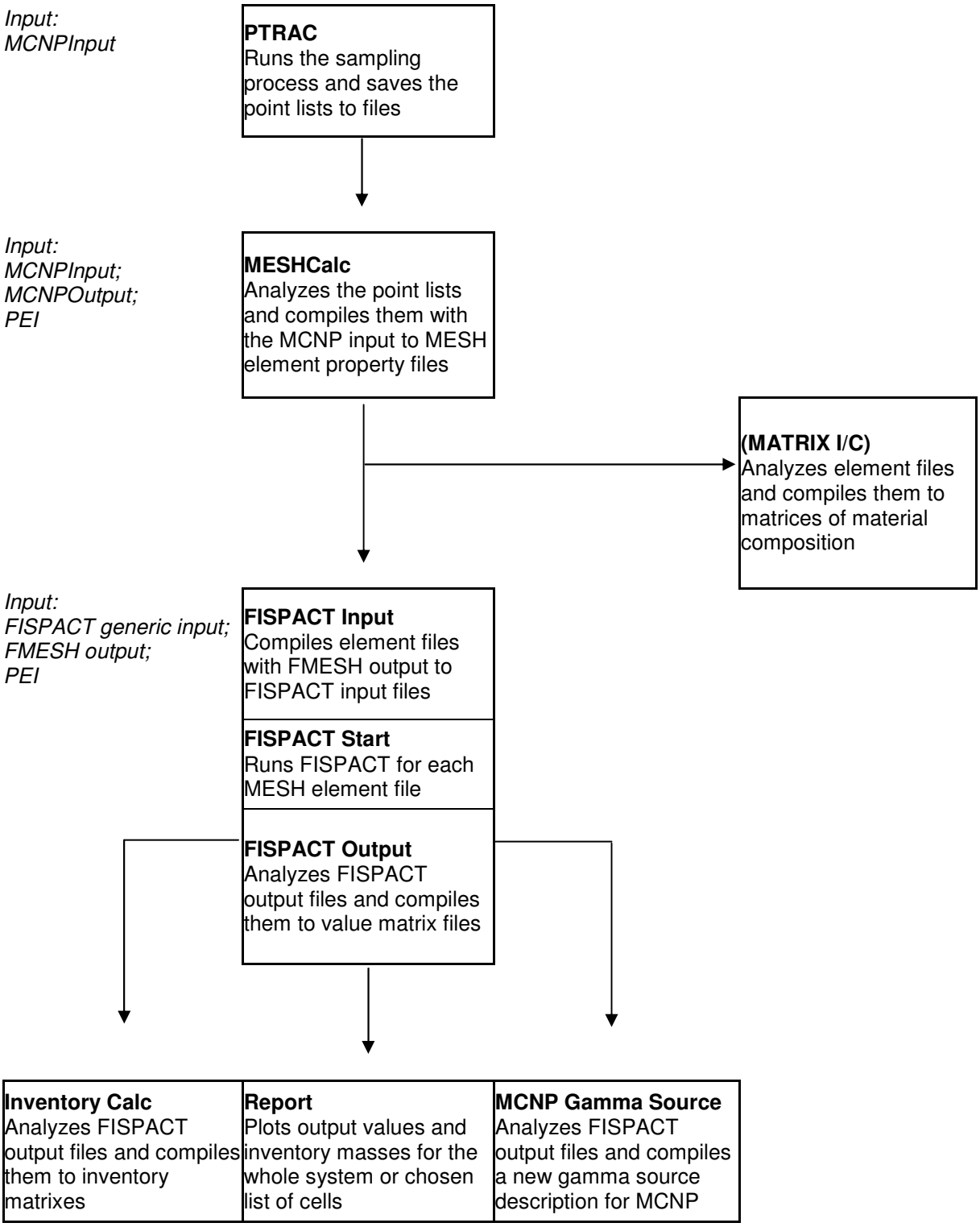

Figure 37: MCNPAct: Flowchart of the program modules

Figure 37 shows a flowchart of the logic sequence of the modules throughout the program execution. The single program modules are described here shortly as an overview and in detail the chapters 4.4.2. to 4.4.9. These modules are usually executed one after another.

1. PTRAC – The code modifies the MCNP input by including the special PTRAC card, which will sample randomly generated points in the geometry. Also a corresponding source routine with a uniform distribution is included together with the VOID card, which removes all materials from the geometry. The MCNP runs are then automatically started and PTRAC data are stored in external log files.

2. MESHCalc – The PTRAC file is analyzed and together with the MCNP input and output files the material composition and mass of every FMESH element is calculated and saved in an external MESH-file

3. Matrix I/C – This module is optional. It searches the MESH files for user specified materials or isotopes and gives out a new file with the distribution map of that material/isotope inside the geometry that can be directly plotted by a suitable visualization program.

4. FISPACT INPUT – The MESH files are analyzed and together with the corresponding FMESH tally file the single FISPACT input files are generated and stored to the hard disk.

5. FISPACT START – This module will start a FISPACT run for every single generated input file. Output files are renamed according to their position in the geometry for later analysis.

6. FISPACT OUTPUT – All of the single FISPACT output files are analyzed and data of activity and heating are collected and written in new files that can directly be visualized by suitable programs. This is repeated for every time step defined in the FISPACT input file.

7. Inventory Calc – All of the single FISPACT output files are analyzed again in more detail and this time the activity and masses of single isotopes are collected and stored so that one new map is generated for every single nuclide. This again will be done for each time step defined in the FISPACT input file.

8. Report –An analysis is made, where the activation parameters for the whole structure are summed up from the FISPACT files.

9. MCNP Gamma Source – The single FISPACT output files are read and searched for the gamma emissions. These data are compiled together to a new MCNP compatible gamma source that is saved in three external files and can directly integrated into the MCNP input file with the help of a modified MCNP5 version (external source definition). This is done for a time step defined with help of the GUI.

In the following paragraphs, the modules are explained in detail.

4.4.2. PTRAC

The PTRAC module of the MCNPAct code starts the sampling process that generates the point list, from which the cell volumes are calculated later.

The user at first has to define the desired region in the geometry for analyzing. This can simply be done by giving the minimum and maximum coordinates for all of the three axis X,Y and Z with help of the GUI. Also the user is supposed to give the number of steps into each dimension that the program will use to segment the geometry in two or in three dimensions. When only a 2D picture or slice is needed the user has to set the other dimension to only one step. Furthermore the plane of the maps (XY, YZ or XZ) has to be defined. It can be chosen from three buttons underneath the text boxes inside the GUI.

If the analysis is run in threedimensional mode (by choosing more than one step in every direction), there will be a map generated for each step of the axis that is positioned perpendicular to the chosen mapping plane. For example, if the mapping plane is XY and the Z axis segmentation has been set to 10 there will be 10 different PTRAC runs for slices along the Z-axis.

This definition of the boundary conditions of the calculation should be consistent to the definition of the FMESH Tally, which delivers the neutron flux data for the later computation, i.e. it should have the same dimensions and segmentations along the axis and the mapping plane should be the same as defined in the FMESH card in the original MCNP input file.

Also the user has to prepare the MCNP input file with code words for adaption by MCNPAct. At first the complete source routine must be removed from the file, because MCNPAct will introduce its own one. At the position of the removed source, the user has to introduce the comment line

“**c source**”,

where the new source routine is supposed to be inserted into the input file. Furthermore the end control line has to be removed or commented out. This affects the NPS, CTME and KCODE card, as MCNPAct will introduce again its own one. It is also important, that the analyzed region does not contain any cells with zero importance and that there is no CONTINUE card at the beginning of the input file.

Finally the user sets the number of sampling points for each PTRAC computation. The more points are chosen, the more accurate the results will be. A good compromise between time and accuracy are 100,000 to 300,000 points, but this is of course dependent on the number of MESH elements in one slice. As the points are later deposited for calculations in the RAM memory of the computer, the maximum number of points used is dependent on the machine, but can be estimated at about 500,000.

When the user activates the module with the "**PTRAC**" button on the GUI, a file dialog will open in a new window, which asks for the original input file. MCNPAct will then read every single line in the input and write these in a new file, so that the original input remains unchanged. When the code finds in a line the keyword "**c source**", the new source routine that respects a cuboid region inside the geometry will be introduced as shown in the example below:

```
c source
sdef   x=d1 y=d2 z=d3
si1 0 1500
sp1 0 1
si2 -300 -150
sp2 0 1
si3 -750 750
sp3 0 1
void
```

After the source description, a **VOID** card is automatically inserted. It replaces automatically all materials with a void, what reduces significantly the amount of time needed for the computations, as only source events are counted and scattering events will not occur anymore. The particle track immediately ends, when it enters the region with zero importance around the geometry.

MCNPAct will then again transfer line by line of the original file to the new input file until the file ends. Then the code inserts a PTRAC card, which is equal in dimensions to the source description so that a random distribution of the sampling points inside the analyzed region is guaranteed. Finally an NPS card is introduced, that ends the run after reaching the desired number of source points.

```
PTRAC EVENT=src WRITE=pos TYPE=n MAX=-20000
     FILE=asc FILTER=0,1500,x -300,-150,y -750,750,z
NPS 20000
```

MCNP is then run with the new input file. After finishing, the new ptrac-file will be renamed according to its position in the coordinate system of the model. The generated input file, the MCNP output file and run file will be deleted, as they are not needed anymore. If the analysis is supposed to be 3D rather than 2D, all this steps from MCNP input generation to MCNP run will be repeated for every slice along the axis perpendicular to the mapping axis. The PTRAC files, called "**pt_#**", are then ready for further work and generation of them is necessary before starting the next module.

4.4.3. MESH Calc

This module transforms the PTRAC information together with data from MCNP input and output to a number of files, which includes the material composition, masses and volumes of each element.

At first the user has again to ensure, that the dimensions, number of steps and the mapping plane for the matrix have been chosen right inside the GUI. Here the user also has to provide the volume of each matrix element. This can be computed automatically from the data given at the axis descriptions by pressing the button "**Vol Calc**".

After starting the module, the user is asked in a file dialogue to give the name of the first PTRAC file and also the name of a suitable MCNP output file. From the output file MCNPAct reads the gram densities of the cells described in the input file as these will be calculated in a typical MCNP run. So it is useful to have a MCNP run done with the original input file. It must not include a void card and must not be an output from a continue run as these outputs don't include the desired material data.

After that MCNPAct will ask for the original input file. Here some rules for the format have to be considered. At first it is important, that the materials descriptions begin with "**m1**", if there is no material one, the user is supposed to make one, even if it is not used, as the program interprets the code word "**m1**" as the beginning of the materials section of the MCNP input file. Then it is important, that only one isotope description is in one line, i.e. there is at first the ZAID and then the relative abundance of the isotope and then a line-break at the end. At the end of the materials section the user is supposed to introduce a commentary line reading "**c endmat**", so that MCNPAct will finalize the material reading process.

When the user starts the module by clicking on the "**MESH Calc**" button, the code opens the ptrac file generated at the previous step at first and reads it line for line. Usually a PTRAC file made of source events consists of some header lines followed by the single points with each described in three subsequent lines as shown in the example below:

```
3     1000
9000        1        40        1    11094        0
0.10675E+04 -0.29729E+03 -0.18737E+03
```

This example shows particle number 3 as seen in line one. Second line gives the information, that the log describes a source type event (9000) and that it generates the particle trajectory in cell 11094 with the specific Cartesian coordinates in line number three. Sometimes MCNP causes trouble, when a particle is lost or is generated in a region with a geometric error. Then there are additional lines in the ptrac description.

As MCNPAct is supposed to be insensitive to minor geometric errors, the ptrac-file will be analyzed at first line by line as a means of a cleaning process and non-sense parts of the list, for example lost particles data, are removed.

After this step the file is analyzed again from the beginning for a necessary preprocessing of the data. An internal four-dimensional array is generated, which is sorted by the sequence of the MESH elements. Inside this specific array the sampling points with their associated cell numbers are written down, so that finally there is a sampling point list for each single element of the MESH.

Then every single element is analyzed with help of the sampling point list. A new list is generated in the memory that contains the numbers of the geometrical cells that are sampled inside the element and the number of points that occurs for this cell is counted. With the number of sampled points the volume of this cell can be determined statistically with help of the Monte Carlo method.

To compute the mass of the cells inside a specific element, the MCNP-output is opened and the density is read out of the cell description and with its help the mass is calculated and added to the internal element-cell list. This information is written into an external file, called MESH-File that is in ASCII format and can be opened by the user for control purposes. The first lines show the cell composition of an element as shown in the example below.

```
CellNo  Counts   PercentVol  Volume MatNo Density Mass
8876 5 0.247770069375619 35678.8899900892 4 7.84528 279.910882061447
8979 1990 98.6124876114965 14200198.2160555 0 0 0
```

The first line shows for cell number 8876, that there have been counted 5 sampling points, what correlates with 0.25% of the overall volume and corresponds with 35679 cm³. The material number of this cell in the MCNP input is 4 and the density of it counts 7.84 g/cm³. The mass of this cell inside the element is then 280 kg.

By this way it is a useful side application of MCNPAct to analyze the whole geometric input or a specific part of it when limiting the number of steps to one in each dimension. Masses and volumes of the single cells are calculated what is not done by MCNP itself, but in certain situations MCNP or the user needs the volumes and/or masses for computations with the tally, what can sometimes lead to time consuming efforts, when several cells with a complex geometry have to be computed manually to assess the volumes of these.

To determine the material composition, the MCNP input is analyzed and the material compositions of the cells inside the element are compiled and written into an internal array. If the isotopic abundance of a material is given in atomic fraction, this number is computed to the weight fraction by multiplying with their atomic mass. With the overall mass of the element

computed earlier, the absolute weight of the isotopes inside the element is determined and given out as a list in the MESH-File, which can again be read by the user.

```
5010 0.000515371158702212
5011 0.00228183966130789
6012 0.0279725225236621
```

The example above shows for the MESH element a material composition of boron and carbon with their respective isotopic masses given in kilograms. The sum of these numbers matches the overall mass of the element, what is important as the FISPACT input file later needs them in that special format.

This computation is repeated for every single element of the FMESH array and for each element a specific MESH file is stored on the hard disk, that can be viewed by the user and that will be opened and used again by other modules of the code. If a MESH element contains no materials at all, MCNPAct detects this and writes only “void” into the output file since this of course needs no further computation.

4.4.4. Matrix I/C

This module is optional and is intended for plotting material maps over the original geometry. The module opens the MESH files generated in the module MESHCalc one after another and reads the material mass of the one specified by the user on the GUI. A new matrix is created as external file and the material mass of one element is inserted at the corresponding position in the matrix.

If the MESH files are made for 3D analysis the user has to provide the slice number of the picture plane, as the material matrix is only intended to display 2D maps, that can again easily be opened by suitable visualization tools. By switching on or off a button at the GUI the results are given in its absolute value or in a logarithmical scale as some visualization programs will not switch the scale by themselves.

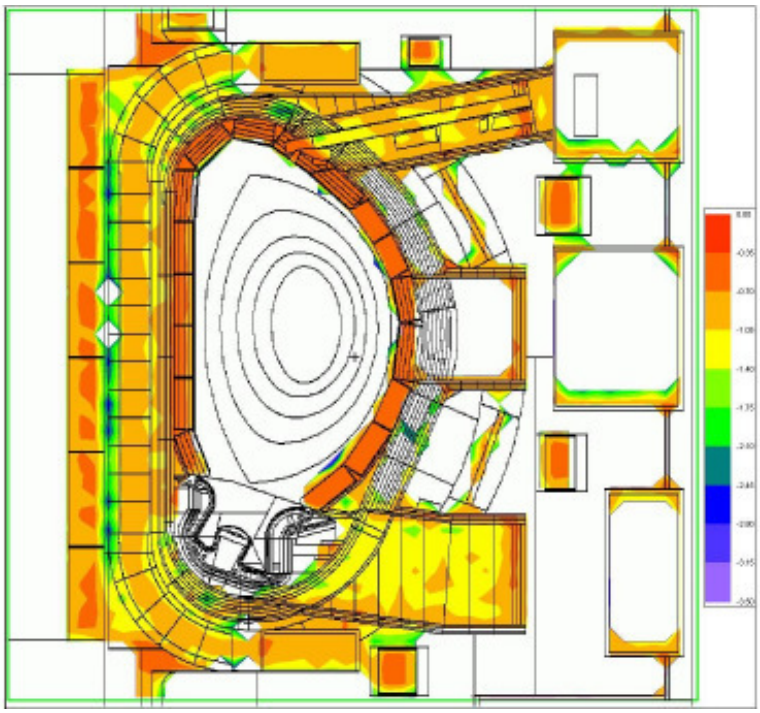

Figure 38: Abundance of iron in the MCNP input of ITER mapped over the geometry plot

4.4.5. FISPACT INPUT

This module is responsible for generating FISPACT input files from the generated MESH files, a basic FISPACT input, a material converter file and the FMESH output from MCNP. Before starting, the user has to be sure, that data given on the GUI are correct, namely the dimension and step numbers, plane and volume.

Furthermore the paths for the FISPACT executable file and the working directory of the MCNPAct process have to be provided. When activating the button, the user is at first asked for a translation file ("PEI") that is an external file of MCNPAct. As FISPACT and MCNP use different identifiers for the materials, this file provides the translations for all of them. They are opened by the code and saved in an internal array.

MCNPAct asks then for a basic FISPACT input file in which the mass, material composition and neutron flux is inserted automatically. The user can use every FISPACT input, but has to remove the masses and material composition. At that specific positions the user is supposed to make a commentary line:

"*** MCNPAct**".

This will lead to the action, that the code will remove the commentary line with the actual materials of the MESH element as determined.

Furthermore the user has to include additional commentary lines reading

"*** MCNPFlux**".

That comment will be replaced by the code with the actual neutron flux for the specific element. The user also has the ability to include more than one of this keywords if more than one irradiation step is used in a longer timescale.

Sometimes for fusion calculations in FISPACT several irradiation pulses are combined in one longer time period by using the average neutron flux over that time period, so the user has the ability to change the neutron flux by a factor he can include in a field in the GUI.

Next the code asks for the first MESH element file and finally for the corresponding MCNP FMESH output file. In the FMESH output it is important, that there is only one FMESH Tally. If in the users output more then one tally is present, it is necessary to copy the desired one into a new text file and use this one for processing with MCNPAct.

MCNPAct reads then for every element of the geometry the FISPACT input file line by line and includes at the correct position the overall mass of the element and its material composition, which has been translated into the FISPACT format with the help of the PEI translation file. Next the corresponding position of the FMESH output is read and the neutron flux is included at the defined positions in the FISPACT input file.

4.4.6. FISPACT START

This module will start a FISPACT run for every single generated input file. The user has to ensure, that the number of steps in each dimension has been set correctly and that the path names are given in the GUI. Furthermore the user has to define the slice number in a 3D computation for that the mapping should take place together with the plane for the mapping.

After pushing the button, MCNPAct will begin copying the first input file from the working directory to the FISPACT directory and activation calculation will start.

When the spectrum button in the GUI has been activated by the user, the code knows, that the associated FMESH file contains also spectrum data. These spectrum data can have a user defined group structure. MCNPAct starts then before each activation calculation a separate FISPACT run, in which only the spectrum data is analyzed and compiled to a 172 standard group structure, with which the activation calculation is started. If no spectrum data is given in the FMESH file, the standard spectrum file in the FISPACT working directory is used. This can be the case, if only small structures are computed and a common spectrum file has been generated manually by the user and provided in the working directory.

After MCNPAct detects the run to be finished, the FISPACT output will renamed to identify it according to its position in the matrix and it will be copied back to the working directory. The old input file is deleted then and the procedure will be repeated for each element of the matrix. When a matrix element is detected to have no materials inside, no FISPACT run will take place to save computation time.

When larger element sizes have to be calculated, this step can take a longer amount of computation time. In further versions of the MCNPAct computer code it would make sense to implement a parallel computation of this step with multiple FISPACT calculations at the same time.

4.4.7. FISPACT OUTPUT

This module will collect the desired data from all of the FISPACT output files and assembles them to data maps that reflect the whole geometry. The user again has to ensure, that the number of steps in each dimension has been set correctly. After activation of the module by clicking on the respective button in the MCNPAct GUI, the code will ask for the position of the first FISPACT output file.

The code will open them and searches the text files line by line for keywords that announce the desired data. So when detects the keyword “TOTAL ACTIVITY” it writes the following number value into the respective position in a internal array. One matrix is generated for the values of total activity, heat production and total dose each and one set of these matrices is generated for each time step defined in the FISPACT input file.

At the end of the module, all of these matrix arrays are written in external text files that can be imported into the visualization program. As this module only generates data for two dimensional matrices, the user has to define the position of the slice in a three dimensional volume.

4.4.8. Inventory Calc

This module is optional for detailed analysis. It works similar to the last module and opens the FISPACT output files but will search inside them for the activities and masses of the different activation products. It will give out maps for activity and mass of each single daughter isotope and each single time step.

The user has to be aware that this will generate a huge amount of data, usually hundreds or thousands of files and that it will take some time to compile them, especially if the number of geometric segmentations is high. Also this module only generates data for two dimensional matrices, so the user has to define the position of the slice in a three dimensional volume.

4.4.9. MCNP Gamma Source

MCNP can be used for determining dose rates, when introducing the appropriate tally cards. But for activation gammas, at first the source has to be defined. [HEUEL-FABIANEK 05]

This module will again read the FISPACT output files and collects the gamma emission for each element resolved in a 24 group spectrum. Two methods have been implemented and tested for this purpose.

Internal Source routine

The internal source routine method had the goal to introduce a simple text source into the standard MCNP input file for a easy computation.

The user has to give the time step, when several of these are defined in the FISPACT calculation. The data are gathered in an internal array and are then given out in an external text file as MCNP gamma source. This file can be opened by the user with a text editor and copied directly to a MCNP input file for the calculation of the gamma transport due to activation. The source is then a composite of blocks with different intensities and energy distributions that resemble the geometrical segmentation.

As the source is independent on MCNP cells with the source simply super positioned to the geometry, the model itself will not change. The user can then insert regular tallies into the MCNP input or use FMESH tallies to take again use of its mapping functions. Furthermore this module generates a second external file that resembles a 2D map of the gamma activity itself according to the slice chosen in the GUI that can be visualized as shown in the twodimensional representation of the source displayed in Figure 39.

The method works and has been tested with the ITER input for the CXRS Port Plug. A visualization of a FMESH-Tally for the computed gamma flux can be seen in Figure 40.

The problem is, that the size of the MCNP input file for the gamma source is growing exponentially with increasing number of MESH-Elements. Due to this problem the number of elements is limited in a way that higher grades of discretization as necessary with the ITER geometry are not possible. Another way had to be found for calculating the shutdown dose rate and the internal sorce routine method has been abandoned completely.

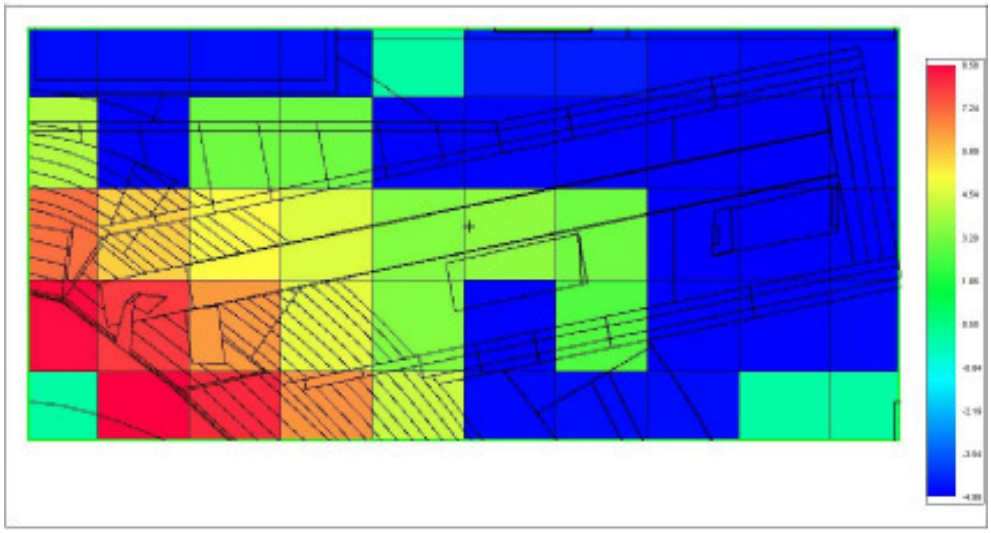

Figure 39: 2D Map of a simple gamma source with 10x5x5 elements plotted over geometry.

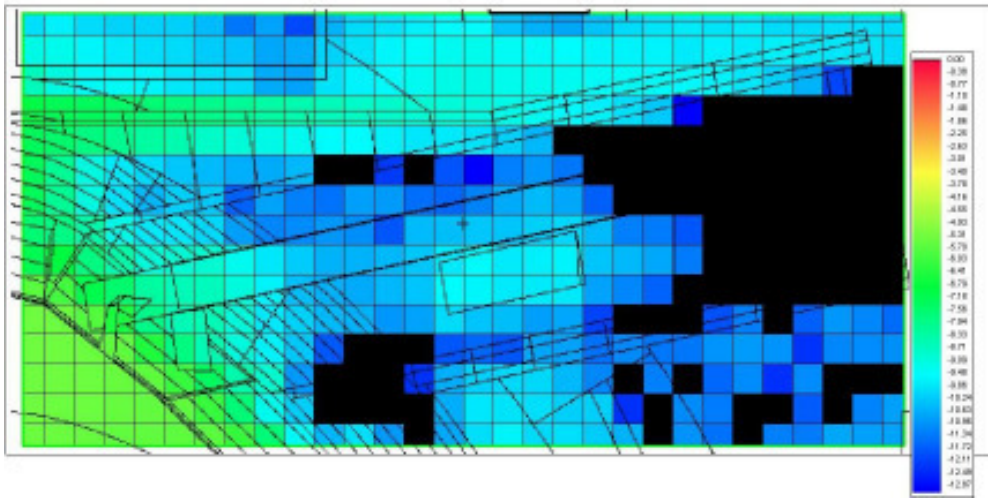

Figure 40: Map of MCNP gamma transport calculation test results with automatically generated source

External Source routine

MCNP gives the possibility to provide an external source that can be programmed in FORTRAN and is then integrated into MCNP after compilation. This external source is activated, if no source description is given in the MCNP input. The FORTRAN code of the external source can be found in the appendix.

As preparation for the source generation, all FISPACT outputs are read by MCNPAct and the necessary values are written in two text files that will then be opened by the MCNP FORTRAN source routine.

The source routine reads at first a file called ‘gsrc’, which has been prepared by MCNPAct. In this text file, the first nine lines serve as header files, providing the new source routine in MCNP with information about the number and dimension of mesh elements. After that, each

value given in the file is corresponding to a specific element and gives data about the relative gamma population of this element. The number of gammas created in the system per second is provided by MCNPAct and must be entered into the MCNP input file by the user.

Another external text file called ‘spectr’ contains the relative gamma spectrum of each of the single elements. FISPACT provides a 24 group spectrum that is taken over by the MCNP external source routine.

After all data are stored inside internal arrays, a random number generator chooses one of the elements to be starting point of the first gamma. All elements are weighed in a way, which the overall number of gammas created in an element is proportional to its gamma activity, determined by FISPACT. Inside this cell, an arbitrarily coordinate is chosen by another run with the random number generator and the cell number associated with this coordinate is determined by an internal query, as MCNP needs it as an input.

The source routine reads a list of cells from an external file that has to be provided by the user and is called ‘ixcel’. If the coordinate position cannot be associated to a cell name, the random generator chooses a new coordinate. By this way it can be realized that gammas are only starting inside material cells, if cells with no materials are omitted in the cell list file.

As a last step, the relative spectrum inside the specific element is loaded from the ‘spectr’ file and the actual gamma energy is chosen with the help a random number generator again in a way, that the overall number of gammas started in that specific element is representing the associated spectrum with the help of weighting factors.

The process is now repeated until the defined number of source particles has been started. The general tally results are normalized by 1 starting particle. The user has to multiply the tally values with the overall number of gammas created by the gamma activity. This value is provided by MCNPAct when compiling the gamma source files.

5. Results of the simulations

5.1. Neutron Flux, spectrum and heating

The computer runs have been performed with the JUMP and JUROPA supercomputers at the Research Center Jülich.

JUMP (JUelich Multi Processor) is an IBM p690-Cluster and was first run at Feb 10th, 2004. The system consists of 1312 processors in 41 node servers with 5.2 Terabytes Memory and a theoretical computation capacity of 8.9 Teraflops/s.

The second supercomputer JUROPA is based on a cluster configuration of NovaScale servers, and on blade servers with Intel Nehalem processors. The system was designed by experts from the Jülich Supercomputing Centre and implemented together with the partner companies Bull, Sun, Intel, Mellanox and ParTec. It consists of 2208 computing nodes with a total computing capacity of 207 teraflop/s.

The neutron flux in a zone of the system is defined as the number of neutrons crossing the unit surface in a second and is calculated in MCNP by using the tally for cell flux. The time integrated flux is

$$\int_v \int_E \int_s N(\vec{r},E,t)dsdE\frac{dV}{V}$$

Because $N(\vec{r},E,t)ds$ is a track length density, MCNP estimates this integral by summing WT_l/V for all particle tracks in the cell, time range, and energy range. Because of the track length term T_l in the numerator, this tally is known as a track length estimate of the flux. It is generally quite reliable because there are frequently many tracks in a cell (compared to the number of collisions), leading to many contributions to this tally.

The final computer run for the neutron and gamma flux computations, that have been also used for the activation calculations with MCNPAct and FISPACT, have been accomplished in several steps to a number of 560 million source neutron histories. After each step results were checked for errors and given back to MCNP by using the restart tool of the code.

The results in the output file are given in particles counted P in the respective parts of a tally normalized to one particle. So the result had to be divided by the volume V of the tally, which has been determind using the MCNPAct code described above.

Furthermore the resulting values have to be multiplied with the overall neutron generation rate of the reactor (n=1E+19 n/s) to give the neutron flux Φ in the specific component of the reactor.

$$\Phi = \frac{P}{V} n$$

For this task a long term simulation run was performed and mesh tallies with a high level of details for whole ITER as well as for the selected parts were generated. These results were used for the activity calculations with FISPACT using the interface tools. The values for the activity, inventory activation products and masses for selected locations and structures are compared with the results of other groups, especially for the upper port plug structures.

5.1.1. Verification of model and methods

To verify the methods and the MCNP model used, an older version of the CXRS Port Plug has been modelled. This outdated geometry without retractable tube and only five mirrors has been computed in the past by another group and neutron flux and nuclear heating data are available for the mirrors [SHATALOV 02].

The geometry of the 2002 version of the PP has been generated with the dynamic geometry generating method and was then manually included into the ITER Feat MCNP model. A MCNP geometry plot can be seen in Figure 41. The system consists of five mirrors, all positioned on the centre of the Port Plug x-axis with no deviation to the side, unlike the actual Port Plug.

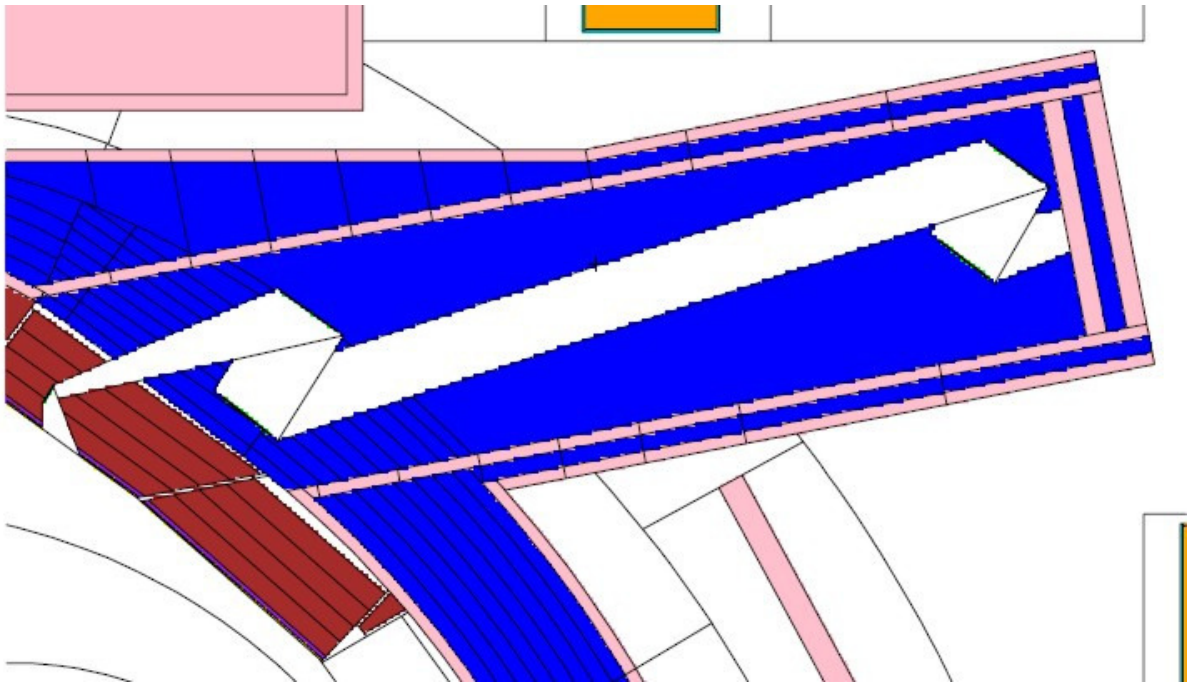

Figure 41: Plot of the newly modeled input based on the geometry used by [SHATALOV 02]

Regular type 4 and type 6 tallies have been made at the positions of the mirrors to get the neutron flux and nuclear heating values. The model has been run with the JUMP supercomputer with 16 processors and an accumulated processor time of 700 minutes, what was enough for 870,000 neutron histories.

The results are given in Table 13. Value of the neutron flux at the first mirror is 7.2E+13 n/cm²s in the new model and 5.62E+13 n/cm²s in the reference. The difference is in the order of 30% what is also true for mirrors #3 and #4. The Value for mirror #2 is differing by almost 100% and for mirror five by 300%. This can be explained due to the high statistical error or minor variations in the position and alignment of the mirrors.

Furthermore it has been pointed out, that there are flaws in the old model geometry. Presumably ba a computation error the angles of the mirrors have been chosen wrongly, so that the correct alignment is not provided in that model. As the dynamic model generator used can only design mirrors with a correct alignment for the optical system, the models are differing from each other, what is presumably a source of the differences in the results.

CTME=700 / 43x16 NPS=870000

Position	Shatalov et al.	error	Bourauel	error	f
m1	5.62E+13	0.02	7.20E+13	0.08	1.28
m2	1.68E+11	0.06	2.50E+11	0.17	1.49
m3	1.75E+11	0.02	1.30E+11	0.06	0.74
m4	4.13E+08	0.3	3.70E+08	0.3	0.90
m5	5.43E+07	0.27	1.60E+08	0.7	2.95
W	1.41E+07	0.1	N/A	N/A	

Table 13: Results of the neutron flux verification model compared with [SHATALOV 02]

Compliance is better when statistical errors are lower. When looking at Figure 42 where the values are plotted in logarithmical scale, it can be seen that the values are in good compliance, when noting that the differences in the overall model are varying by six orders of magnitude in an environment, where small changes in the position and angle of the mirrors can be responsible for big differences in the result.

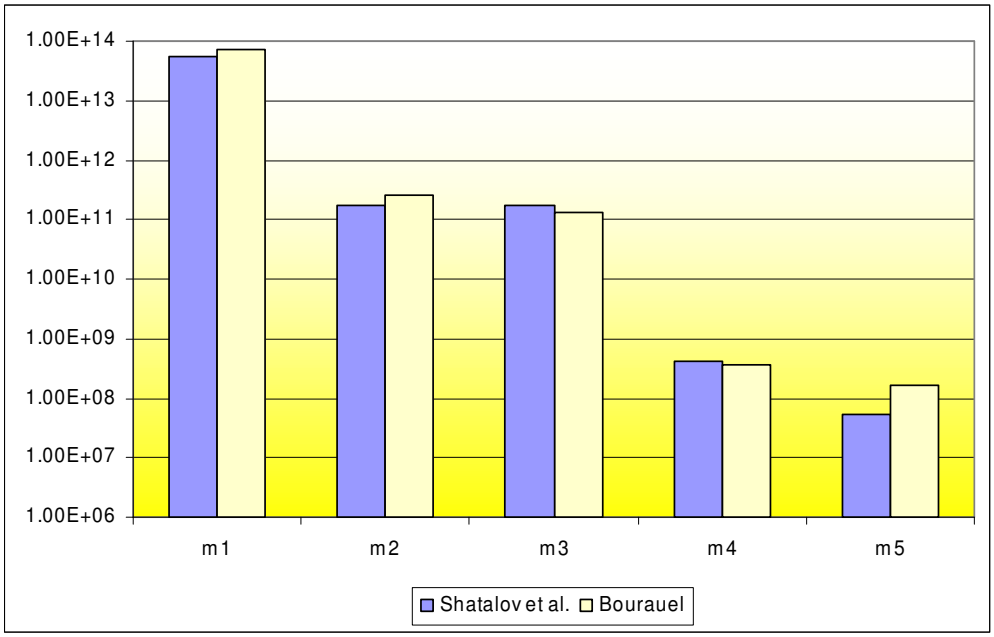

Figure 42: Results of the neutron flux verification model compared with [SHATALOV 02]

5.1.2. Neutron Flux, gamma flux and spectrum in ITER

Due to the complexity of the geometrical model of the reactor and the large number of particle histories, the computing time was reduced significantly by the application of the parallel version of MCNP5 [BRIESMEISTER 03]. In total 560 Mio source particles were simulated resulting in a relative error (neutron flux) of less than 1 % around the front opening and less than 15% at the back windows of the structure.

Tallies were introduced at the position of the mirrors for neutron flux and energy deposition. Additionally several rows of raw and fine mesh tallies (FMESH) were introduced to sample the areas around the mirrors, the Port Plug as a whole and the complete ITER section for neutron flux, gamma heating, neutron heating and radiation damage.

An overview of the neutron flux field in the complete ITER reactor is shown in Figure 43. Black spaces indicate regions where no results were obtained due to shielding effects and low weighting factors that have been introduced to raise effectivity of the computation in the areas of interest. Some of the FMESH tallies were later used with MCNPAct to compute the activation with FISPACT according to the developed method.

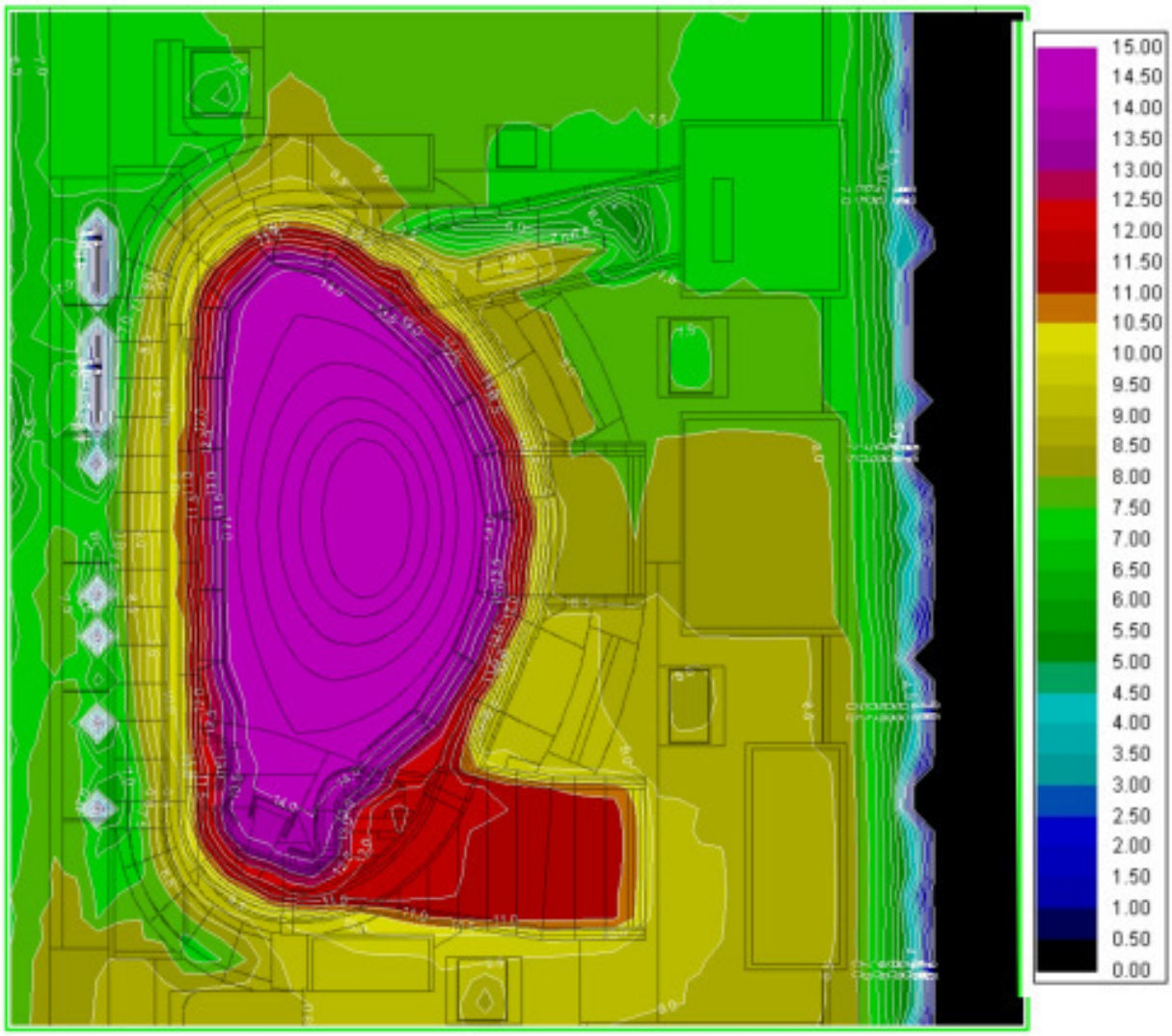

Figure 43: Neutron Flux in ITER computed with ITER Feat model [log(n/cm²s)].

Neutron flux is highest in the centre of the plasma chamber as expected with about 1E+14 n/cm²s. When entering the Blanket Shield Modules, neutron flux is decreasing fast within the material to lower than 1E+13 n/cm²s when entering the shielding. A high flux with more than 1E+13 n/cm²s is also expected in the whole of the divertor region. At the outer limit of the shielding, values in the order of magnitude around 1E+9 n/cm²s are expected.

The radiation background inside the voids behind the shielding is strongly dependent on the position. So the radiation in the lower parts of ITER, namely around the divertor region, is higher by around two orders of magnitude. The reason is the significant lower amount of shielding at the divertor port. Due to this reason the neutron flux in the different port cells is also varying strongly.

In the divertor port cell the neutron flux is around 2E+8 n/cm²s, in the equatorial port cell it is around 1E+8 n/cm²s and in the upper port cell the neutron flux is lowest with lower than 2E+7 n/cm²s.

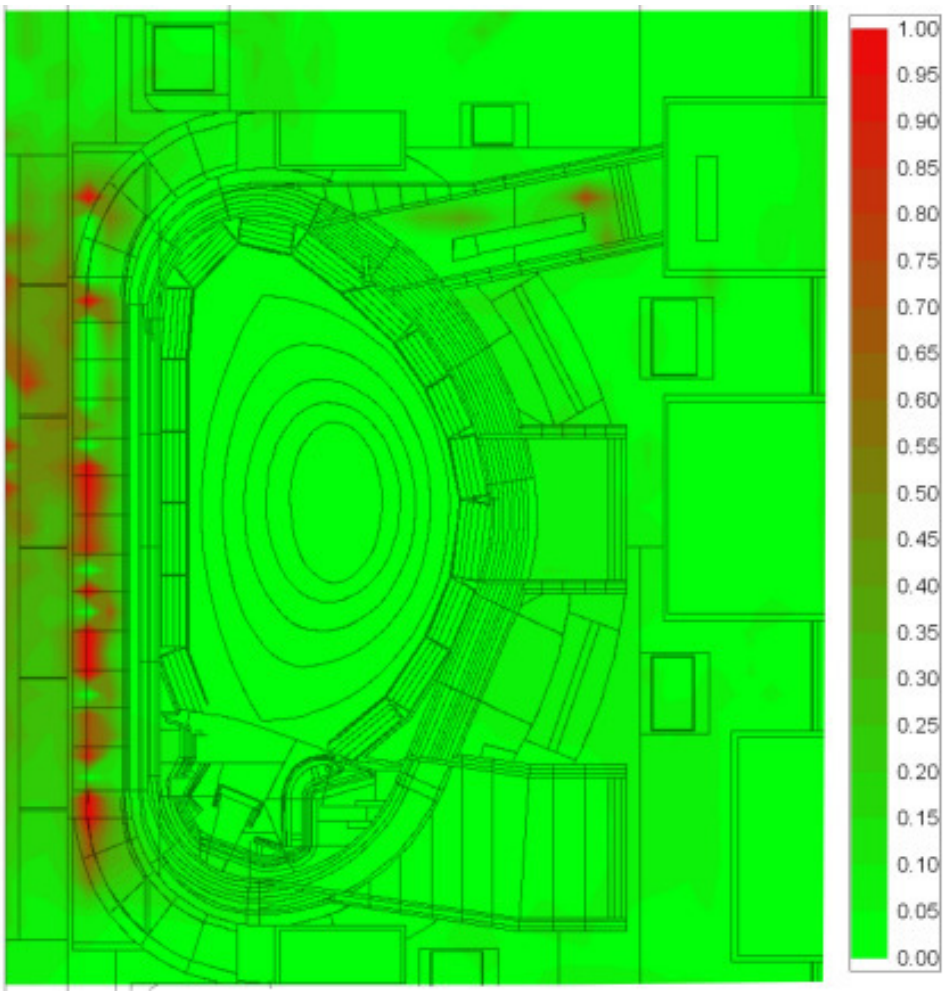

Figure 44: Statistical error in ITER neutron flux calculation

Figure 44 shows the statistical error inside the ITER. It can be seen, that the error at the most parts of the geometry is below 0.05 or at least 0.1 what means that the values are mostly reliable. There are only some minor parts where the error is to high for reliable values. These regions are located inside the innermost shielding and coils of ITER.

This is due to a low neutron flux because of the massive shielding of that region and also because of low importance factors to reduce the amount of computation time as this region is not of interest for the actual problems of this work.

But there is also a limited region inside the CXRS Port Plug with a statistical error higher than 0.5. This is mainly due to the high amount of shielding at the back part of the Port Plug, where the neutron flux drops below 1E+6 n/cm²s what is below the background radiation outside the Plug.

This fact leads to the conclusion that some part of the shielding inside the CXRS Port Plug could be saved as it has no effects on the radiation level in the port cell. This should be analyzed by further work and also it could be helpful to further increase the importance as a method of variance reduction at the back region of the Port Plug.

An overview of the gamma flux field in the complete ITER reactor is shown in Figure 45. The chart is very similar to that of the neutron flux in ITER. Highest gamma flux of course in the plasma region, divertor and the blanket modules next to the first wall. Outside the shielding blocks, the gamma flux is between 1E+6 and 1E+9 1/cm²s. Especially in the regions around the divertor port values are high because of the lower amount of shielding there.

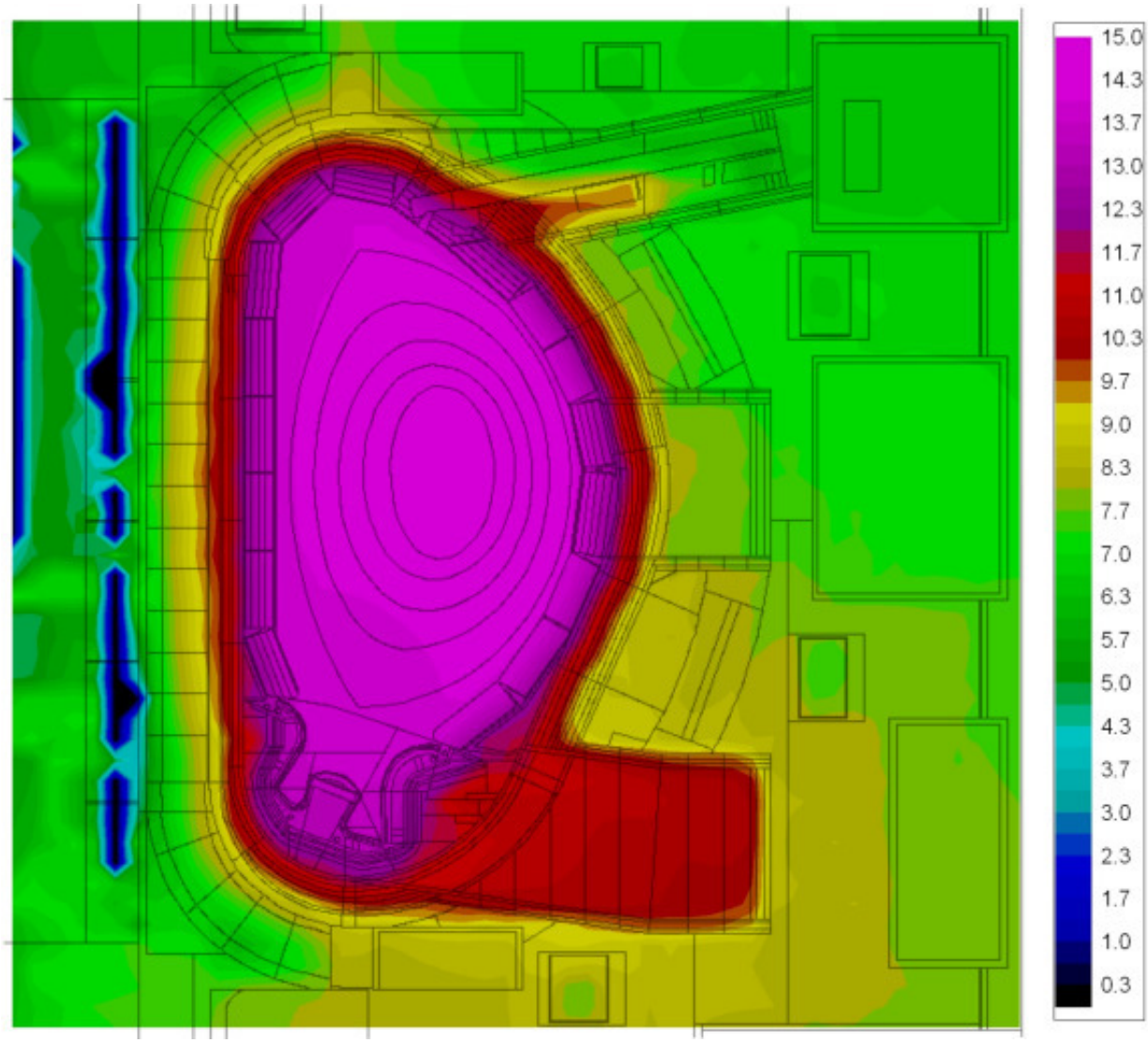

Figure 45: Gamma Flux in ITER computed with ITER Feat model [log(1/cm²s)].

FMESH tallies have also been used to compute line distributions of neutron flux at several parts of the geometry.

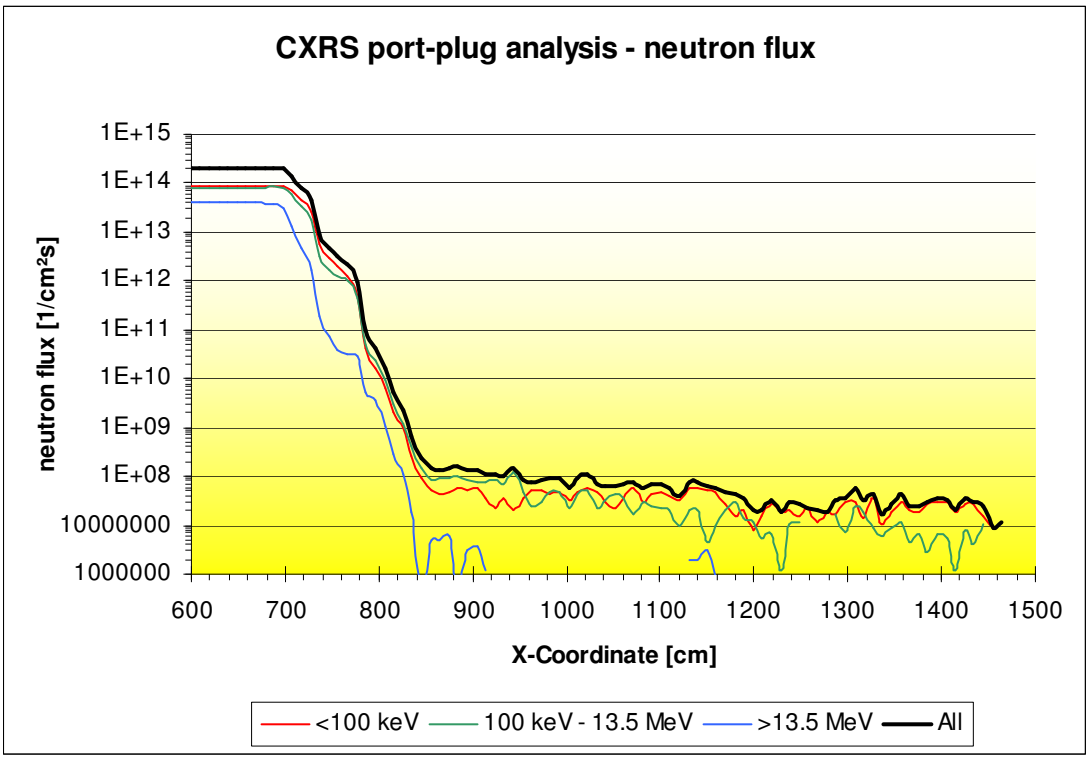

Figure 46: Line profile through the neutron flux distribution

Figure 46 shows a line profile of the neutron flux in the shielding of ITER at different energies. The line is positioned slightly below the Upper Port Plug level. The overall neutron flux drops from about 2E+14 n/cm²s at the 1st wall of the BSM to about 2E+8 n/cm²s at the back side of the shielding module after about 150 cm.

High energy neutrons are dropping faster what leads to the conclusion that the energy of the neutron is given to material very fast within the first atomic collisions. After the shielding, the neutron flux is decreasing more slowly because there is no more material but only the drop due to the increasing distance from the neutron source.

The shape of the curve is rougher behind the shielding because of variances in the values due to higher statistical errors.

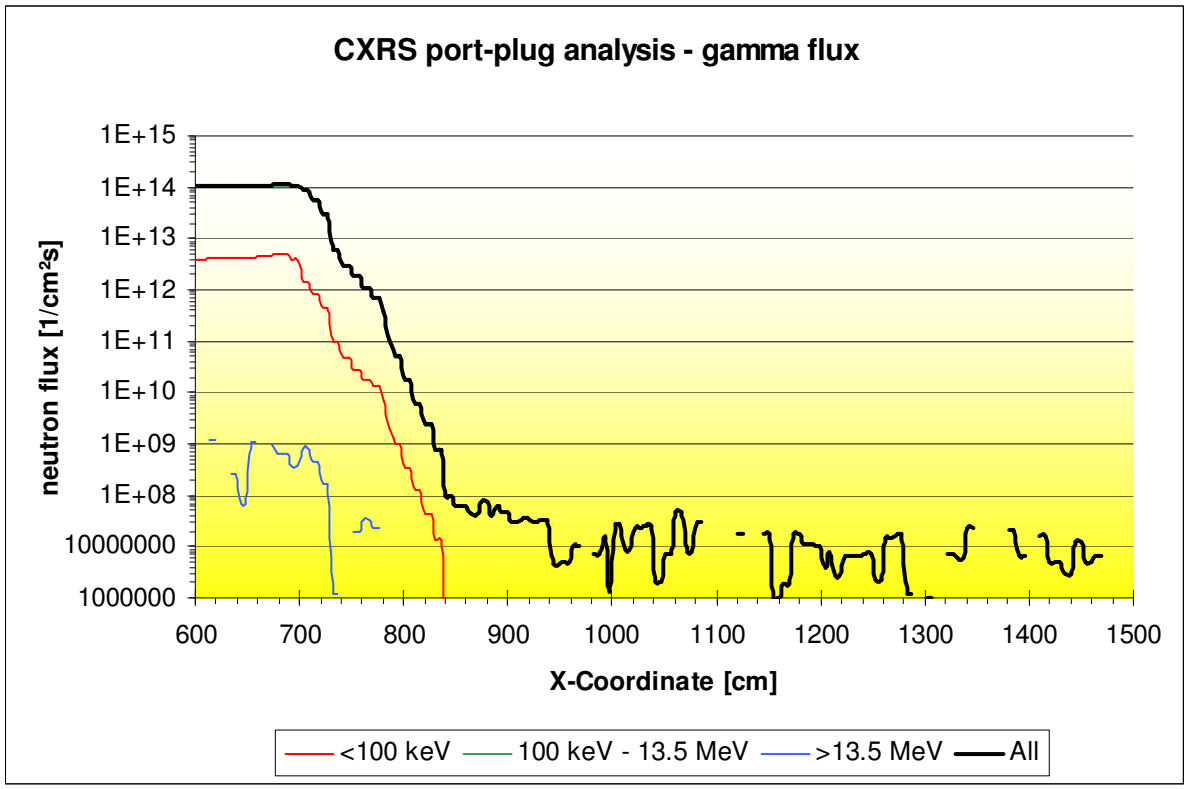

Figure 47: Line profile through the gamma flux distribution

Figure 47 shows a line profile of the gamma flux in the shielding of ITER at different energies. The line is again positioned slightly below the Upper Port Plug level. The shape of the curve is equivalent to that of the neutron flux. The overall gamma flux drops from about 1E+14 γ/cm²s at the 1st wall of the BSM to about 1E+8 γ/cm²s at the back side of the shielding module after about 150 cm.

As the gamma flux is proportional to the neutron flux within same materials and if the neutron spectrum is the same, the attenuation within the shielding is the same for gamma and neutron flux. Behind the shielding, the curve is again getting very rough because of higher statistical errors.

5.1.3. Neutron Flux, Gamma Flux and spectrum inside CXRS PP

Other FMESH tallies have been introduced into the model to get the neutron flux distribution within the CXRS Port Plug. This distribution is given in Figure 48. White spaces mark regions where no values could be obtained due to high statistical errors. It can be seen, that the region inside the Port Plug, where bad statistics is located is bigger than that in Figure 43. This due to the reason, that the volume of the FMESH elements is now significantly lower and more matrix elements are getting no results.

No neutrons have been sampled in regions with a neutron flux lower than 2E+5 n/cm²s. To deal with that problem a conservative approach has been chosen and values have been set to 2E+5 n/cm²s in further computations.

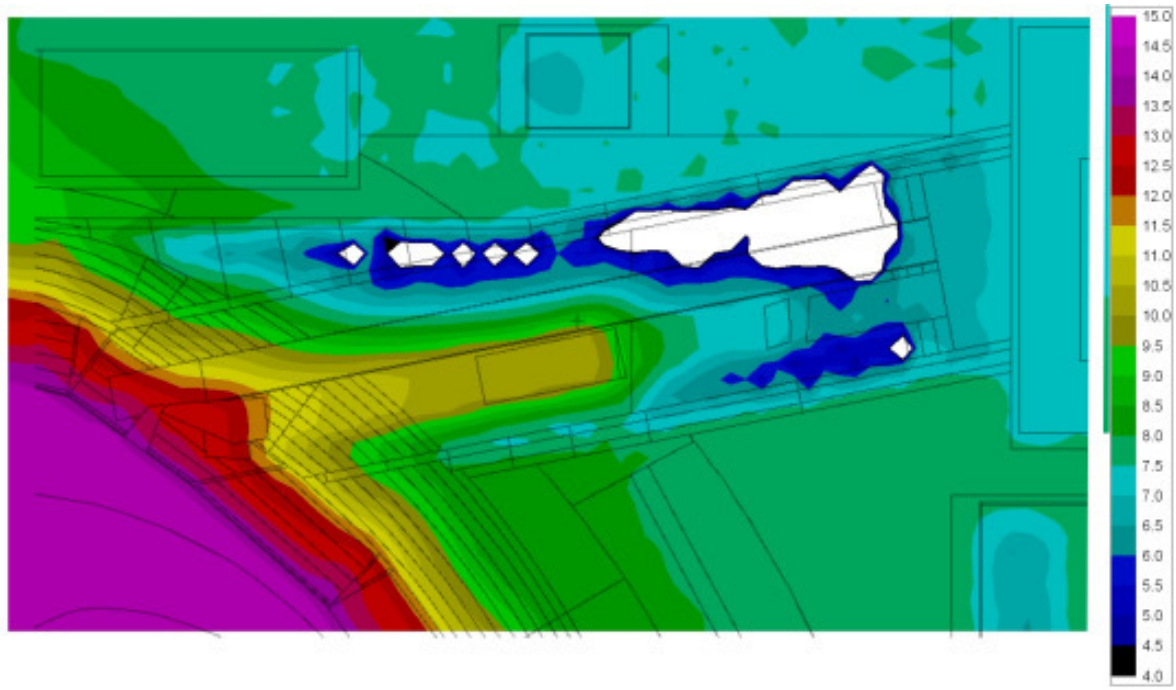

Figure 48: Neutron Flux in ITER CXRS PP [log(n/cm²s)].

In contrast to the low flux at the back part of the CXRS Port Plug the neutron flux in the port cell is again be seen to be lower than 2E+7 n/cm²s. The consequence again would be the insight, which a certain mount of shielding can be saved, as it has no influence on the neutron flux in the port cell due to background radiation.

Other values are as expected. The neutron flux at the first wall is again in the order of magnitude of about 1E+14 n/cm²s. Inside the Port Plug there is a long barrelling in the isofluency lines. Of course there are big spaces of undisturbed neutron flux due to the voids in the mirror labyrinth.

Some additional FMESH tallies have been included into the interior of the CXRS Port Plug to show the behaviour of the neutron flux at some critical positions. For example, Figure 49 shows the neutron Flux at the area where mirror #5 and mirror #6 are located. The picture shows the XY-Plane and the way of the light is clearly seen.

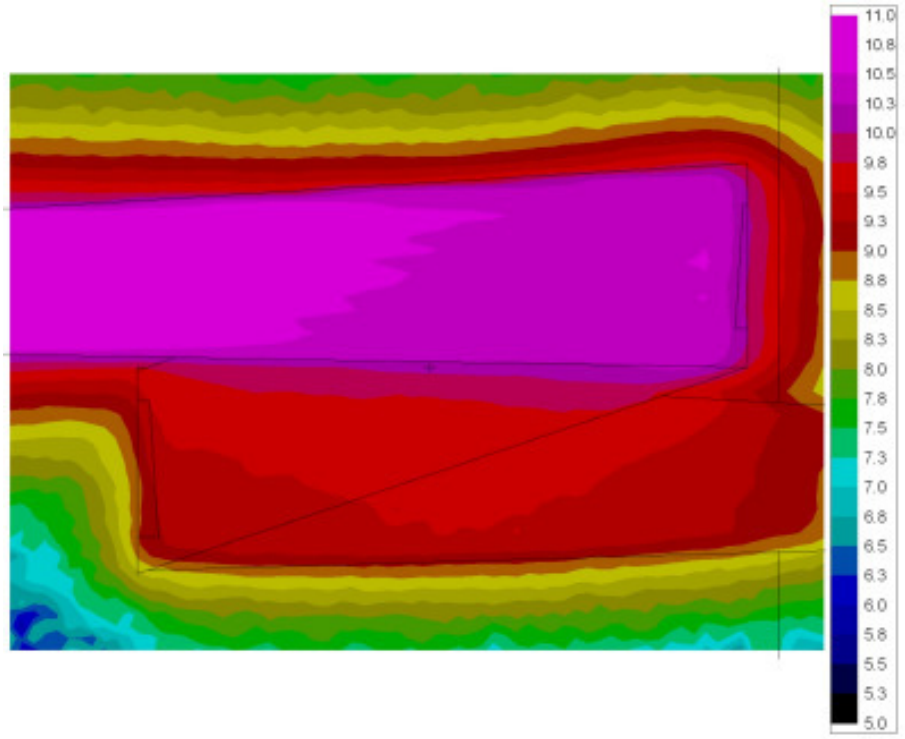

Figure 49: Neutron Flux in ITER CXRS PP at position of mirror 4 and 5 [log(n/cm²s)].

The space between mirror #4 and #5 is in the upper edge of the picture, what corresponds to the +Y direction and neutron flux is significantly higher with about 1E+10 n/cm²s than in the area below, that shows the space between mirror #6 and #7 with a neutron flux of about 1E+9 n/cm²s to 1E+10 n/cm²s. The drop in the neutron flux is relatively sharp, where no line of sight to mirror #5 is present. Also it can be seen in the figure, that the neutron flux is dropping also very fast inside the material of the Port Plug shielding.

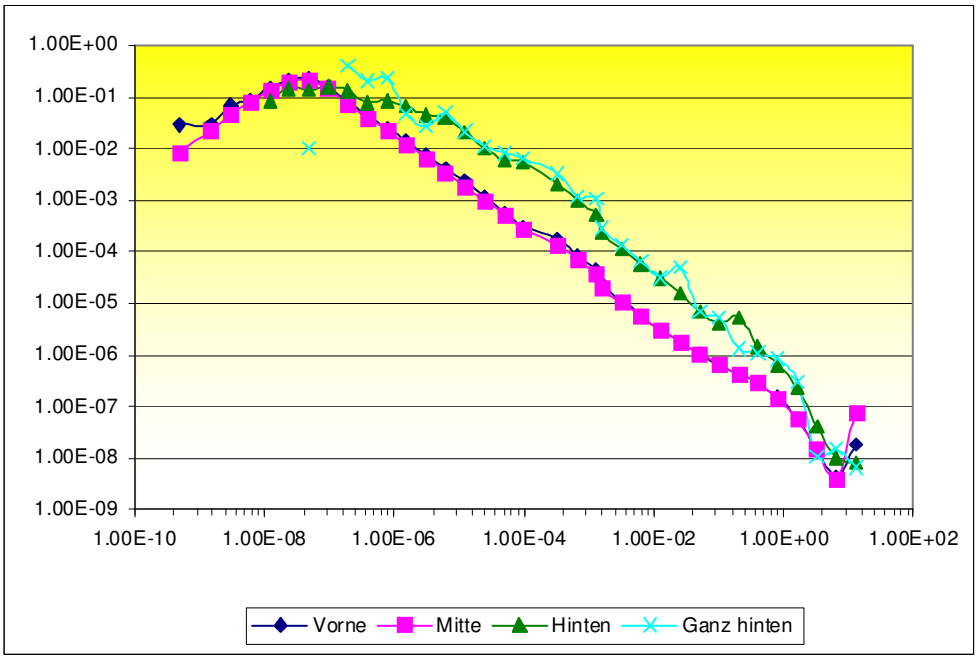

Figure 50: Relative Neutron Flux Spectrum [MeV] at different locations in ITER CXRS PP

In a separate simulation run a more detailed analysis of the spectrum has been made as shown in Figure 50. The picture shows the relative neutron spectrum at four positions of the Port Plug. It is interesting to see the maximum all curves in the thermal region of the spectrum. Higher relative energies were expected at the front of the Plug and lower energies in the back, when the 14.1 MeV fusion neutrons lose their energy. But only a minor 14.1 MeV peak can be seen in the curve for the front, which vanishes, when progressing outward with the other curves.

It seems that a high amount of the neutrons is reflected back very often to show also a maximum peak at thermal energies even inside the plasma region. The fact, that the relative neutron spectrum is very similar at all analyzed points is of some particular importance. As the neutron spectrum is important for further nuclear reactions, especially for activation reactions, it would reduce the difficulty of these computations if the same spectrum for all points can be used. More work should be done to investigate this into more detail.

5.1.4. Heating inside ITER and the CXRS Port Plug

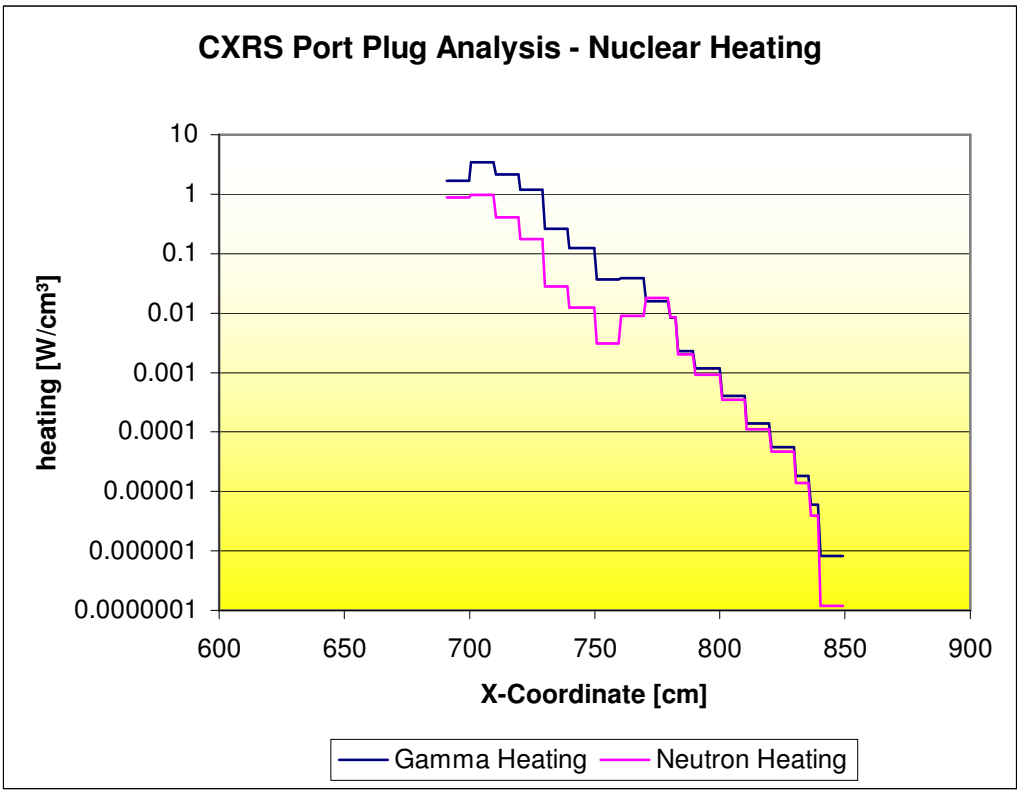

Figure 51: Line profile through the neutron and gamma heating distribution [W/cm³]

Detailed analysis has not been made only for neutron flux but also the same FMESH-tallies have been used for neutron and gamma heating determination to plot 2D- and line distributions. Figure 51 shows the nuclear heating in [W/cm³] throughout the ITER shielding at a position slightly underneath the CXRS Upper Port Plug much like the neutron and gamma flux in Figure 46 and Figure 47.

The neutron flux is mostly linear in shape, only two edges are occurring. One edge is located directly after the first wall, where the heat is rising suddenly what can be explained due to different materials at that position and at x-value 760 cm, where a small void is located between the BSM and the shielding. After that void, the relative amount of neutron and gamma heating is the same.

Up to that point, neutron heating is significantly lower than the gamma heating. A reason could be the fact, that the material composition in the BSM is another than in the shielding, namely the amount of water relative to the steel is higher in the BSM, what could lead to other behaviour of neutron scattering.

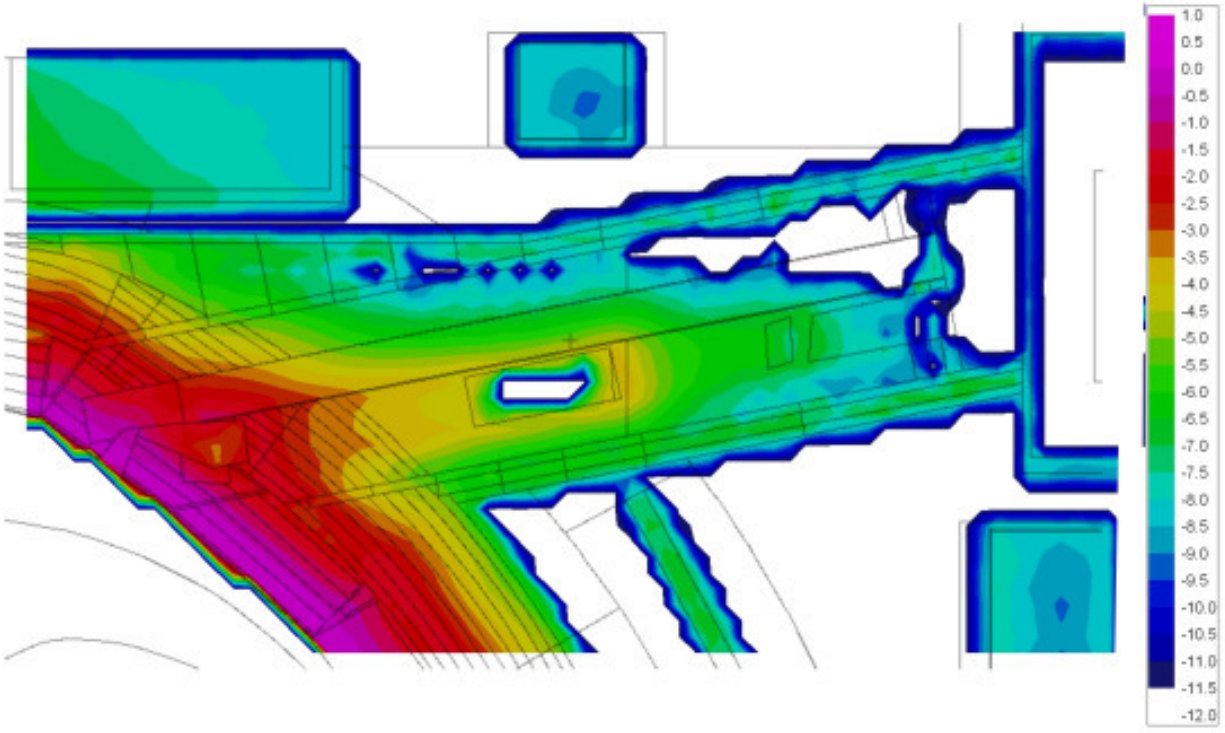

Figure 52: Neutron Heating in CXRS PP (log[W/cm³])

Figure 52 and Figure 53 show the twodimensional distribution for neutron and the gamma heating respectively. It can be seen, that the gamma heating is higher with half an order of magnitude in most parts of the Port Plug, especially at the front.

In other components the difference is even more obviously, for example in the magnetic coils, where the gamma flux is higher by a whole order of magnitude.

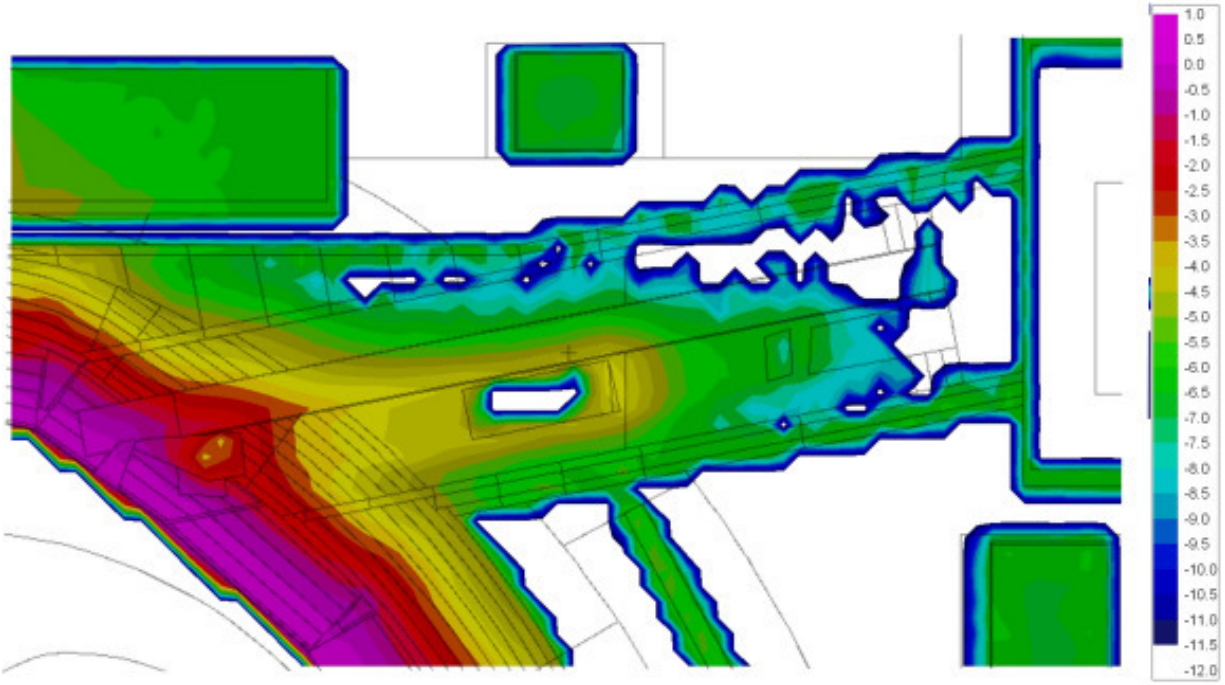

Figure 53: Photon Heating in CXRS PP (log[W/cm³])

5.1.5. Loads on the mirrors

Simple type 4 and type 6 tallies have been included into the MCNP input besides the formerly described FMESH results, to give information about the neutron flux and nuclear heating inside the mirror materials. Heating tallies include neutron as well as gamma heating.

At the location of the first mirror 3.76E+13 n/cm²s and 1.29 W/cm³ were calculated for neutron flux and nuclear heating respectively, representing the highest values in the Port Plug. Both values are in order of magnitude again comparable to that given in [SHATALOV 02]. The neutron flux for the mirrors two and three is 5.82E+12 and 1.21E+13 n/cm²s respectively, showing an increase at the position of mirror three.

This is due to the fact, that a higher fraction of neutrons is penetrating the shield than streaming to the position through the optical labyrinth. The nuclear heating rate at the position of mirror #2 and #3 was calculated to be 1.31E-1 and 3.89E-1 W/cm³ respectively.

	Neutron Flux [1/cm²s]		Heating [W/cm³]
	Flux	Statistical Error	Heating
Mirror 1	3.76E+13	0.01	1.29
Mirror 2	5.82E+12	0.01	1.31E-01
Mirror 3	1.21E+13	0.01	3.89E-01
Mirror 4	3.28E+10	0.01	6.41E-4
Mirror 5	2.31E+09	0.01	2.62E-5
Mirror 6	4.46E+08	0.09	7.67E-6
Mirror 7	1.58E+07	0.20	1.47E-7
Port Cell	2.42E+07	0.03	N/A

Table 14: Results of the CXRS PP neutron flux and nuclear heating calculations using MCNP

For each following mirror, the neutron flux and heating decrease rapidly due to the shielding effect of the structures. An evaluation of the calculations for the model with retractable tube shows, that the relative error for the neutron flux remains below 10% for the first six mirrors and is lower than 20% at the last two mirrors and the port cell. The value inside the port cell is 2.42E+7 n/cm²s for the neutron flux.

The neutron flux inside the port cell with 2.42E+7 n/cm²s is higher than that in mirror #7. This is due to the fact, that the neutron flux in the port cell is mainly influenced by the background radiation in the machine and not by the port plug. This is again a hint, that some amount of the shielding in the CXRS port plug model could be saved.

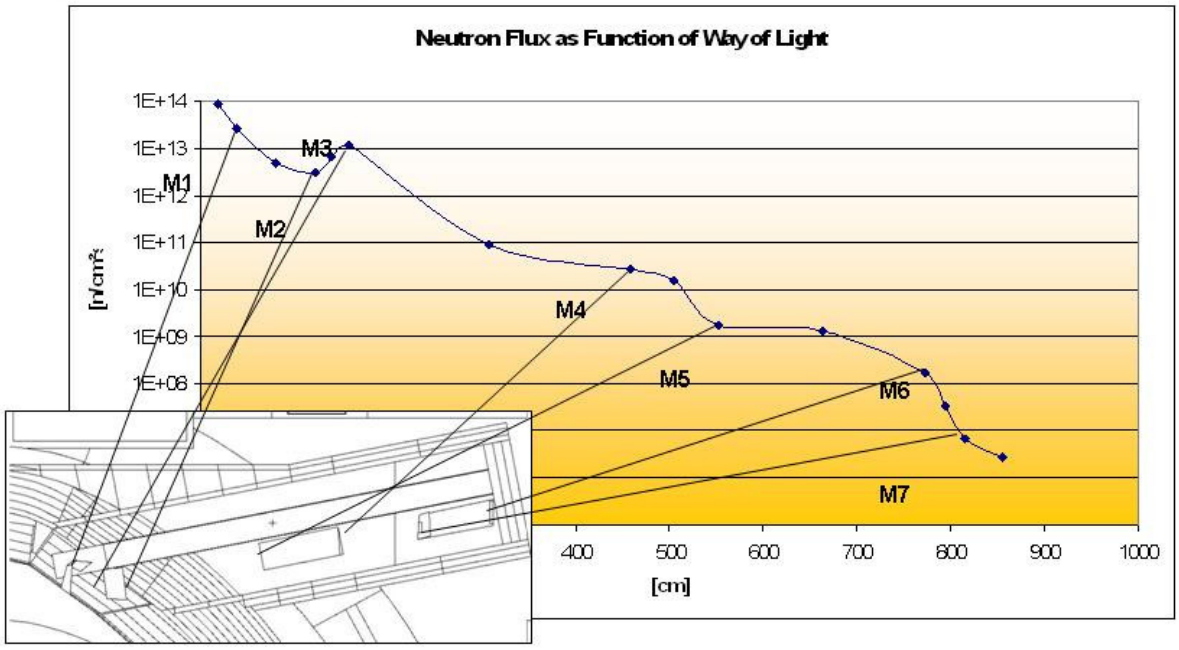

Figure 54: Neutron flux along CXRS PP mirror labyrinth way of light [log(n/cm²s)]

Figure 54 shows the change in the neutron flux along the way of light from the plasma to the port cell. Highest value is as expected at the 1st wall with about 1E+14 n/cm²s and drops throughout the way from mirror #1 and mirror #2 but is rising again on its way to mirror #3 because of the fact, that more neutrons are moving there through the shielding than by streaming effects of the mirror labyrinth.

After that the flux is dropping more constantly but with some sharper drops behind mirror #4 and mirror #6. The value of the port cell is not included in that figure but the curve would be increasing again after the last point due to the higher background radiation inside the port cell.

5.1.6. Comparison with results of other groups

To explain some differences in the results of the neutronics analyses performed by FzJ and by NRG the proposal has been made by NRG to compare line-profiles of the neutron and gamma flux distributions as well as the nuclear heating profile in the shielding. The line-profile is generated along a line through the points (570, 0, 330) and (1500, 0, 505) to match the computations made by NRG.

The line profiles have been generated by including FMESH tallies in the ITER Feat model around the area to be sampled. The FMESH output was then analyzed with MCNPAct. The code extracted the line profile from the 2D distribution between the mentioned coordinates. For the heating values, multiplicator cards have been used.

The detailed results are given in Figure 55 and Figure 56. To show, that the ITER-FEAT- and the ALite-model are identical in its coordinates, a plot of both models in superposition has been given in Figure 57.

Results of the computations of the flux-profiles are in good accordance with the results of NRG. The higher radiation levels at higher X-values can be explained by the higher amount of shielding in the divertor port region in the ALite-model.

The heating results are in good agreement after X=750 cm. Before that coordinate, values are differing by up to a factor of two near the front wall. The area before X=750 belongs to the Blanket Shield Module. It's possible, that there are some differences with the material composition or the density, but this is subject to further analysis.

Another comparison has been made with a publication by ITER Organisation [POLUNOVSKIY 08]. Figure 58 shows the overall nuclear heating – sum of neutron and gamma heating – at the same position than the comparisons with NRG, but with the ITER Org values included as red line. These values are slightly lower than FzJ results, but this can be explained by a slightly different position of the sampling points. The ITER Org sampling points are positioned about

ten cm higher than the FzJ line distribution, where neutron and gamma flux is also somewhat lower because of the increased distance from the core.

When taking this fact into account, there is fairly good agreement with the ITER Organisation heating calculations.

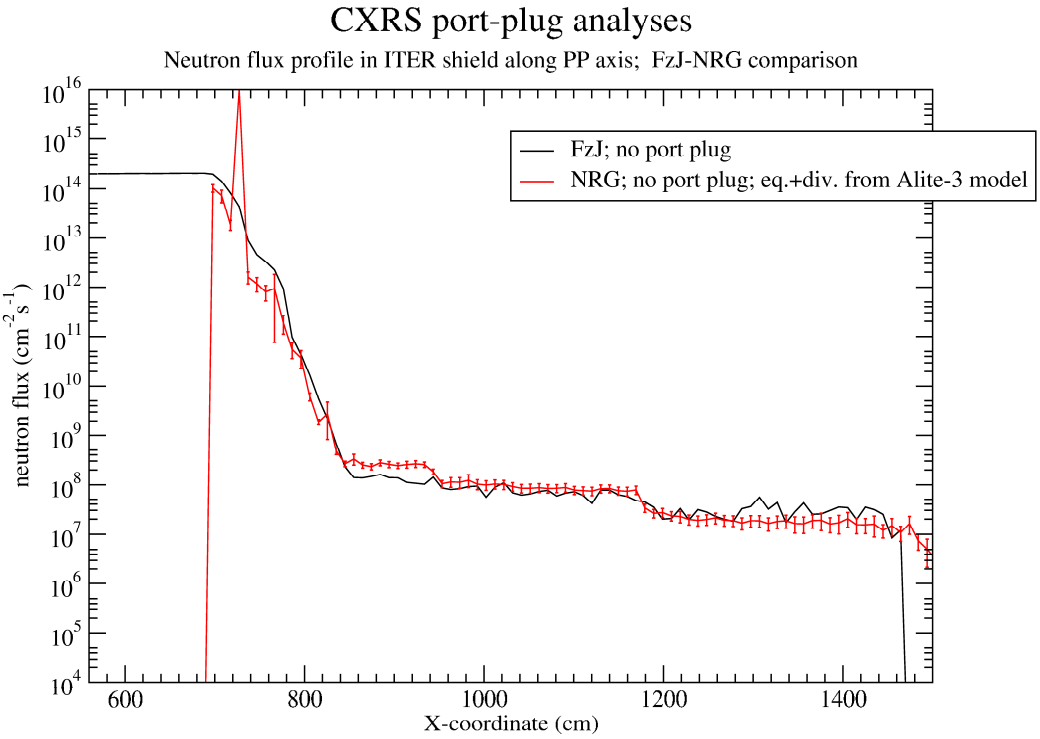

Figure 55: Comparison with the neutron flux profile of NRG (FzJ/NRG)

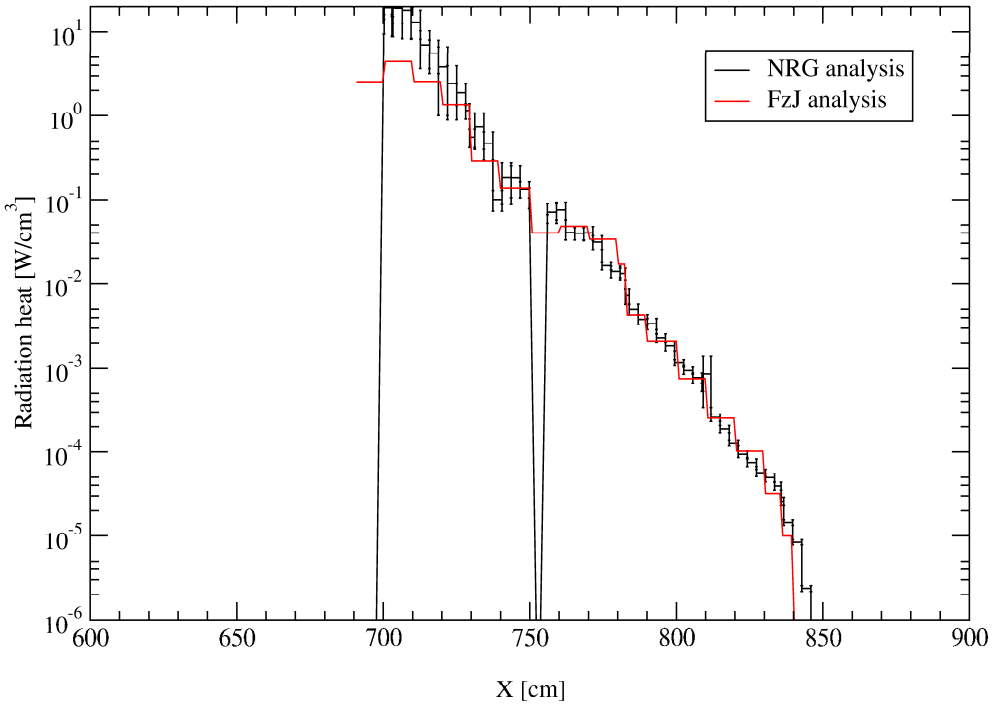

Figure 56: Comparison with the heating profile of NRG (FzJ/NRG)

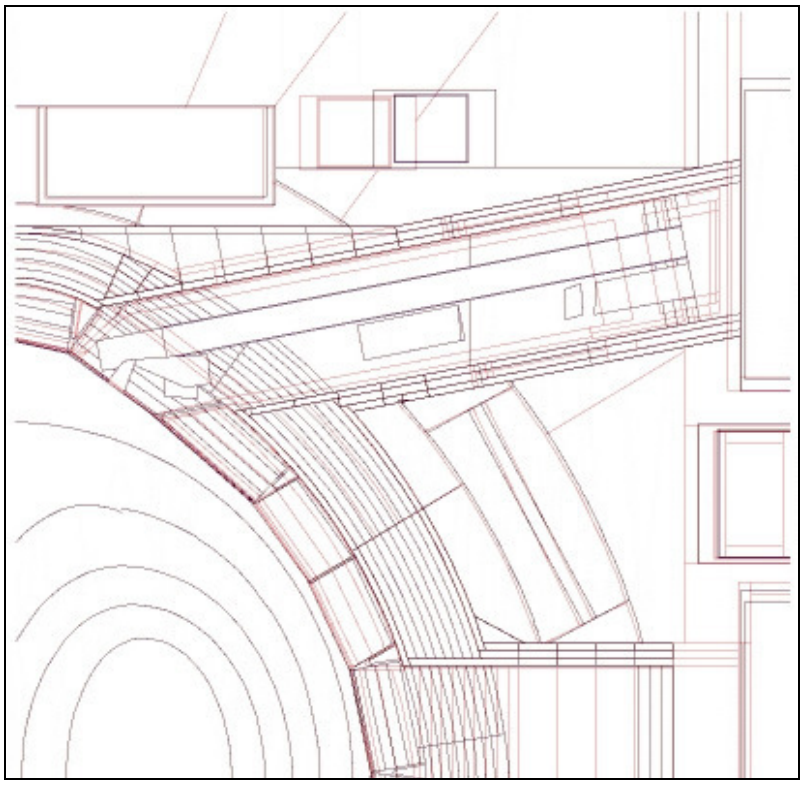

Figure 57: Superimposed image of the ITER-FEAT- (black) and ALite-MCNP-model (red)

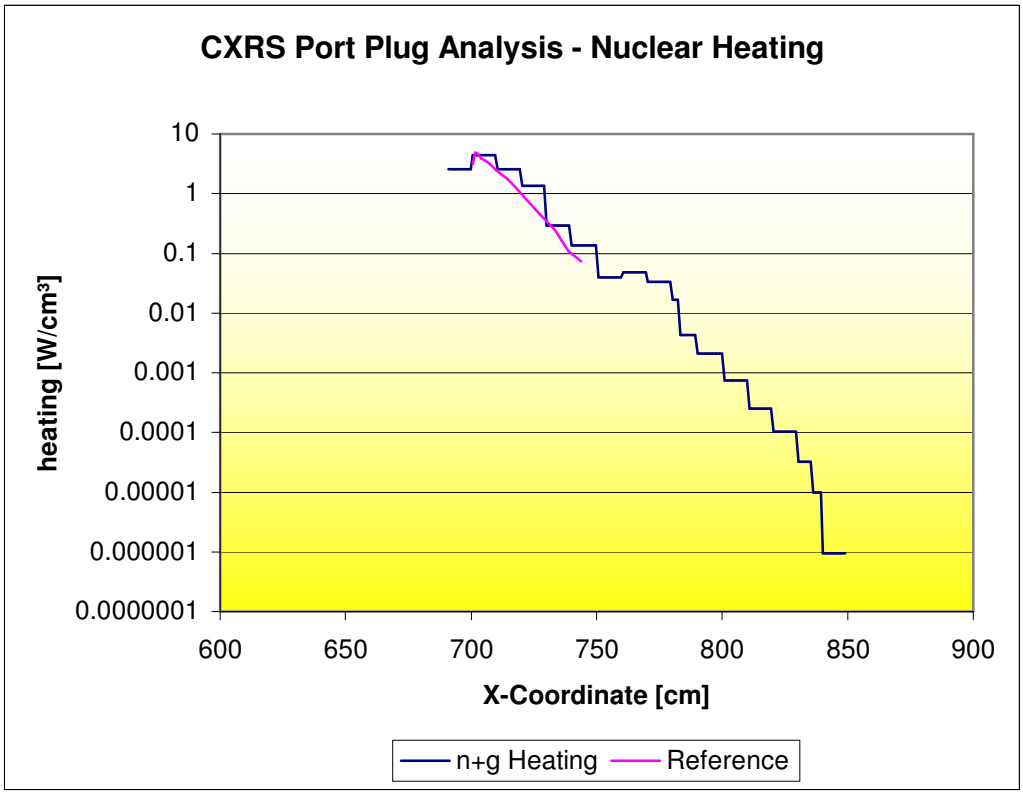

Figure 58: Line profile through the nuclear heating distribution and verification with ITER reference

5.1.7. Impact of materials on mirror heating

Figure 59 shows the results of some calculations on influence of materials on mirror heating, here done fore the second mirror. They differ from other values for the mirrors in this work because of certain statistical errors due to the short computation time, but for a quantitative comparison it should be sufficient. The PP model was computed with different materials. Also some variations have been done in different simulations with size and mass of the mirrors, but that has only minor influence.

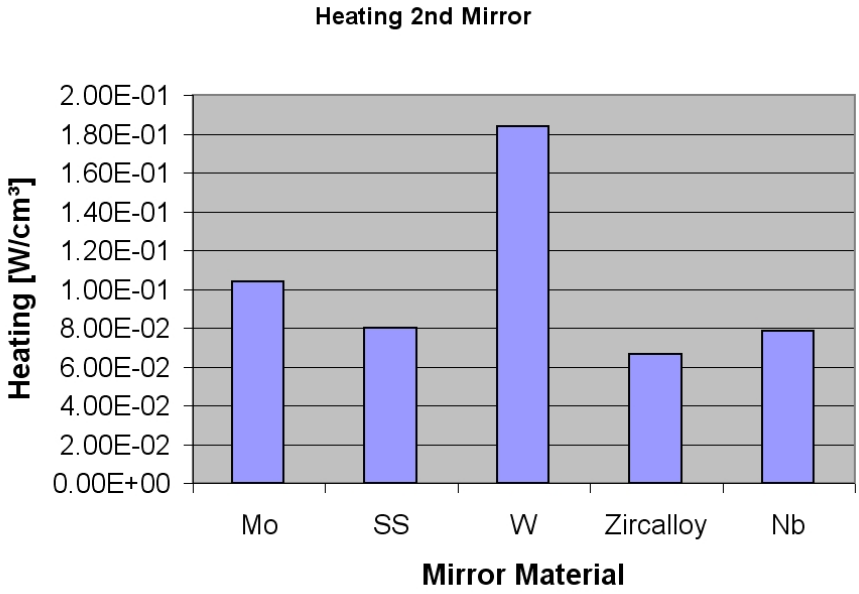

Figure 59: Heating values of the second mirror depending on the material chosen [W/cm³]

It seems that tungsten is responsible for a significantly higher heating than for mirrors made of stainless steel. Molybdenum, the material of the 1st mirror, has only about half the heating values of tungsten. Heating for mirrors made of stainless steel and niobium are only slightly lower, but regarding the mirror materials Zircalloy would be the best choice, when looking only at the heating.

5.1.8. Flux and Heating gradients inside the 1st mirror

Especially in the parts of the Port Plug that are nearer to the front wall, there are huge differences in the neutron flux and heating values when changing the position. This fact implies that gradients could occur also in smaller structures. This could be critical especially for the first mirror, as heating gradients can create tensions and mechanical deformations. To investigate that, a detailed analysis of the first mirror has been made.

The mirror has been surrounded completely by very fine 3D FMESH-grids, with 0.25 x 0.25 x 0.25 cm per voxel. Neutron and photon heating again is identified by multiplier cards. After a 50 hour simulation on four processors with about 45 million neutron trajectories simulated, the

resulting FMESH-files have been analyzed by MCNPAct to create line distributions along the x-axis of the mirror.

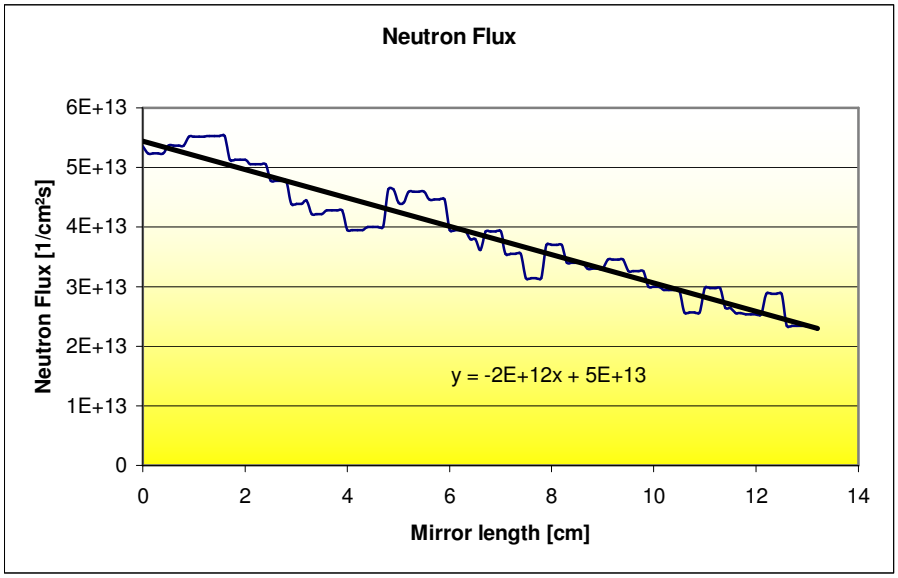

Figure 60: Results of the CXRS PP neutron flux calculations [n/cm²s] for the first mirror.

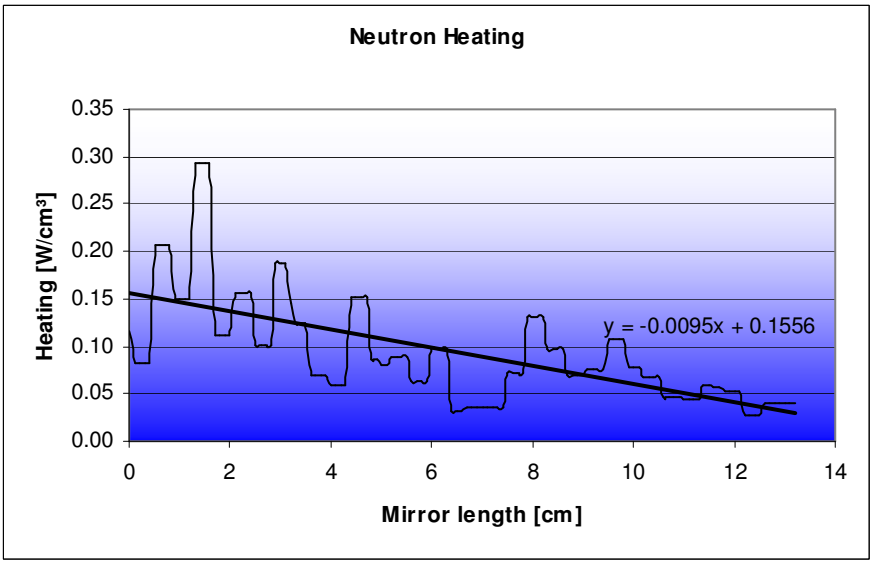

Figure 61: Results of the CXRS PP neutron heating calculations [W/cm³] for the first mirror

The results can be seen in Figure 60 and Figure 61. The neutron flux profile shows a drop throughout the length of the mirror from 5.3E+13 n/cm²s to 2.2E+13 n/cm²s, what reduces the flux by more than a factor of two or about 0.25E+13 n/cm²s per cm. The shape of the curve is almost linear when smoothed.

The same is true for the neutron and the photon heating. The neutron heating drops from 0.15 W/cm³ to 0.04 W/cm³, as seen in Figure 61, and the photon heating decreases from 1.8 W/cm³ to 0.8 W/cm³, as seen in Figure 62. It must be said that statistical variance is high with that simulations due to the high special resolution, but the trend is clearly visible.

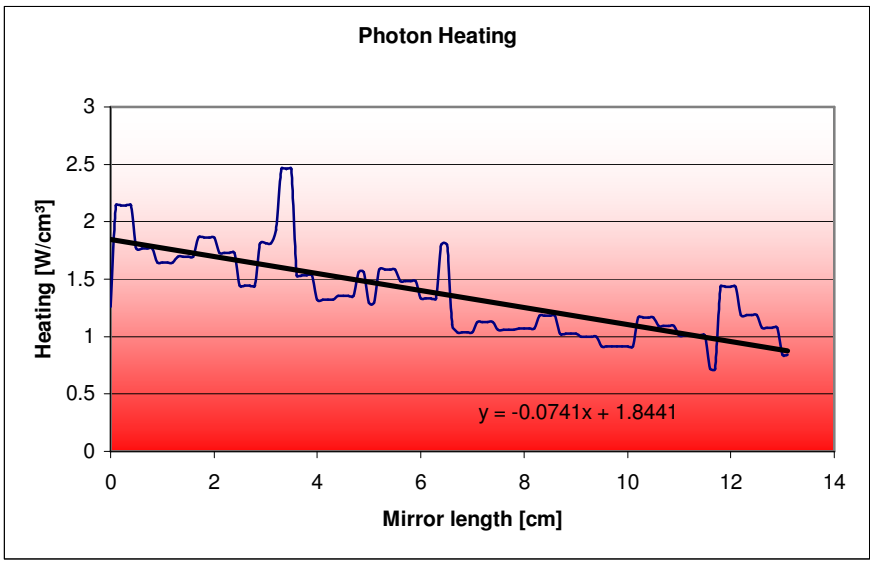

Figure 62: CXRS PP photon heating [W/cm³] for the first mirror

5.2. Material Damage

Of particular interest is the material damage in critical structures of the CXRS Port Plug. Structural materials can be brittle after too much radiation damages and the optical components, for example the mirrors can be degrade, due to lattice defects, when atoms are knocked out of their original positions.

The results were again obtained by the Monte Carlo Code MCNP with the standard ITER Feat model with Port Plug included. For the sampling of the neutronic results several 40x40 element FMESH-Tallies were introduced at the regions of interest, namely the vicinity of the mirrors as well as some F4 type tallies for the mirrors themselves. Statistical reliability at the first three mirrors in this simulation was within 0.01. Neutron transport was simulated correctly with cooling water in the shield, but tally multipliers have been modified for structures of stainless steel.

The material damage has been calculated via FM cards according to the standard Norgett-Robinson-Torrens (NRT) model [NORGETT 75], [MACFARLANE]. Results were computed in dpa/FPY. They can be modified easily for any operation time as the damage is linear to the time. There are also other methods, that can be used for radiation damage calculations. [HOGENBIRK 08]

An overview of the situation at the front part of the Port Plug is shown at Figure 63.

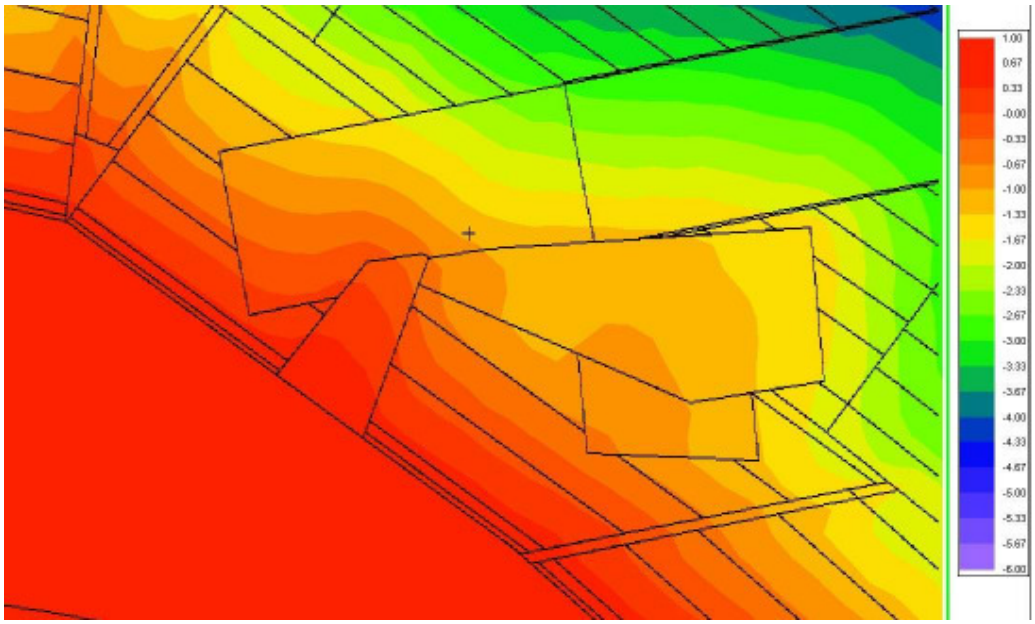

Figure 63: Neutron damage in CXRS PP in [log(dpa/FPY)]

The picture shows a damage of about 0.5-1 dpa/FPY in the structures of the retractable tube surrounding the first mirror. Situation of the other mirrors is shown in Figure 64 and Figure 65. At the 2nd mirror the material damage is about 0.02 to 0.05 dpa/FPY.

Mirror three damage is again higher because of its nearer position to the front wall, with about 0.1 to 0.25 dpa/FPY. At mirror number four a production rate of 1E-4 to 3E-4 dpa/FPY is expected and at number five the production rate is lower than 5E-4 dpa/FPY. Table 15 gives an overview.

Mirror	Neutron damage (dpa/FPY)
1	0.5 - 1
2	0.02 – 0.05
3	0.1 – 0.25
4	1E-4 – 3E-4
5	1E-5 – 5E-4

Table 15: Neutron Damage in CXRS PP in [dpa/FPY]

Research in the last years [BACON 04], [VOSKOBOINIKOV 08], [OSETSKY 02] allows concluding that NRT damage calculations are overestimated for metals. This leads to the conclusion, that NRT damage results are safely conservative in their impact on metal properties of the CXRS Port Plug.

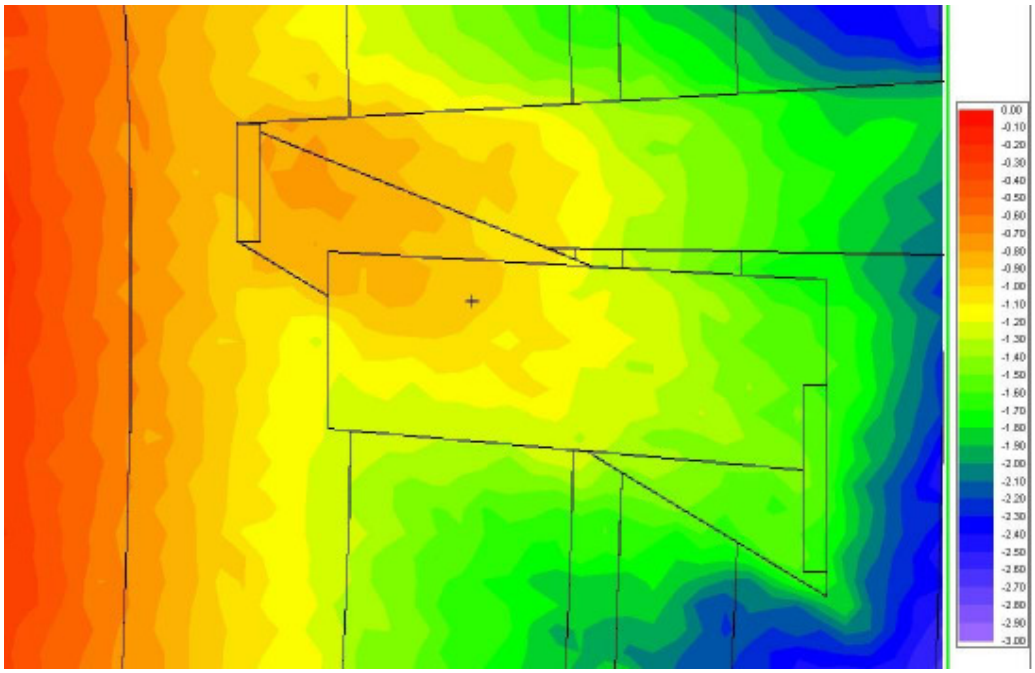

Figure 64: Material Damage in CXRS PP (2nd and 3rd mirror) in [log(dpa/FPY)]

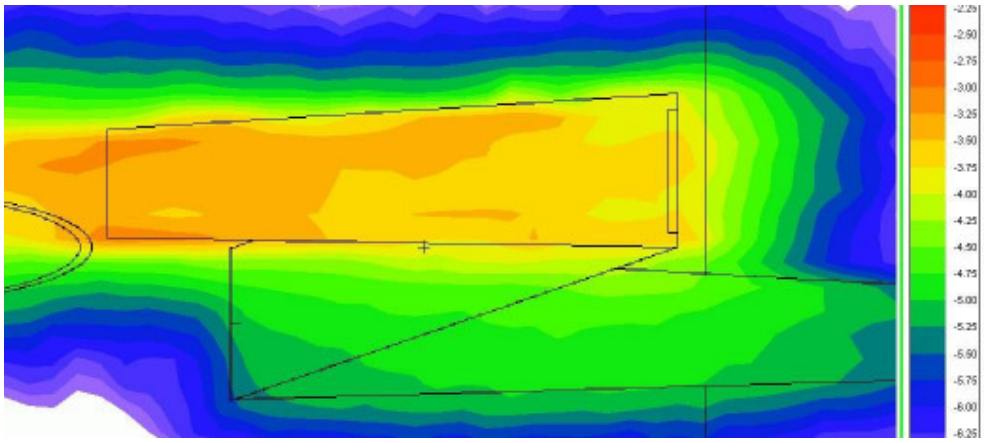

Figure 65: Material Damage in CXRS PP (4th and 5th mirror) in [log(dpa/FPY)]

5.3. Neutronic effects on the TF coil insulation

Investigations have been made on the effects of neutron and gamma radiation during ITER operation on the TF coil insulation. At first computer simulation runs with MCNP were done for detailed geometrical models of ITER with CXRS Upper Port Plug installed.

Figure 66 gives an overview of the neutron distribution around the port plug and the coils. Numbers are given in [log (n/cm²s)]. Most of the neutrons that have effects on the front side of the coils and insulation are moving directly from the shielding around the torus and not from the interior of the port plug.

The values for the insulation on the front side of the coils are varying between 6E+7 n/cm²s and 2E+8 n/cm²s with a statistical reliability of lower than a factor of two. Gamma induced absorbed energy is varying between 6E-8 W/cm³ and 3E-7 W/cm³. Neutron induced energy deposition is higher with 1.5E-7 W/cm³ up to 7E-7 W/cm³. With an estimated ITER operation over 10 years and an accumulated burn time of 25,000h the total neutron flux will be at maximum 9.4E+19 n/m². The energy absorption of the insulator material is then 225 kJ/kg, what is equivalent to 0.225 MGy. Values are in order of magnitude similar to that of other groups.

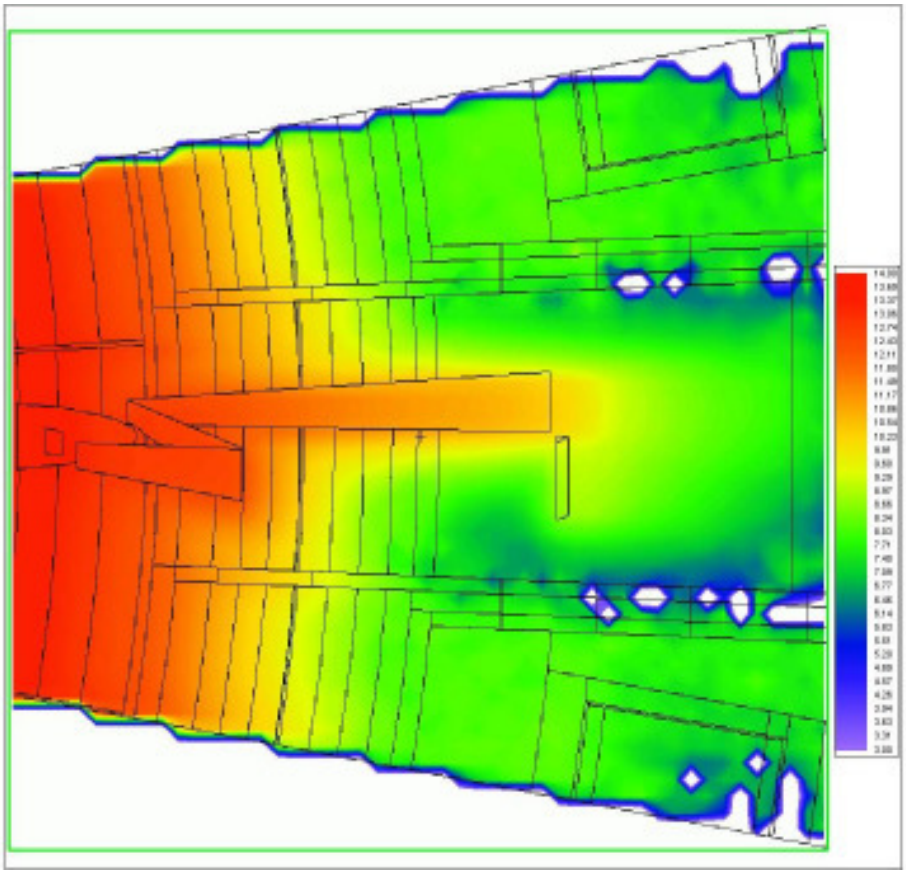

Figure 66: Neutron Flux around the port plug [log(n/cm²s)]

A second computation has been made with a model without Port Plug, as can be seen in Figure 67 but only with the regular shielding of the vacuum vessel. Values for the insulation on the front side of the coils are again varying between 6E+7 n/cm²s and 2E+8 n/cm²s with a high statistical reliability. The neutron flux distribution can be seen in Figure 68.

Gamma induced absorbed energy is varying between 6E-8 and 4E-7 W/cm³. Neutron induced energy deposition is higher with 1.2E-7 up to 4E-7 W/cm³. The results are the same as in the model with PP and variations are within the statistical reliability.

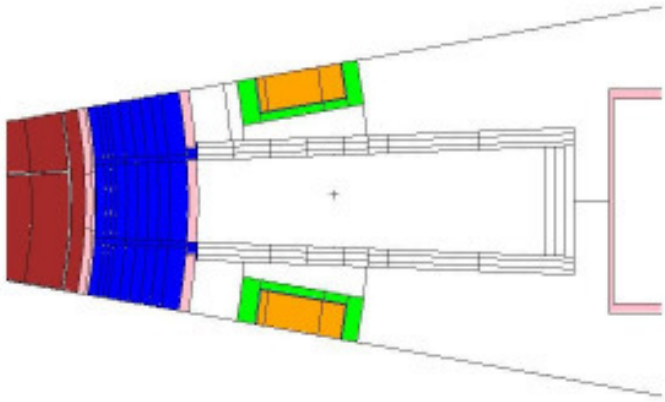

Figure 67: Plot of the MCNP model without Port Plug

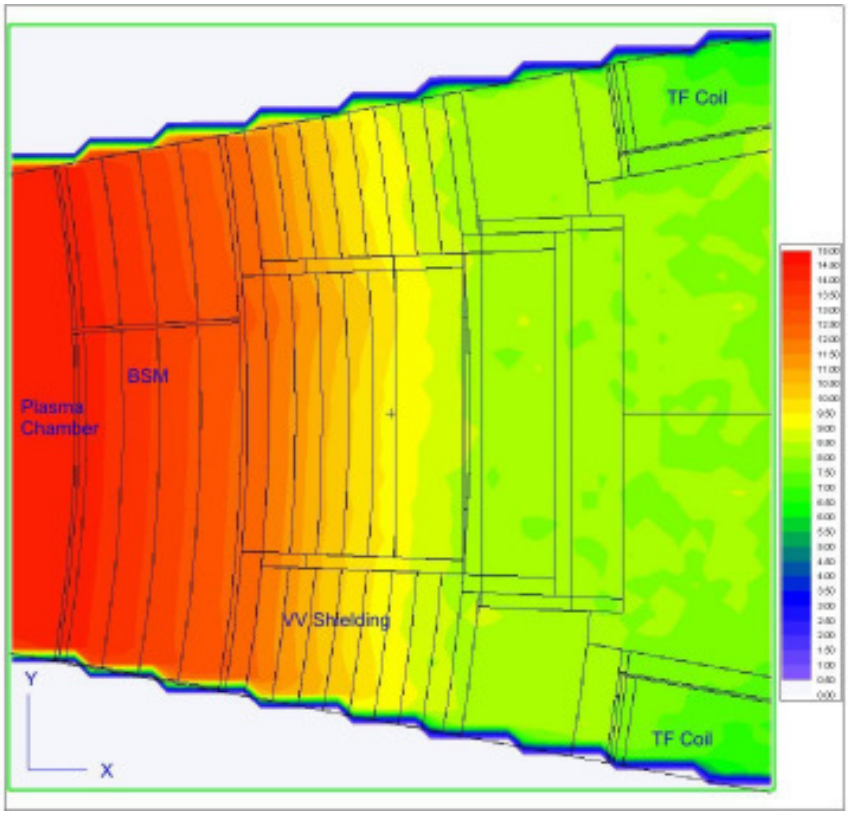

Figure 68: Neutron Flux in model without Port Plug [log(n/cm²s)]

According to the Nuclear Analysis Report (NAR) [IDA 06], that contains all of the neutronics limits regarding ITER, the limits for the magnet insulation over the lifetime of ITER are:

- Peak gamma- and neutron-radiation: 10 MGy
- Total neutron flux: 5x10^21 n/m²

The data are regarding to the epoxies used in the insulation, where radiation will break up the long polymers of the material and is responsible for gas generation inside the insulator. There is

also mentioned that switching to other insulation materials like Polyimides or Bismaleimides would increase the tolerance to radiation by a factor of 10.

The simulation is showing that the neutron flux and absorbed energy is in this port plug configuration at least two orders of magnitude lower than the design limits Table 16. But it should also be mentioned that the presented data are calculated for operational loads only. This is sufficient for determining the accumulated neutron flux but due to activation processes within the ITER structures, there will be additional gamma radiation and thus a higher dose rate at the end of the ITER lifetime.

This should be assessed in a separate activation calculation and by an additional gamma transport calculation, with the codes R2S or MCNPAct, what is however a very time-consuming process.

Furthermore the used MCNP model does not include any gaps in the port plug model besides the mirror labyrinth. A further assessment should be made for effects of them to the coil insulation. When looking at the overall neutron flux distribution of ITER (Figure 43) it becomes clear, that the values are higher at the lower levels of the reactor. Especially at the divertor port region neutron flux is higher by two orders of magnitude, so that violations of the limitations are possible here. A detailed analysis is highly recommended.

	Model with PP	Model without PP	ITER Limits
Max. Neutron Flux [n/cm²s]	2.00E+08	2.00E+08	N/A
Max. Absorbed Energy [W/cm³]	8.00E-07	1.00E-06	N/A
Total Neutron Flux [n/cm²]	9.40E+19	9.40E+19	5.00E+21
Peak Radiation [MGy]	0.225	0.28	10

Table 16: Results of the computations for the coils

Further investigations should concentrate on simulations with models including gaps and on the effects of walls with lower steel to water ratio. Furthermore the material damages in the critical components should be determined by separate computations.

Used steel to water ratios in the current model are as followed:

BSM: Stainless Steel 80% with water 20%
VV shielding: borated Stainless Steel 60% with water 40%
VV hull: 100% Stainless Steel

5.4. Activation

5.4.1. Activation Calculations for ITER

MCNPAct has been used for the activation calculations. To demonstrate the capabilities of the coupling method, the code has not only been used for the CXRS Port Plug but also for the ITER fusion reactor as a whole.

As a preparation a three dimensional MESH tally with the dimension of 50 x 50 x 30 segments, resulting in 75,000 elements, has been introduced into the ITER Feat MCNP model with integrated CXRS Port Plug. That FMESH then has further been segmented into 24 energy groups, leading to an overall number of more than 1.8 million sampled values. A MCNP plot of the ITER geometry used for the activation calcultion can be seen in Figure 69.

In total 560 Mio source particles were simulated resulting in a relative error of the energy integrated neutron flux of less than 1 % around the front opening and less than 15% at the back windows of the CXRS Port Plug structure. The computation time for that MCNP run was more than 2,200 CPU-hours.

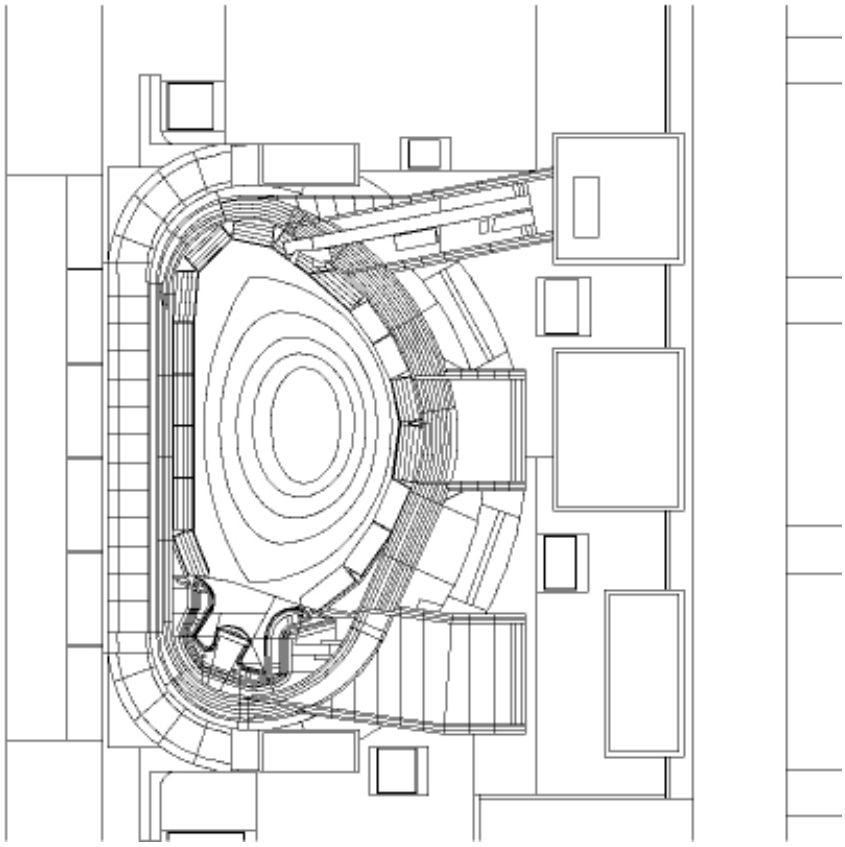

Figure 69: MCNP plot of the ITER geometry used for the activation analysis

The activation calculations with FISPACT have automatically been carried out with MCNPAct, one for each element in the three dimensional matrix. The computation time for the analysis was about 24 hours. FISPACT results have then compiled for activation, activation heating and gamma dose for all occurring daughter products. An overview of the most active isotopes, ten years after shutdown of ITER, has been compiled in Figure 70.

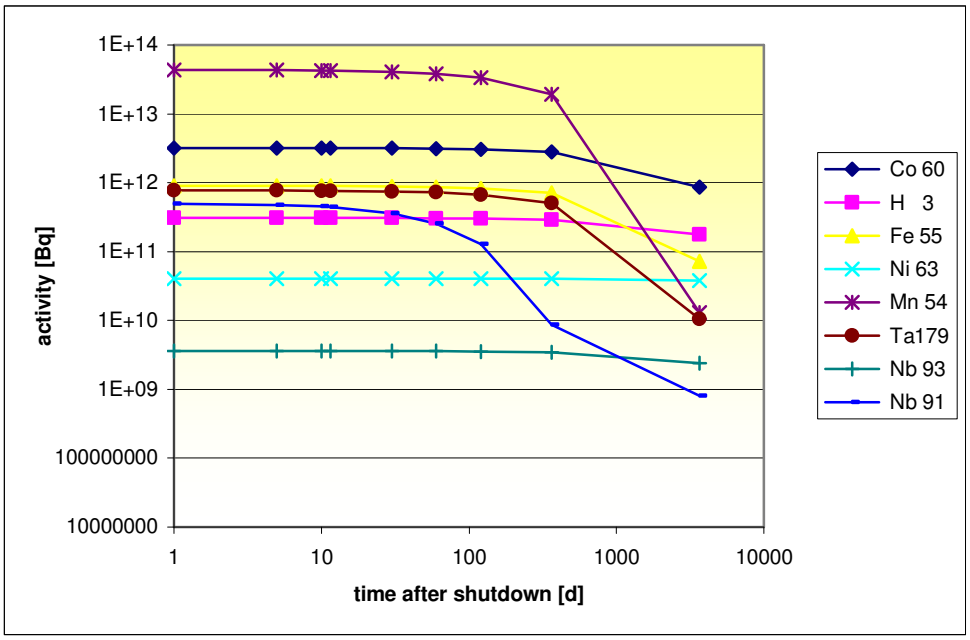

Figure 70: Activity of the most active isotopes inside ITER structures due to activation after shutdown

After ten years of cooling time most of the activation comes from Cobalt 60 with almost 1E+12 Bq. This is generated due to the irradiation of steel. More than 1E+11 Bq are coming from tritium. As mentioned earlier, the computation should be repeated with water removed from the water-steel mixture to determine the amount of tritium generated inside the cooling water. Further contributing isotopes are iron55, nickel63 and manganese54, all originating by the irradiation of steel. These numbers have additionally been compiled in Table 17.

Isotope	Activity [Bq]
Co 60	8.56E+11
H 3	1.76E+11
Fe 55	7.20E+10
Ni 63	3.79E+10
Mn 54	1.31E+10
Ta179	1.04E+10
Nb 93	2.39E+09
Nb 91	8.10E+08
C 14	5.47E+08
Co 57	1.97E+08
Mo 93	1.47E+08

Table 17: Activity of most active isotopes in ITER 10 years after shutdown

When looking at the most active isotopes shortly after shutdown, there are other isotopes in the focus. The most active ones have been compiled in Table 18 for one day after shutdown of the ITER reactor.

Isotope	Activity [Bq]
W 187	1.7776E+18
Cu 64	1.1521E+16
W 185	3.9041E+15
W 181	9.5352E+14
Mn 56	6.5221E+14
Co 58	1.8411E+14
Mo 99	1.6608E+14
Tc 99	1.4803E+14
Na 24	9.7587E+13
Ta184	5.3255E+13
Cr 51	5.0557E+13

Table 18: Activity of most active isotopes in ITER 1 day after shutdown

The highest activity shortly after shutdown is originating from tungsten187 with 1.78E+18 Bq. Also the tungsten isotopes number 185 and 181 are responsible for a very high activity with 3.9E+15 Bq and 9.5E+14 Bq respectively. These numbers show clearly, that the use of tungsten should be limited, when the activity shortly after shutdown is analyzed. High activity is also originating from copper64 and manganese56 with 1.15E+16 Bq and 6.52E+14 Bq respectively.

When looking back at Table 17, where the activities after ten years are listed, none of these isotopes are occurring anymore. So the high activity of the isotopes after 1 day is originating from relatively short half-lifes. This has the advantage of a rapid decay for reducing the mount of nuclear waste after shutdown but results in high activity and heating valus after shutdown and at the end of the operation phase.

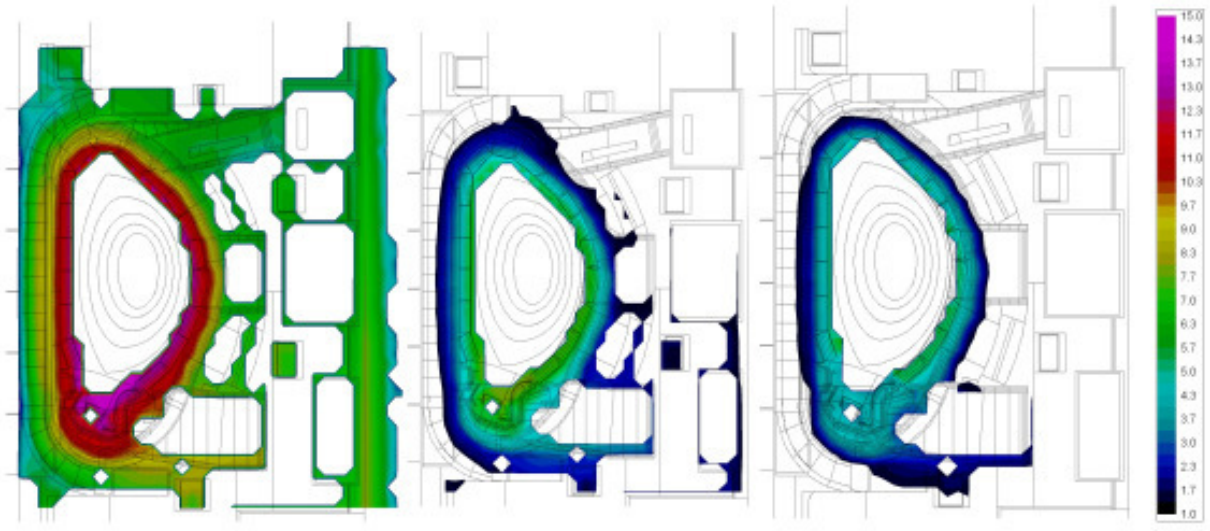

Figure 71: Activity in ITER 1 day (left), 1 year (middle) and 10 years (right) after shutdown [log(Bq/kg)]

Of special interest is also the tritium generation during the operation as the amount of tritium is limited by ITER regulations. When looking at Figure 72, where the overall tritium abundance is shown dependent on the time after shutdown, it can be seen, that the mass of the volatile gas is 0.9 gram. As tritium has a half life of about 12 years, the amount is decreasing only slowly in the first years but reduces to about 5 gram after ten years.

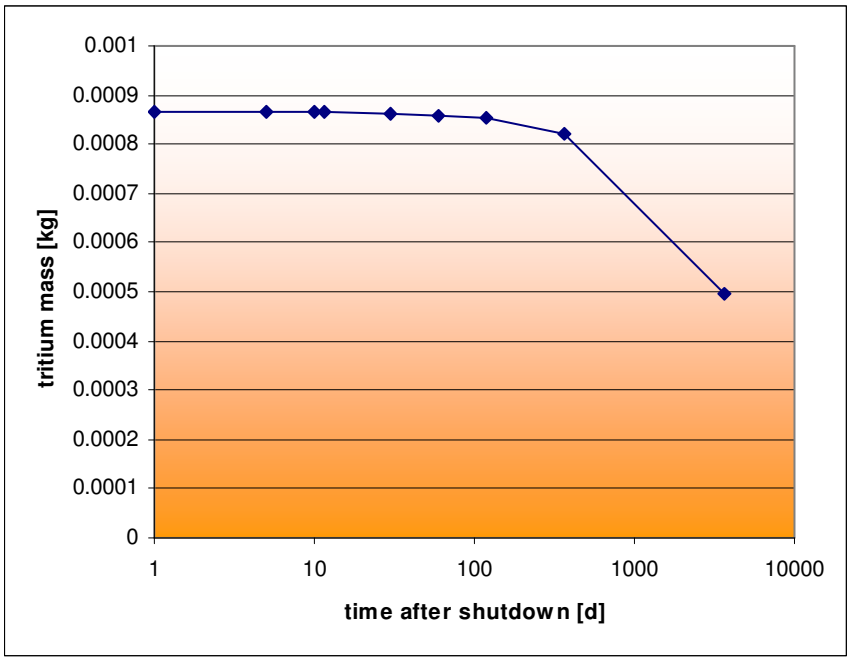

Figure 72: Tritium content inside ITER structures due to activation after shutdown

Figure 73 shows the tritium activity dependent on the position inside ITER for one day after shutdown on the left side and for ten years after shutdown on the right side. As the colour scale is plotted logarithmically, it can be seen, that there is almost no difference between the two plots.

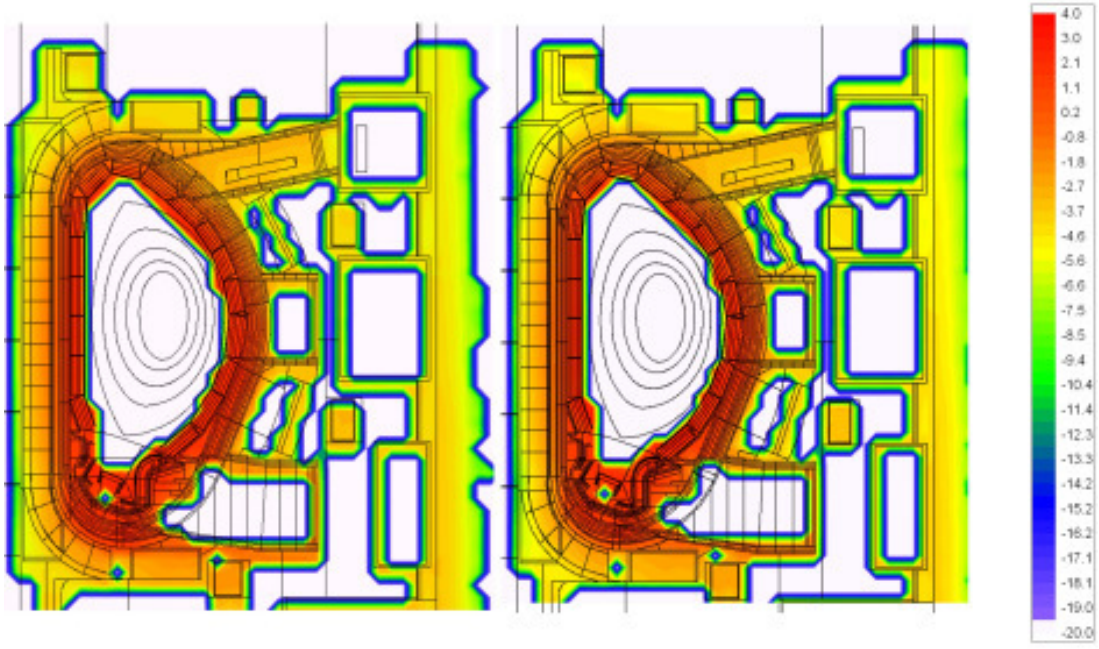

Figure 73: Tritium activity in ITER 1 day (left) and 10 years (right) after shutdown [log(Bq/cm³)]

Highest concentrations occur next to the first wall of the BSMs with up to 1E+4 Bq/cm³. Main contribution to the tritium generation is the irradiation of the coolant water. As mentioned earlier, the same model should be calculated without water added in the water-steel mixture of the shielding. Fortunately it is possible to calculate other MCNP input files in the activation calculations with FISPACT than in the neutron field simulations as the cooling water should be present in the latter for a realistic model.

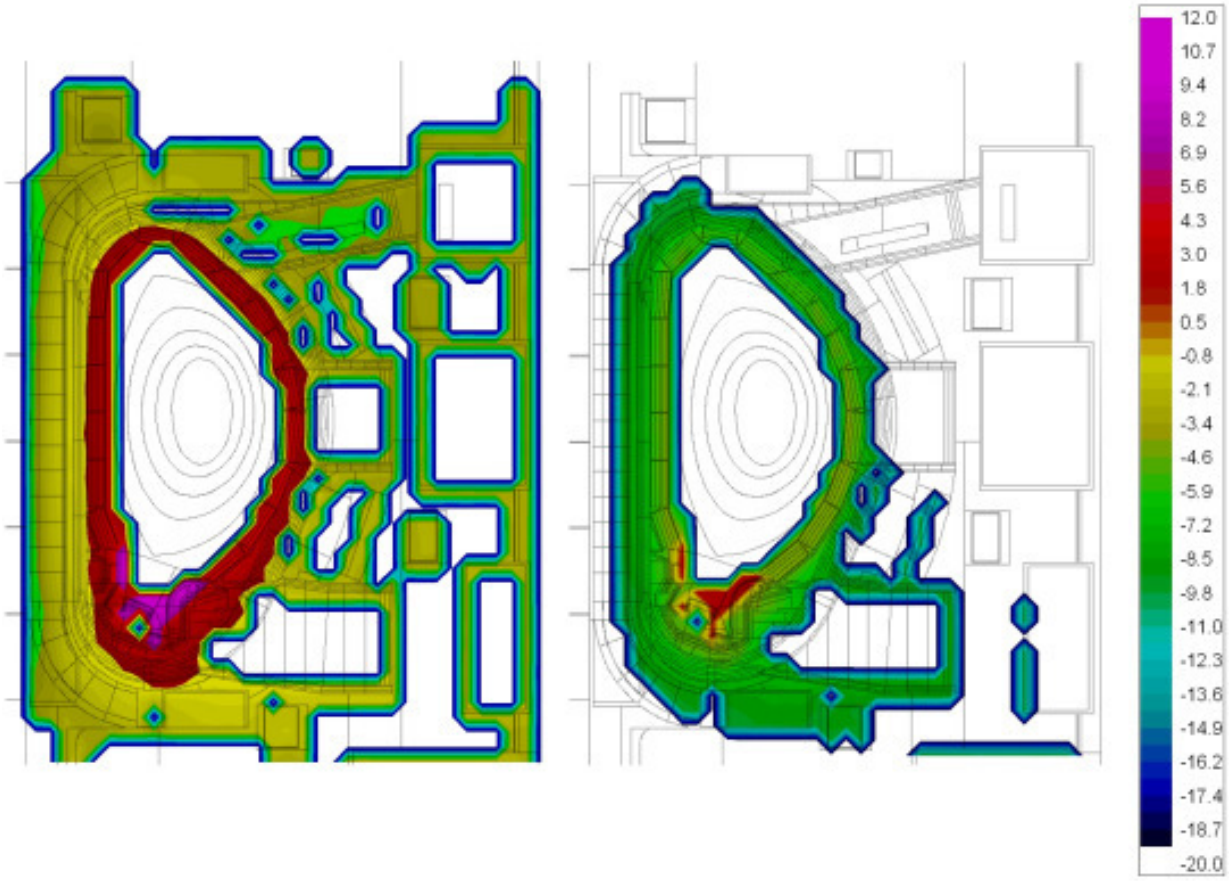

Figure 74: W-187 activity in ITER 1 day (left) and 30 days (right) after shutdown [log(Bq/cm³)]

In the activation calculations also the abundance of single isotopes has been calculated and listed. Figure 74 shows the activity due to tungsten 187 in the different parts of ITER, what is the most active isotope one day after shutdown as listed in Table 18. The left side of the picture shows the activity one day after shutdown. Highest activity of that isotope is located in the BSM next to the 1st wall with up to 1E+5 Bq/cm³ and especially in the divertor cells with up to 1E+12 Bq/cm³.

Due to the short half life of tungsten 187 the activity decreases strongly in the first years after shutdown. The right side of the picture shows the situation ten years later, where the high activity in the divertor region has been reduced to about 4 to 5 Bq/cm³. In the BSMs the activity dropped to lower than 1 Bq/cm³.

As a rapid decay is an advantage for the nuclear waste situation, it can lead to problems due to activation heat shortly after or even during irradiation, when adding to the neutron and gamma heating absorbed in the structures. The decay heat is also calculated by FISPACT and has been collected and compiled by MCNPAct in Figure 75.

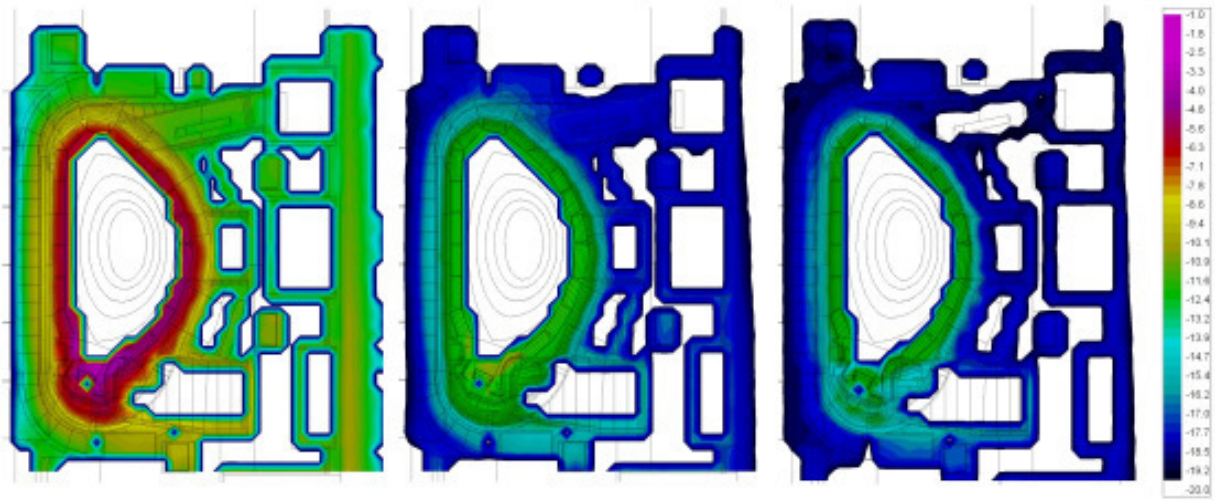

Figure 75: Activation heat 1 day (left), 1 year (middle) and 10 years (right) after shutdown [log(kW/cm³)]

The situation is as expected with high amounts of activation heat shortly after shutdown, that is decreasing by several orders of magnitude within the first year. The activation heat is highest in the divertor region and inside the BSMs next to the 1st wall, what is like expected due to the high activity there. Values can rise in the divertor up to 100 W/cm³. These values then drop to 1E-7 W/cm³ ten years after shutdown.

5.4.2. Activation Calculations for the ITER CXRS Port Plug

For the activation calculations of the CXRS Port Plug the standard ITER Feat model with the dynamically generated Port Plug model with retractable tube as described above for the reference model 2008 has been used. A FMESH tally has been introduced in the area around the Port Plug. This tally was a threedimensional structured tally with 41 x 20 x 20 elements, what amounts a resolution of 16,400 geometrical elements.

The tally has been further structured in 24 energy groups to resemble changes in the spectrum throughout the geometry. The overall number of sampled data in the tally amounts to 393,600 sampled values that have been used for the activation calculations with FISPACT.

A MCNP plot of the ITER CXRS Port Plug geometry used for the activation calculations can be seen in Figure 76. In total 560 Mio source particles were simulated resulting in a relative error of the energy integrated neutron flux of less than 1 % around the front opening and less than 15% at the back windows of the Port Plug structure. The computation time for that MCNP run was more than 2,200 CPU-hours. Again, MCNPAct has been used as a coupling mechanism for the data transfer between MCNP and FISPACT to support the activation calculations.

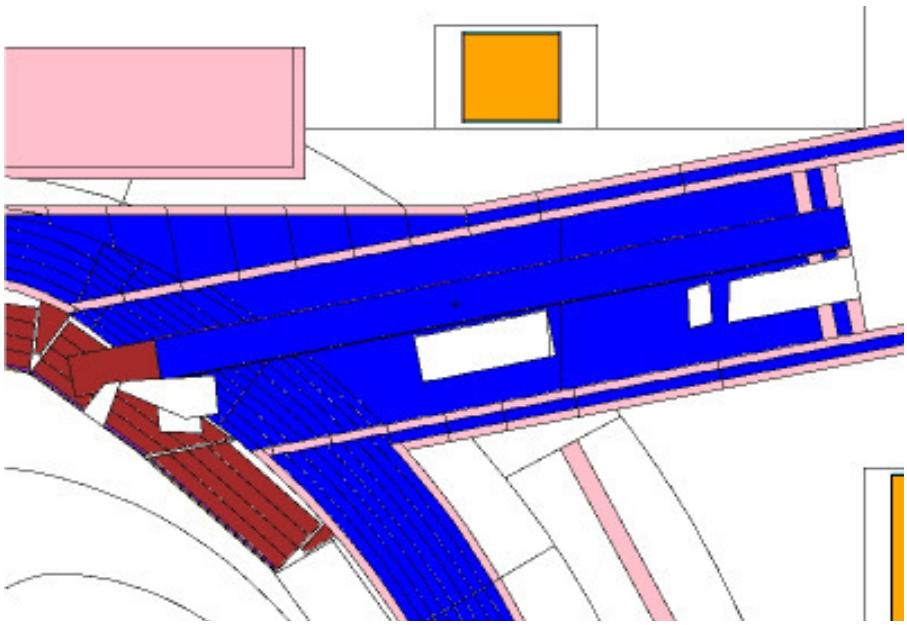

Figure 76: MCNP plot of the ITER CXRS Port Plug geometry used for the activation analysis

The overall activity distribution in the model geometry at different time steps after shutdown of ITER was analyzed first.

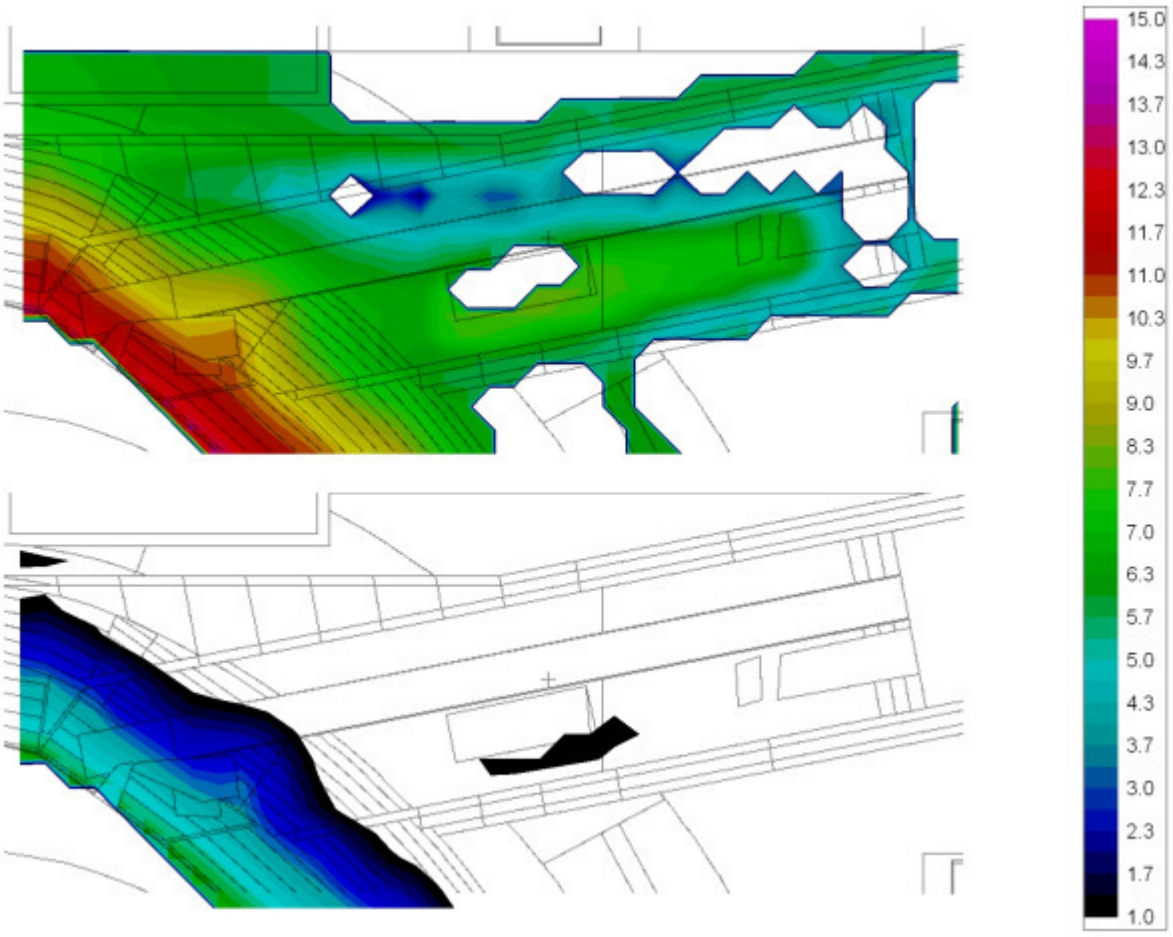

Figure 77: Activity in the CXRS PP 1 day (up) and 10 years (down) after shutdown [log(Bq/kg)]

A visualization of the activity is shown in Figure 77. The upper picture depicts the activity one day after shutdown and the lower picture displays the same for a time step ten years after shutdown to show the effects of the cooling time.

The highest activity in the system is next to the first wall inside the Blanket Shield Module (BSM) as expected with up to 1E+13 Bq/kg after one day of cooling time. Throughout the BSM, the activity is decreasing fastly by several orders of magnitude until reaching 1E+10 Bq/kg at the front of the shielding modules.

In the vicinity of the mirror labyrinth there is an area of higher activity reaching inside the shielding module with up to 1E+11 Bq/kg. This can be clearly seen as a buckle in the picture, showing the effect of the higher neutron flux values in the voids of the labyrinth.

At the more distant parts of the Port Plug the activity is decreasing below 1E+5 Bq/kg, especially at the parts located at the back side above the retractable tube because of the high amount of shielding present. As these are regions where no neutron flux could be detected by MCNP there will also be no more activation.

When looking to the situation after ten years, the activation has decreased significantly. Activation values next to the first wall dropped below 1E+7 Bq/kg. behind the BSM the activation is further lowered, reching very fast values below 1E+1 Bq/kg where the values are not displayed anymore. Still clearly visible is the buckled shape of the activation field that is reaching some dozens of centimetres inside the Port Plug due to the voids of the mirror labyrinth.

Figure 78 is showing the activation in the CXRS Port Plug one day after shutdown due to the isotope cobalt60.

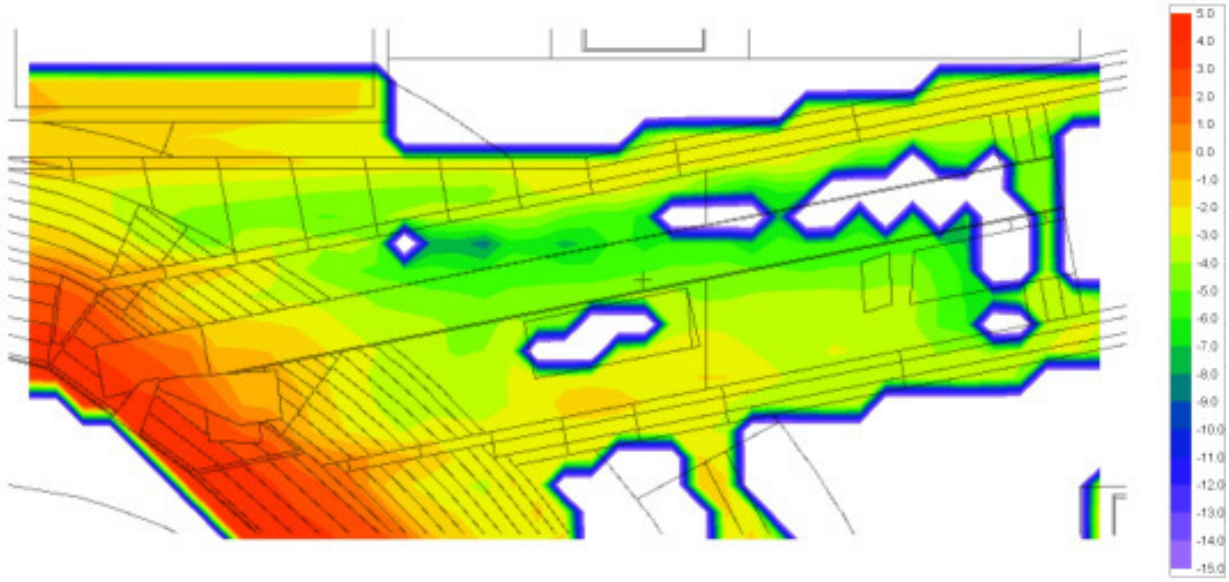

Figure 78: Co60 activity in the Port Plug one day after shutdown [log(Bq/cm³)]

Cobalt60 is generated by neutron irradiation of iron, decay of iron59, what leads to the formation of cobalt59, what is transmuted easily with high cross section into the highly radioactive cobalt60. [BECKURTS 64]

Another possible source of cobalt60 is the activation of nickel, what is a alloying element of stainless steel. Nickel58 is transmuted into nickel59, which decays to cobalt59 (although with a very high half-life), what again is easily transmuted into cobalt60. It could be interesting to analyze the relative fractions of the two ways responsible for the buildup of cobalt60.

Cobalt60 has a half-life of about 5 years and will thus decay away, when looking at longer cooling-times. However, one day after shutdown the contribution of Co60 to the activity will amount to about 1E+5 Bq/cm³ next to the first wall of the BSM. In the shielding modules the maximum value is dropping fast below 1E+2 Bq/cm³.

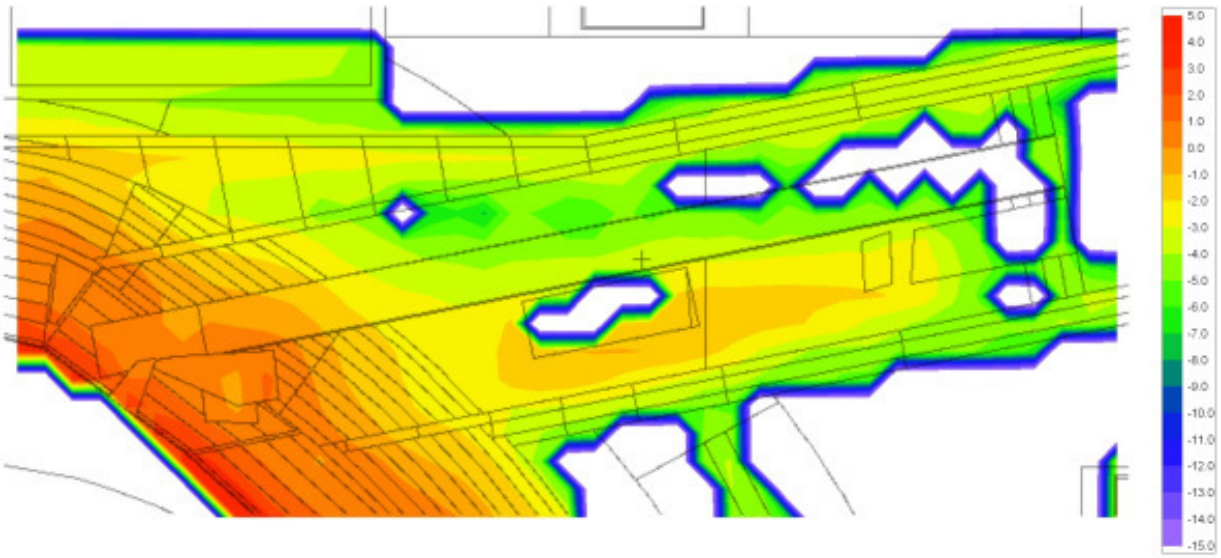

Figure 79: Tritium activity in the Port Plug one day after shutdown [log(Bq/cm³)]

Also of interest is the tritium production inside the ITER CXRS Port Plug. Highest concentrations occur next to the first wall of the BSMs with up to 1E+4 Bq/cm³, what amounts to the same value determined in the activation calculations for ITER done earlier. Main contribution to the tritium generation is by the irradiation of the coolant water.

Again, the same model should be calculated without water added in the water-steel mixture of the shielding. Fortunately it is possible to calculate other MCNP input files in the activation calculations with FISPACT than in the neutron field simulations as the cooling water should be present in the latter for a realistic model.

As mentioned earlier, a rapid decay is an advantage for the nuclear waste situation, but it can lead to problems due to activation heat shortly after or even during irradiation, when the decay heat is added to the neutron and gamma heating absorbed in the structures. The decay heat has been also calculated by FISPACT for the CXRS Port Plug and has been collected and compiled by MCNPAct in Figure 80.

The situation is as similar to that calculated for the sum of the ITER structures in the last chapter with high amounts of activation heat present shortly after shutdown, but is decreasing by several orders of magnitude within the first year. The activation heat is highest in the inside the BSMs next to the 1st wall, what is like expected due to the high activity there. But values here are comparatively small with about 0.01 W/cm³. These values then drop further down to 1E-10 W/cm³ ten years after shutdown.

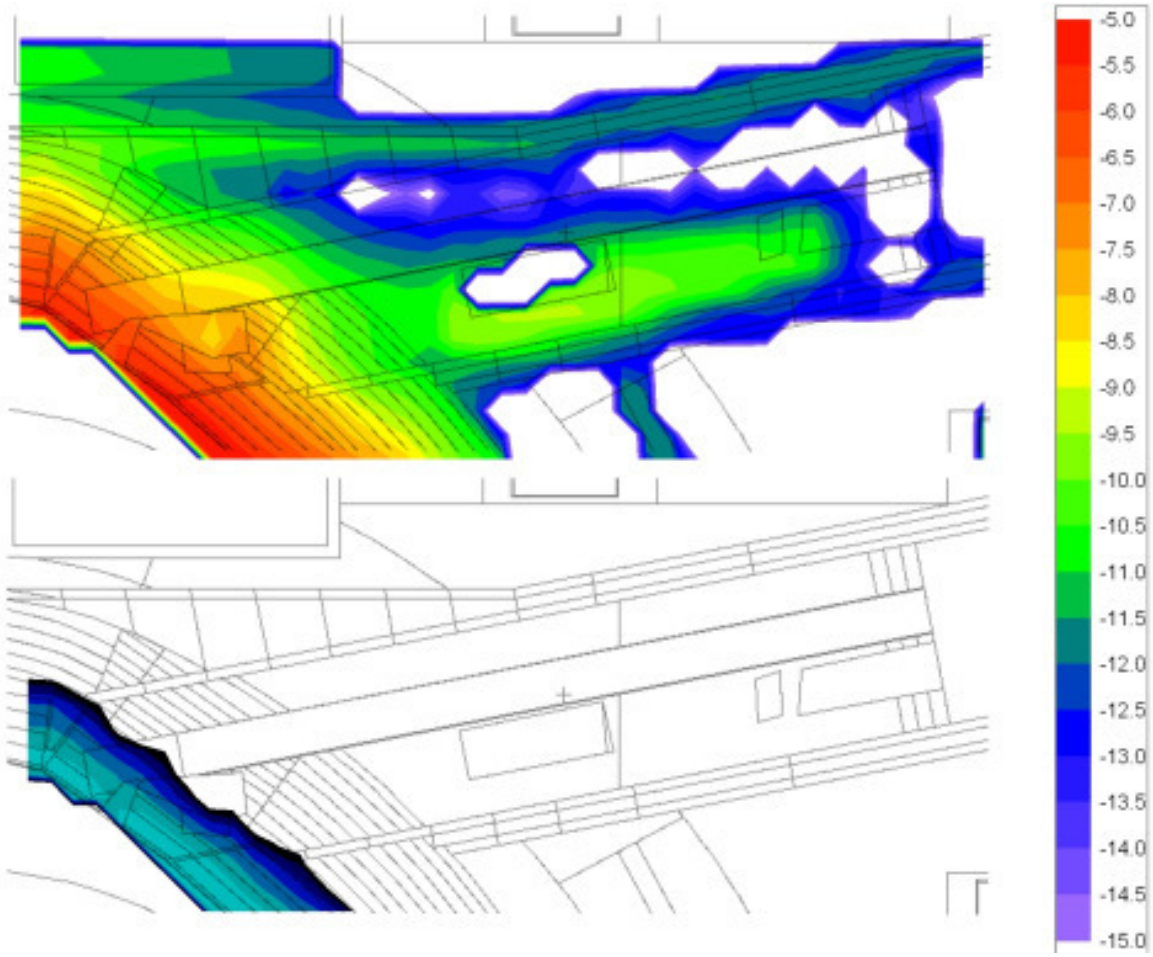

Figure 80: Activation heat production 1 day (up) and 10 years (down) after shutdown [log(kW/cm³)]

5.4.3. Gamma Dose Rate before and after ITER Shut Down in the Upper Port Cell

A first look into the dose rates present in ITER can be done with MCNP alone during the operation by introducing appropriate multiplier cards to the tallies. An example of this is shown in Figure 81, where the dose rate due to gamma radiation has been computed with MCNP. A FMESH tally has been combined with a dose energy (DEn) and a dose conversion (DFn) card. The results are given in rem/h but can simply be converted to Sv/h. Thus the expected dose in the plasma region reaches up to 1E+13 µSv/h. This is by a factor of 20 lower then computed by [IIDA 06], but here only the activation due to gammas has been computed and the fraction by neutrons should be significantly higher due to the higher weighting factors for neutrons, when calculating the equivalent dose. When computing the dose rate after shutdown, activation will be the responsible mechanism and has to be computed with activation codes like mentioned earlier.

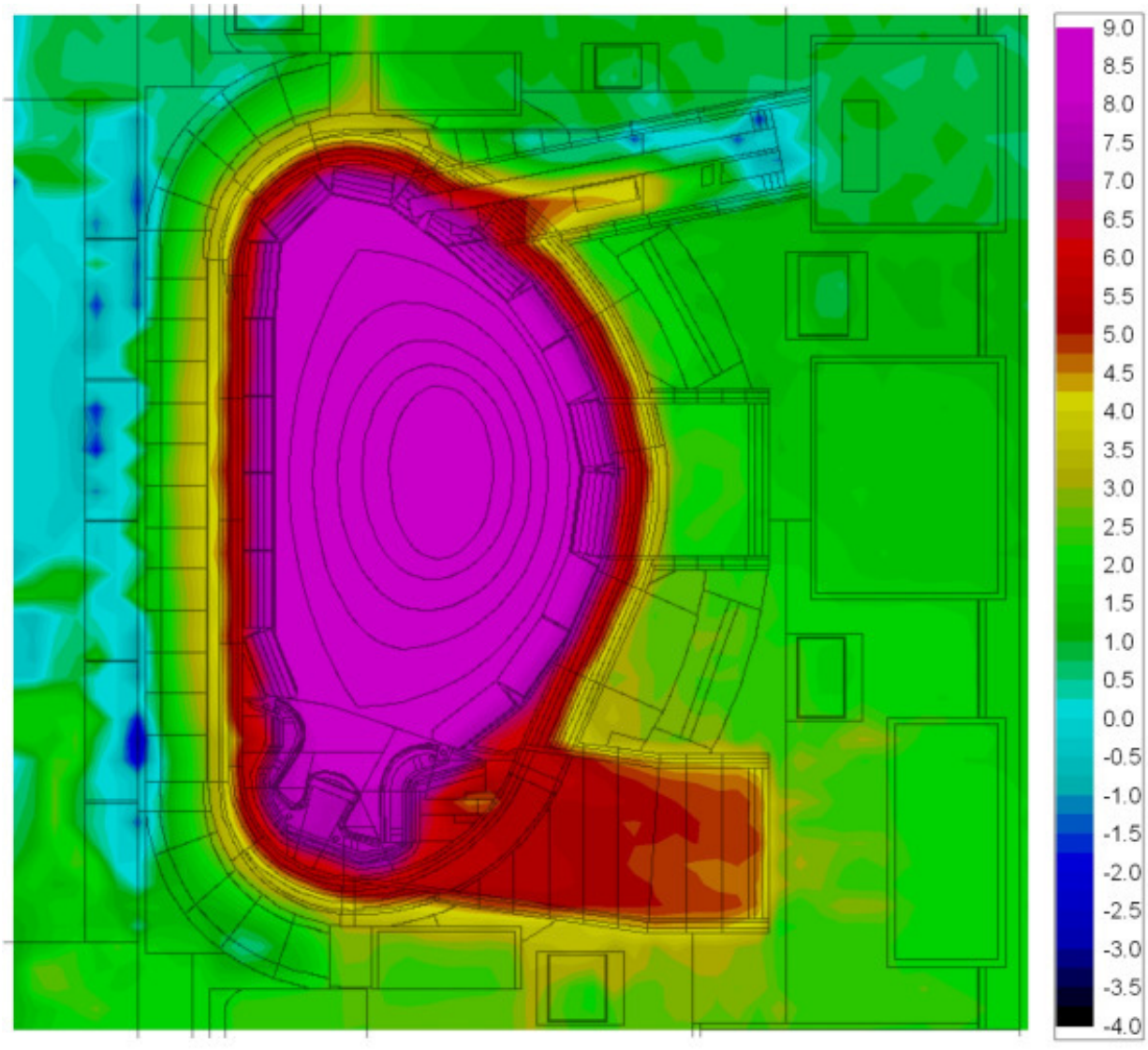

Figure 81: Dose Rate during operation due to gammas in ITER [log(rem/h)].

ITER regulations demand, that the dose rate in the Upper Port Cell after shutdown of the reactor is lower than 100 microSv/hr after 10 days of cooling, so MCNPAct has been used to calculate the Dose Map in the Upper Port Cell behind the CXRS Port Plug. A MCNP plot of the Port Cell model can be seen in Figure 82.

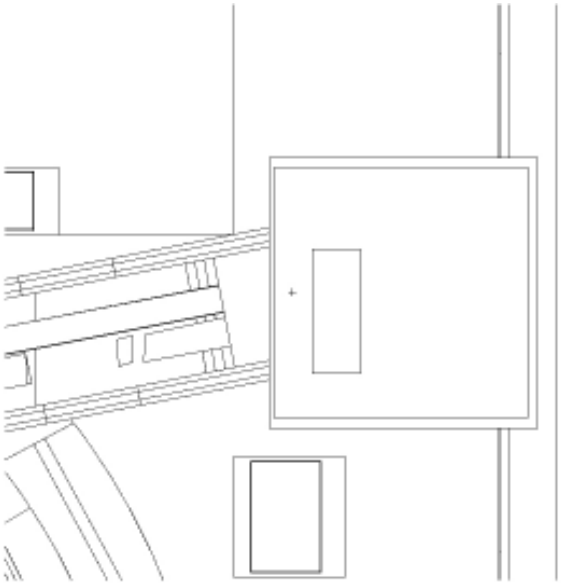

Figure 82: Port Cell in MCNP model

In order to verify and to compare the results with other groups, a situation has been modelled to match that of the NRG partners, who have done a manual calculation based on MCNP neutron flux results. In that computation only the activity of the Port Cell wall has been taken into account. With that method, the NRG result for the dose rate in the Port Cell amounts to 45 microSv/hr.

For the calculation with MCNPAct, a first simulation of the neutron flux and its spectrum in ITER has been made. This simulation is identical with that shown in Figure 43. A second FMESH tally has than been introduced to sample the neutron flux and its spectrum only in the area around the Port Cell. This FMESH tally is a 3D matrix with 6x6x8 elements, which segments the Port Cell in 288 single volumes.

This matrix was then the base for the activity calculation with MCNPAct and for each of these elements an activation calculation has been done by FISPACT. The output files have been restructured and analyzed and a new MCNP gamma source has been compiled based on the activation gamma spectrum computed by FISPACT. The source has been linked to the cell number of the Port Cell, so that virtual gammas in MCNP have only been started in the activated material of the port wall.

Results of the simulation have also been visualized by FMESH tallies, like displayed in Figure 83. Here it is clearly seen, that activation gammas only have started in the area of the Port Cell, as only this has been simulated. The highest dose rate in the Port Cell amounts to about 20 microSv/hr what is in good agreement with computations done for [IIDA 06(3.5-2)].

Compared to the results of NRG this seems very low for a verification of the result, while the same order of magnitude at least show, that there are no rough, systematical errors in the coding. Reasons for the differences could be different neutron fluxes in the area of the Port Cell, rounding of activation results, differences in the materials or different activation scenarios.

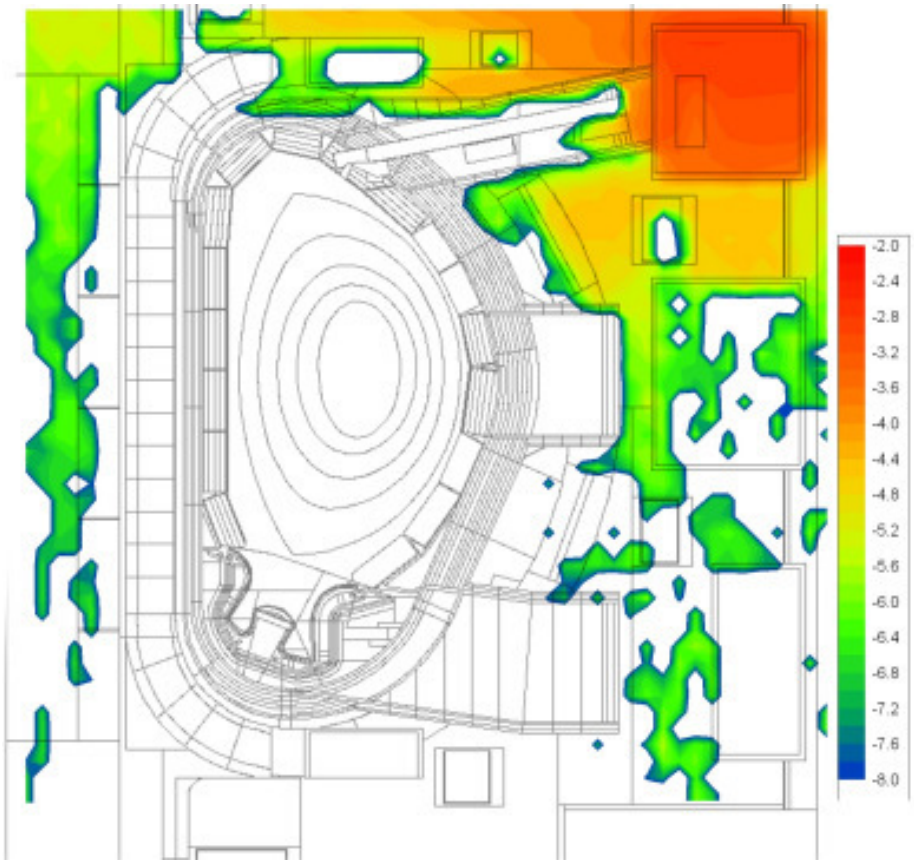

Figure 83: Dose Rate due to activation gammas from Upper Port Cell structure in ITER in [log (rem/h)]

While both the results of NRG and the computations with MCNPAct seem to indicate a lower than demanded dose rate, it must be clearly said, that these results can be only preliminary. On the one hand, the calculation must be done with the other structures of ITER included for the activation and not only for that of the Port Cell. On the other hand, while MCNPAct is clearly able to do this, the new method first have to bear up against a more detailed and demanding verification.

For ITER related activation calculations, there exists a verification package called SINBAD, which includes experimentally verified activation calculations that could be used for verification of MCNPAct [KODELI 05]. Unfortunately a detailed verification and error estimation of the MCNPAct based activation calculation method is beyond the scope of this work, but should be carried out in the future.

5.5. Helium Production

The results were again obtained by the Monte Carlo Code MCNP and the activation code FISPACT with the help of the coupling code MCNPAct. The MCNP 3D model used is the standard ITER Feat model with a dynamic CXRS Port Plug model of the 2008 reference option included. Variance reduction was modified to raise the computation efficiency in the outer parts of the shielding, especially at the UPP coordinates.

For the sampling of the neutronic results several 40x40 element FMESH-Tallies were introduced at the regions of interest, namely the vicinity of the mirrors. Statistical reliability at the first three mirrors is within 0.01 at mirrors four and five at least lower than 0.1. Neutronic results and material composition of the FMESH-elements were compiled via MCNPAct to FISPACT input files. The FISPACT input was then changed for simulation of stainless steel structures. So neutron transport was simulated correctly with cooling water in the shield, but activation analysis was carried out only for structures of stainless steel.

One FISPACT input for each mesh element was generated and computed. FISPACT output was then compiled to 2D plots of the respective geometry. Results were computed for an ITER operational time of 10 years. They can be modified easily for other operation times as the helium production is linear to the time. An overview of the situation at the front part of the PP is shown at Figure 84.

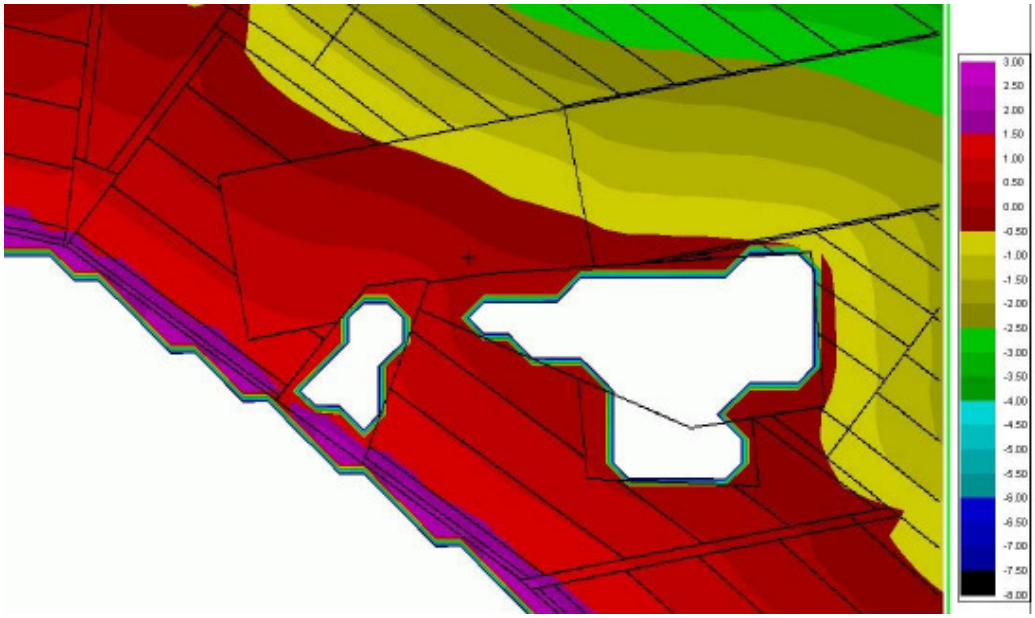

Figure 84: Helium Production in CXRS PP in [log (appm)]

The picture shows a helium production of about 5-10 ppm in the structures of the retractable tube surrounding the first mirror. At the 2nd mirror the helium production amounts to about 0.2 to 0.6 ppm. Mirror three helium production is again higher because of its nearer position to the front wall, with about 1 to 2 ppm. At mirror number four a production rate of 0.01 to 0.05 ppm

is expected and at number five the production rate is lower than 0.01 ppm. Table 19 gives an overview.

The main mechanisms for helium production are (n,α)-Reactions and to a lower degree decay of tritium. Only helium production by irradiation and decay in the SS structures can be simulated by the used method. The amount of accumulated helium may be appreciably higher due to diffusion and subsequent decay of tritium in the material [FABRITSIEV] and also by alpha implantation [LOUTHAN 01].

Mirror	Helium Production (ppm)
1	5-10
2	0.2-0.6
3	1-2
4	0.01-0.05
5	<0.01

Table 19: Helium Production in CXRS PP in [appm]

As mentioned earlier, the helium quantity in welded parts is lmitet to one ppm in welded parts. A separate computation has thus been made for the most endangered regions of the Port Plug, namely the connections to the surrounding shielding at the front of the Port Plug, where the shielding blocks next to the BSM are located, as shown in Figure 85. The helium produced in these parts amounts to a maximum of 0.5 ppm per fpy what is similar to results of other groups for other Port Plugs and thus the rewelding helium limits are met.

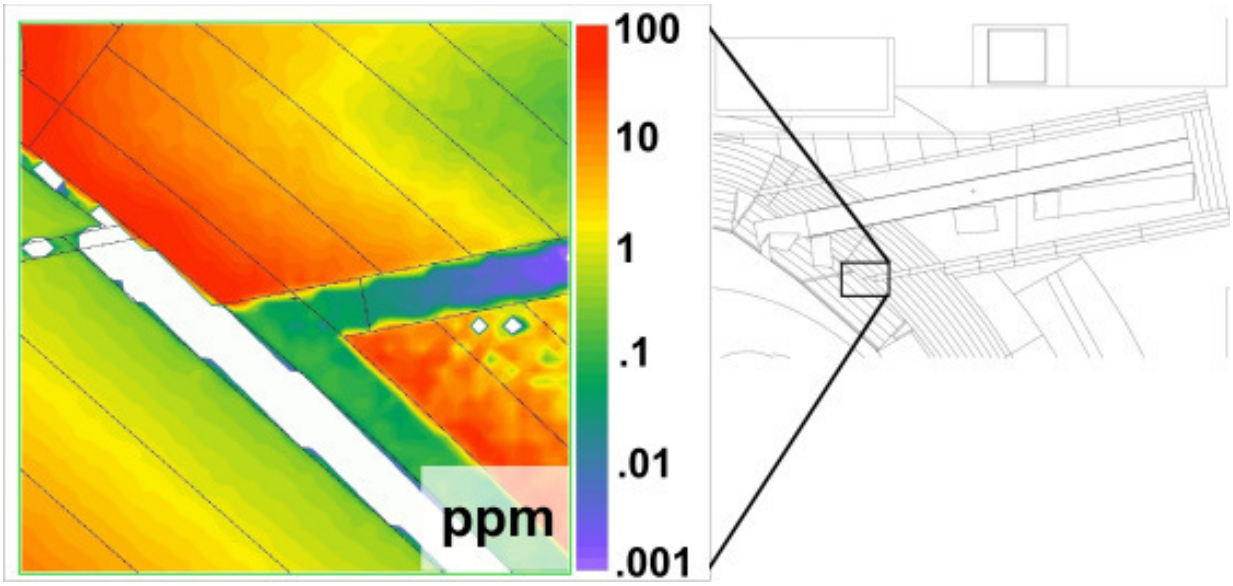

Figure 85: Helium production in welded parts of the CXRS Port Plug

5.6. Nuclear Heating in Coolant of the ITER CXRS PP Retractable Tube

For the thermal analysis of the CXRS Port Plug Retractable Tube the nuclear heating is needed as an input. These values again have been calculated with the standard ITER Feat model using Monte Carlo Code MCNP.

A cell of cylindrical shape filled with water as material has been integrated into a simplified Port Plug model at the position of the x-axis of the retractable tube to simulate a long cooling channel. This cylinder has been divided into a number of segments to get a line distribution along the x-axis of the Port Plug.

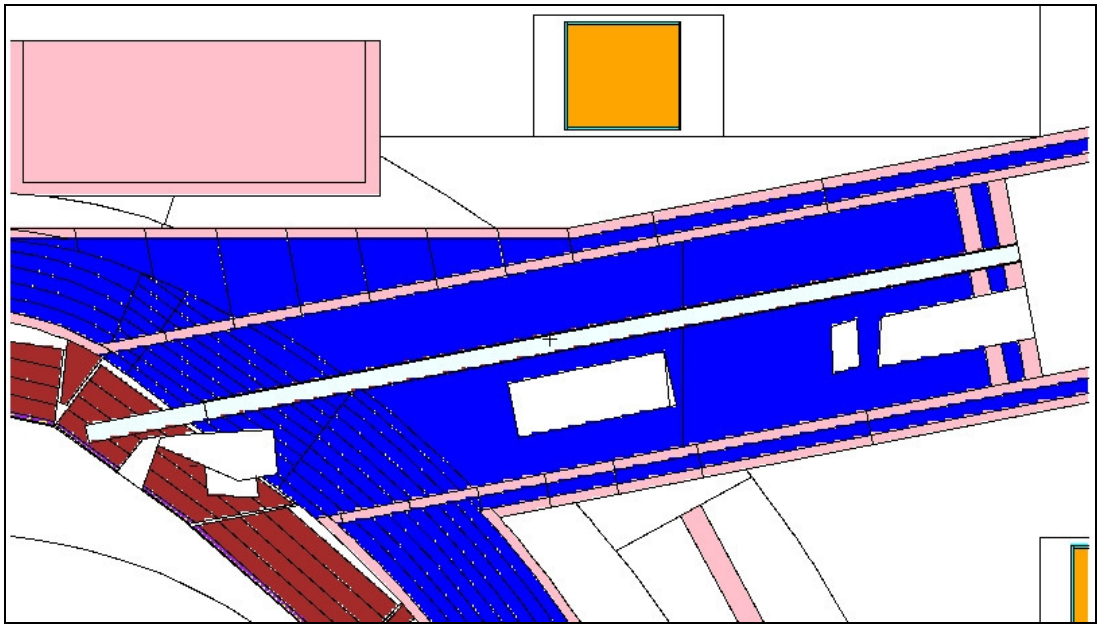

Figure 86: Geometry plot of the model used

In this simulation the local coordinate x is positioned at global coordinate x = +610 cm. This is equal to a front wall distance of 21 cm. This should be taken into account when calculating with the given formulas.

Results are given in Figure 87. Contribution to the values is 67% from neutron heating and only 33% from gamma heating. Highest values at the front of the retractable tube are 0.615 W/cm³. The numbers are decreasing exponentially with rising distance from the Front Wall. Edges in the curve are a result the unsymmetrical shape of the nearby mirror labyrinth.

Due to these edges in the curve it makes sense to use two best-fit curves and formulas. For the first 40 cm of the geometry the resulting formula is Y = 0.6016e (-0.1166X) and behind that point the resulting formula is Y = 0.0279e (-0.045X) with X in [cm] length of the retractable tube and Y in [W/cm³].

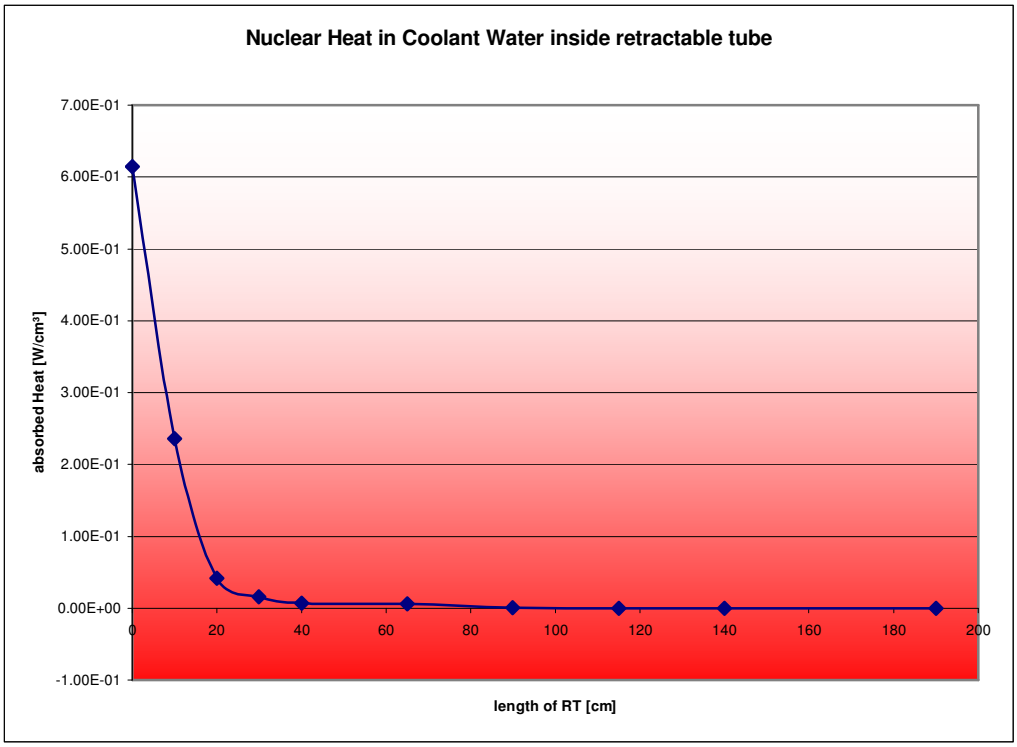

Figure 87: Nuclear Heating in Retractable Tube Coolant Water

6. Summary and Conclusions

Suitable methods and tools have been developed to compute the parameters and data needed for the construction of the CXRS Port Plug. The parametric MCNP-model building can support the design process of the machine with its frequent geometric modifications. With this technique, the geometry representation is only approximative and neutronix results will be converged only to a certain degree. But for a preliminary design calculation this method should be sufficient, if there is some margin to the limit.

Furthermore, tools have been developed to visualize general MCNP-FMESH-outputs instantly for any point of the geometry on a two-dimensional and also three-dimensional base. Also line profiles can be generated between points in the model.

The most important work was the development of a software tool, that combines the computer code MCNP with the activation code FISPACT and is able to deliver the original zero-dimensional activation data as two-dimensional maps or three-dimensional distributions and is also capable to compile the activation-output to a new MCNP gamma source for determination of activation gamma dose data.

This can be done not only for the ITER problems but for any MCNP input as the tool has been written in a general form. The methods and tools have been verified up to a certain degree with models and data from other groups and have been used to deliver critical values needed for the construction of the ITER CXRS PP.

Neutron and gamma flux as well as neutron and gamma heating values have been determined for all points in the model and especially for the positions of the mirrors. The highest v alues for the mirrors are 3.76E+13 n/cm²s and 1.29 W/cm³ for neutron flux and nuclear heating respectively. Statistical errors are below 0.01 for the first five mirrors. Values are in good agreement with ITER Org generated results and also with that of [SHATALOV 02], but are differing up to an order of magnitude with that computed by NRG for certain parts of the geometry, especially next to the first wall. Reason could be different materials or differences in the MCNP model. This should be analyzed in detail as further work.

Some parametric studies have been made for the mirrors, for example the heating of different choices of materials has been calculated. It could be shown, that tungsten would have the highest heating with more than 1.8E-1 W/cm³, while Zircalloy would be the best choice with a heating value of less than 7E-2 W/cm³ for the second mirror.

Regarding the first mirror also an analysis of the gradients for flux and heating has been made, showing diffrences between different sections of the mirror by about a factor of two. Material damage has been determined for the Port Plug as a whole and for the single mirrors with the

highest value of about 1 dpa/fpy for the first mirror and 10 dpa as maximum value of the front wall areas.

Table 20 shows the most important limits for the Port Plug and the actual values determined by the computer simulations. The shutdown dose rate has been determined preliminary with about 20 microSv/hr at a time of 10^6 seconds after ITER shutdown. Agreement is differing by a factor of two of that of NRG, leaving room for a more sophisticated analysis in the future. Also the dose rates have to be determined by a more rough computation, taking into account also the other activated areas besides the wall of the port cell.

Criterion Number	Definition of Criterion	Value in PP Design	General Design Limit	Met Criterion?
1	Dose rate behind PP is below 100 microSv/hr after 10 days of shutdown	20 microSv/hr	100 microSv/hr after 10^6 s=ca10d	yes
2	Fast neutron fluence behind PP is kept below 10^20 n/m² (0.5 fpy)	1x10^19 n/m²	1x10^20 n/m²	yes
3	Helium production in the joining areas of the vacuum vessel is below 1.0 appm (0.5 fpy)	0.1 appm	1 appm	yes
4	Compatibility with conservative limit for nuclear heating of 10^-3 MW/m³ at the outer housing of the VV	<2x10^-4 MW/m³	10^-3 MW/m³	yes
5	Nuclear Response in the structure of superconductive magnets of TFC near the launcher in accordance to ITER requirements, in particular fast neutron fluence in isolator is below 5x10^21 n/m² (0.5 fpy)	1x10^19 1/m²	5x10^21 1/m²	yes
6	nuclear heating density in the VV kept below 0.3 MW/m³	<0.1 MW/m³	0.3 MW/m³	yes

Table 20: ITER Regulations and conformity of CXRS PP values

Fast neutron fluence is lower than the design limit by about an order of magnitude with 1E+19 n/m² and also the fluence allowed for the isolator of the TFC with 1E+19 n/m². Nuclear heating and helium production rates limits are met with the used model.

Regarding to the preliminary models used it can be said, that there are no critical conditions that would directly prohibit the use of the designed Port Plug. Reserves are present for all of the ITER limits.

Nontheless there are uncertainties, for example the contradictory results of the NRG calculations. The reasons of these differences should be assessed before progressing with more sophisticated neutronics calculations.

Also the MCNP model of the Port Plug can be only preliminary, because of the approximative character of the dynamic model used for this study. Due to the complicated nature of the MCNP modeling, advanced tools must be used necessarily. The best way to get a sophisticated model would be to obtain one of the MCNP-CAD interfaces, when they finaly get available to simulate also small scale structures like the elastic elements inside the retractable tube or the effects of small coolant tubes, which is not possible at the moment and had to be approximated by homogenized materials.

It has been shown, that the visualization of the results by FMESH tallies with the developed tools is of a great help, especially with complicated geometries. 2D colour plots and spectrum views with MOPAR and also the generation of line profiles with MCNPAct provide a better understanding of the physics inside the computed models and can be done in a very short time. Further development should be made here. Thinkable goals could be the automatic and threedimansional plotting of the geometry together with the results and on-the-fly visualization of particle trajectories and their effects while MCNP is running.

For the activation tool MCNPAct it is possible to accelerate calculations by making the work in a parallel mode. Recoding of the some of the modules is suggested to make a more effective use of the internal computer memory, allowing bigger FMESH files to be analyzed. The most important work to be done in the future would be a detailed verification, not only with simulations done by other groups but also with experimental verified data. This could be done with the verification package SINBAD and is suggested to be done before doing more computations for critical ITER components to evaluate the possible error sources.

As there is a lot of potential in the methods and also a great demand for activation tools it is strongly encouraged to make further developments on this subject.

REFERENCES

[ALDAMA 04] ALDAMA, D. L., TRKOV, A.: ***FENDL-2.1-Update of an evaluated nuclear data library for fusion applications,*** International Atomic Energy Agency, Report, INDC(NDS)-467, Distr. FE

[BACON 04] BACON, D.J, OSETSKY, Y.N.: ***Multiscale modeling of radiation damage in metals: from defect generation to material properties***, Materials Science and Engineering A365 (2004) 46–56.

[BARABASCH 09] BARABASCH, V.: ***Material Needs for ITER – Main components***, ITER document, ITER_D_27VZGX (Draft), 2009.

[BECKURTS 64] BECKURTS, K.H., WIRTZ, K.: ***Neutron Physics***, Springer-Verlag, Berlin, 1964

[BELL 70] BELL, G., GLASSTONE, S.: ***Nuclear Reactor Theory***, Van Nostrand Reinhold Company, New York, 1970, ISBN 0-44220-684-4

[BOURAUEL 09] BOURAUEL, P., NABBI, R., BIEL, W., FORREST R.: ***Coupling the MCNP Monte Carlo Code and the FISPACT Activation Code with Automatic Visualization of the Results of Simulations***, Atw. Internationale Zeitschrift für Kernenergie, 2009,vol.54,n7, [Note(s): 459-461, 432-433 [5 p.]]

[BLOM 04] BLOM, F.J., CHURCH, J.M.: ***Welding Simulation & Helium Damage Modelling***, Proceedings of The International Conference on Metal Fabrication and Welding Technology (METFAB-2003), Nottingham, 2003

[BRIESMEISTER 03] BRIESMEISTER, J.F.: ***X5 Monte Carlo Team MCNP: A general Monte Carlo N-Particle Transport Code***, ***Version 5***, LA-CP-03 0245, Manual vol. II, April 2003.

[BRÖCKER 97] BRÖCKER, B.: ***Atomphysik***, Deutscher Taschenbuch Verlag, ISBN 3-423-03009-7

[CHEN 02] CHEN, Y., FISCHER, U.: ***Rigorous MCNP based shutdown dose rate Calculations: Computational scheme, verification calculations And applications to ITER***, 6th Int. Symp. Fusion Nuclear Technology. San Diego, California, USA 2002

[CHEN 05] CHEN, Y.: ***Coupled Monte Carlo – Discrete Ordinates Computational Scheme for Three-Dimensional Shielding Calculations of Large and Complex Nuclear Facilities***, Karlsruhe, April 2005, FZKA 7075

[CHENG 00] CHENG, E.T., ROCCO, P., ZUCCHETTI, M.: ***Application of SAEFP waste recycling and clearance strategies to ITER***, Fusion Engineering and Design 51-52 (2000) 485-491

[COENEN 09] COENEN, J.W.: ***The Influence of the Dynamic Ergodic Divertor on the Radial Electric Field at the Tokamak TEXTOR***, Jülich, 2009, ISBN 978-3-89336-574-6

[COSTLEY 01] COSTLEY, A.E., DONNE, A.J.H., EBISAWA, K., JANESCHITZ, G.,KASAI, S., MALAQUIAS, A., VAYAKIS, G., WALKER, C.I., YAMAMOTO, S., ZAVERIAEV, V.: ***The Challenge of ITER Diagnostics***, 28th EPS Conference on Contr. Fusion and Plasma Phys., Funchal, 2001

[EGGLESTON 98] EGGLESTON, J.E., ABDOU, M.A., YOUSSEF, M.Z.: ***The use of MCNP for neutronics calculations within large buildings of fusion facilities***, Fusion Engineering and Design 42 (1998) 281-288

[EHRLICH 03] EHRLICH, K.: ***Die Entwicklung von Strukturmaterialien für die Kernfusion***, Materialwissenschaft und Werkstofftechnik 34, 39-48, 2003

[ENGLE 67] ENGLE, W.W..: ***ANISN, A One-Dimensional Discrete Ordinate transport Code with Anisotropic Scattering***, RSICC Computer Code Collection, K-1693 (March 1967), CCC-82

[ERIKSSON 03] ERIKSSON, E., RAEDER, J.: ***Extension of ITER waste assessment***, Fusion Engineering and Design 69 (2003) 727-731

[ETO 06] ETO, M., KOIZUMI, K.: ***Material Properties Handbook***, Japan Atomic Energy Research Institute (JAERI), S 74 TD 09 FJ (JA), D327-1, 1998

[FABRITSIEV] FABRITSIEV, S., VAN DER LAAN, J.: ***Helium Effects on the Reweldability and Low Cycle Fatigue Properties of Welded Joints for Type Cr16Ni11Mo3Ti and 316L (N) Stainless Steels***, Effects of Radiation on Materials, ASTM STP 1270

[FARKAS 05] FARKAS, G., SLUGEN, V., DOMONKOS, P.: ***Nuclear Analysis of the Eurofer 97 Alloy by MCNP-4C2 code***, International Conference on Nuclear Energy for New Europe, Bled, 2005

[FISCHER 03] FISCHER, U., CHEN, Y., HEIDINGER, R. LUO, Y., STRATMANNS, E., TSIGE-TAMIRAT, H.: ***Analysis of Fast Neutron Streaming in the Waveguide Channels of the ECRH System in the ITER Upper Port*** IAEA Technical Meeting on ECRH Physics and Technology for ITER, July 14-16, 2003, Germany

[FISHMAN 95] FISHMAN, G.S.: ***Monte Carlo – Concepts, Algorithms, and Applications***, Springer Series in Operations Research, New York, 1995, ISBN 0-387-94527-X

[FORREST 05] FORREST, R.A.: ***The European Activation System: EASY-005 overview***, UKAEA FUS-513

[GLASSTONE 64] GLASSTONE, S.: ***Kontrollierte thermonukleare Reaktionen*** , München, 1964,

[HAWRYLUK 09] HAWRYLUK, R.J., ET AL: ***Principal physics developments evaluated in the ITER design review***, Nuclear Fusion 49 (2009) 065012

[HEUEL-FABIANEK 05] HEUEL-FABIANEK, B., HILLE, R.: ***Benchmark of MCNP for Calculating Dose Rates at an interim storage facility for nuclear waste***, Radiation Protection Dosimetry (2005), Vol. 115, No. 1-4, pp. 424-427,

[HOGENBIRK 08] HOGENBIRK, A.: ***An easy way to perform a radiation damage calculation in a complicated geometry***, Fusion Engineering and Design 83 (2008) 1828-1831

[HOLTKAMP 09] HOLTKAMP, N.: ***The status of the ITER design***, Fusion Engineering and Design 84 (2009) 98–105

[HULME 69] HULME, H.R..: ***Nuclear Fusion***, Wykeham Publications, London, 1969

[IIDA 06] IIDA, H., KHRIPUNOV, V.,PETRIZZI, L., FEDERICI, G.: ***Nuclear Analyis Report (NAR)***, ITER ref document G 73 DDD 2W 0.2 (v2.0), March 2006.

[ITER 08] ***ITER Vacuum Handbook***, Issue 1.1, IDM Ref ITER D 2EZ9UM

[ITER 01] ***Summary of the ITER Final Design Report***, ITER Document G A0 FDR 4 01-07-21 R 0.4

[JASPERS 08] JASPERS, R.J.E., VON HELLERMANN, M.G., DELABIE, E., BOOM, J.E., DONNE, A.J.H., BIEL, W., HAWKES, N.C., NEUBAUER, O., DI MAIO, M., SADAKOV, S., KLINKHAMER, SNIJDERS, B., HOGENBIRK, A.: ***The CXRS diagnostic for ITER and the CXRS-Pilot Experiment on TEXTOR***, Burning Plasma Diagnostics, CP988, 2008

[KALININ 01] KALININ, G., BARABASCH, V.: ***Material Assessment Report***, ITER Document, G74 MA 10 01-07-11 W 0.2, July 2001

[KAMMASH 75] KAMMASH, T.: ***Fusion Reactor Physics – principles and technology***, Ann Arbor Science Publishers, Ann Arbor, 1975, ISBN 0-250-40076-6

[KODELI 05] KODELI, I., HUNTER, H., SARTORI, E.: ***Radiation shielding and dosimetry experiments updates in the SINBAD database,*** Radiation Protection Dosimetry 2005 116(1-4):558-561

[KONING 09] KONING, J., JASPERS, R., DOORNIK, J., OUWEHAND, B., KLINKHAMER, F., SNIJDERS, B., SADAKOV, S., HEEMSKERK, C.: ***Maintenance implications of critical components in ITER CXRS upper port plug design***, Fusion Engineering and Design 84 (2009) 1091-1094

[LAMARSH 01] LAMARSH, J.; BARATTA, A.: ***Introduction to Nuclear Engineering***, Prentice Hall, 2001, ISBN 0-201-82498-1

[LÄSSER 05] LÄSSER, R.: ***The European fusion program and the role of the research reactors***, 9th Intwernational Topical Meeting on Research Reactor Fuel Management (RRFM), Budapest, Hungary, 2005

[LAWSON 57] LAWSON, J.D.: ***Some criteria for a useful thermonuclear reactor***, Proceedings of the Physical Society B, Vol. 70, p. 6 (1957)

[LILLEY 01] LILLEY, J.S.: ***Nuclear Physics – Principles and Applications,*** Cichester, 2001, ISBN 0-471-97936-8

[LINTNER 62] LINTNER, K., SCHMID, E.: ***Werstoffe des Reaktorbaus mit besonderer Berücksichtigung der Metalle***, Springer-Verlag, Berlin, 1962

[LOUTHAN 01] LOUTHAN, M.R.: ***Tritium Decay, Irradiation and Hydrogen/Helium Effects on Type 316L Austenitic Stainless Steel***, Westinghouse Savannah River Company, WSRC-MS-2001-00040

[MACFARLANE] MACFARLANE, R.M.: ***NJOY99.0: Code System for Producing Pointwise and Multigroup Neutron and Photon Cross Sections from ENDF/B Data***, RSICC Code Package PSR-480.

[MCCRACKEN 05] MCCRACKEN, G.M.: ***Fusion – The Energy of the Universe*** , Burlington, 2005, ISBN 0-12-481851-X

[NABBI 01] NABBI, R., WOLTERS, J.: ***Investigation of radiation damage in the aluminum structures of the German FRJ-2 research reactor***, IGORR Conference Proceedings, Munich, 2001,

[NORDLUND 06] NORDLUND, K.: ***Basics of Monte Carlo Simulation***, Lecture Notes, University of Helsinki, 2006

[NORGETT 75] NORGETT, M, ROBINSON, M., TORRENS,I.: ***A proposed method of calculating displacement dose rates***, Nuclear Engineering and Design 33 (1975) 50–54.

[OSETSKY 02] OSETSKY, Y.N., BACON, D.J., SINGH, B.N.: ***Statistical analysis of cluster production efficiency in MD simulations of cascades in copper***, Journal of Nuclear Materials 307–311 (2002) 866–870.

[PAMPIN 07] PAMPIN, P.; DAVIS, A., JAMES, D.: ***Systematic Study of Neutron Shielding Options for ITER Generic Port Plug Design***, UKAEA, Abingdon, 2007, TW6-TPDS-DIASUP, EFDA/06-1436

[PAMPIN 07B] PAMPIN, P.; LOUGHLIN, M.J.: ***Evaluation of a three-dimensional discrete ordinates radiation transport tool for the support of ITER design***, Fusion Engineering and Design 82 (2007) 2008-2014

[PASHCHENKO 98] PASHCHENKO, A.B., ET AL.: ***FENDL/A-2.0 Neutron activation cross section data library for fusion applications***, Report IAEA(NDS)-173 (IAEA October 1998)

[PETRIZZI 06] PETRIZZI, L., ANGELONE, M., BATISTONI, P., FISCHER, U., LOUGHLIN, M., VILLARI, R.: ***Benchmarking of Monte Carlo based shutdown dose rate calculations applied in fusion technology: From the past experience a future proposal for JET 2005 operation***, Fusion Engineering and Design 81 (2006) 1417-1423

[POLUNOVSKIY 08] POLUNOVSKIY, E.: ***The radial and poloidal variations of the blanket nuclear heating*****,** ITER_D_284MGZ, 2008

[RAEDER 81] RAEDER, J., BORRAß, K., DÄNNER, W., LENGYEL, L., SÖLL, M: ***Kontrollierte Kernfusion – Grundlagen ihrer Nutzung zur Energieversorgung***, B.G. Teubner, Stuttgart, 1981

[RUBEL] RUBEL, M.: ***Fusion reactor materials and components: Issues related to radioactivity and radiation induced effects***, Alfven Laboratory, Royal Institute of Technology, Stockholm

[SADAKOV 09] SADAKOV,S., BAROSS, T.,BIEL ,W., BORSUK, V., HAWKES, N., VON HELLERMANN, M., GILLE ,P., KISS, G., KONING, J., KNAUP, M., KLINKHAMER, F., KRASIKOV, Y LITNOVSKY, A., NEUBAUER, O., PANIN, A.: ***Conceptual design of the ITER upper port plug for charge exchange diagnostic,*** Fusion Engineering and Design 84 (2009) 1671–1675

[SATO 06] SATO, S., IIDA, H., NISHITANI, T.: ***Development of CAD/MCNP interface program prototype for fusion reactor nuclear analysis***, Fusion Engineering and Design 81 (2006) 2767-2772

[SAWAN 09] SAWAN, M.E.: ***Benchmarking FENDL-2.1 with Impact of ENDF/B-VII.0 Release on Nuclear Heating and Damage***, 2009 978-1-4244-2636-2/09 IEEE

[SCHAEFFER 73] SCHAEFFER, N.M.: ***Reactor Shielding for Nuclear Engineers***, US Dept. of Energy, Springfield, 1973, TID-25952, ISBN 0-87079-004-8

[SEIFE 08] SEIFE, C.: ***Sun in a Bottle***, New York, 2008, ISBN 978-0-670-02033-1

[SEKI 86] SEKI, Y., IIDA, H., KAWASAKI, H., YAMADA, K.: ***THIDA-2: An Advanced Code System for Transmutation, Activation, decay Heat and Dose Rate***, Japan Atomic Energy Research Institute, JAERI 1301, March 1986

[SERIKOV 06] SERIKOV, A, FISCHER, U., HEIDINGER, R., LUO, Y., TSIGE-TAMIRAT, H.: ***Radiation Shielding Analyses for the ITER Upper Port ECRH Launcher***, The American Nuclear Society's 14th Biennial Topical Meeting of the Radiation Protection and Shielding Division, Carlsbad, USA, 2006

[SERIKOV 08] SERIKOV, A, FISCHER, U., HEIDINGER, R., SPAEH, P., STICKEL, S., TSIGE-TAMIRAT, H.: ***Nuclear analyses for the ITER ECRH launcher***, Nuclear Fusion 48 (2008) 054016

[SHATALOV 02] SHATALOV, G.E., SHELUDIKOV, S.V.: ***Upper Port #3 Neutronic Analysis***, Moscow, 2002, REF NO. G55MD161 03-10-06W 0.1.

[SNOJ 09] SNOJ, L., LENGAR, I., ZEROVNIK, G., RAVNIK, M.: ***MCNP and Visualization of neutron flux and power distributions***, International Conference on Mathematics, Computational Methods & Reactor Physics (M&C) 2009, Saratoga Springs, USA, 2009

[STEPHENSON 58] STEPHENSON, R.: ***Introduction to Nuclear Engineering***, McGraw-Hill Book Company, New York, 1958,

[THOMAS 07] THOMAS, P., ET AL.: ***Progress in the ITER Physics Basis***, Bristol, 2007, ISSN 0029-5515

[TSIGE-TAMIRAT 07] TSIGE-TAMIRAT, H., FISCHER, U., SERIKOV, A., STICKEL, S.: ***Automatic generation and validation of an ITER neutronics model from CAD data,*** Fusion Engineering and Design 82 (2007) 1956-1959

[VAN RIPER 94] VAN RIPER, K.A.: ***Geometry creation for MCNP by SABRINA and XSM***, Eighth International Conference on Radiation Shielding, Arlington, 1994

[VAN RIPER 97] VAN RIPER, K.A., URBATSCH, T.J., SORAN, P.D., PARSONS, D.K.,MOREL, J.E., MCKINNEY, G.W., LEE, S.R., CROTZER, L.A., BRINKLEY, F.W., BOOTH, T.E., ANDERSON, J.W., ALCOUFFE, R.E.: ***AVATAR – Automatic Variance Reduction In Monte Carlo Calculations***, Joint International Conference on Mathematical Methods and Supercomputing for Nuclear Applications, New York, 1997

[VOSKOBOINIKOV 08] VOSKOBOINIKOV, R.N, OSETSKY, Y.N., BACON, D.J.: ***Computer simulation of primary damage creation in displacement cascades in copper. I. Defect creation and cluster statistics***, Journal of Nuclear Materials 377 (2008) 385–395.

[WALKER 03] WALKER., C.I.: ***Neutronic Analysis of Integrated Structures,*** ITER Memorandum, G 55 MD 160 03-10-02 W 0.1 October 2003

[WANG 05] WANG, M., TAUTGES, T., HENDERSON, D., EL-GUEBALY, L.: ***MCNP/CAD Activities and Preliminary 3-D Results,*** ARIES-CS Project Meeting, Madison, 2005

[WASASTJERNA 07] WASASTJERNA, F.: ***Using MCNP for fusion neutronics***, Espoo, 2008, VTT Publications, ISBN 978-951-38-7129-1

[WURDEN 97] WURDEN, G.A., PETERSON, B.J.: ***Imaging Bolometry Development For Large Fusion Devices***, 1997 Varenna ITER Diagnostic Workshop

[ZENG 06] ZENG, Q., LU, L., DING., A., LI, Y., HU, H., ZHENG, S., HUANG, Q., CHEN, Y., WU, Y., IIDA, H,: ***Update of ITER 3D basic neutronics model with MCAM***, Fusion Engineering and Design 81 (2006) 2773-2778

APPENDIX

A) Changed MCNP Sorce routine for MCNPAct calculations

```
subroutine source
  use mcnp_global
  use mcnp_debug

  implicit real(dknd) (a-h,o-z)

  ! real(dknd), dimension(1:3)::A

  integer Imax

 100 open(21,file='gsrc')
  open(22,file='ixcel')
  wgt=1.0
  read (21,FMT=*) sx
  read (21,FMT=*) sy
  read (21,FMT=*) sz
  read (21,FMT="(e15.6)") swx
  read (21,FMT="(e15.6)") swy
  read (21,FMT="(e15.6)") swz
  read (21,FMT="(e15.6)") stx
  read (21,FMT="(e15.6)") sty
  read (21,FMT="(e15.6)") stz
  step=0
  ax=0
  ay=1
  az=1
  c=0
  sum=0
  value=RANG()
  do while (sum.le.value)
   c=c+1
   ax=ax+1
   if (ax.gt.sx) then
    ay=ay+1
    ax=1
   end if
   if (ay.gt.sy) then
    az=az+1
    ay=1
   end if
   read (21,FMT="(e15.6)") cnt
   sum=sum+cnt
  enddo
  xxx=stx+ax*swx-RANG()*swx
  yyy=sty+ay*swy-RANG()*swy
  zzz=stz+az*swz-RANG()*swz
!  write(iuo,FMT=*) xxx
!  write(iuo,FMT=*) yyy
!  write(iuo,FMT=*) zzz
  read(22,FMT=*) Imax
  close (21)
  tme=0.
  jsu=0
  ipt=2
  i=0
  j=1
  do while ((j.ne.0) .and. (i.le.Imax))
   i=i+1
   read(22,FMT=*) ia
   if (ia.ne.99999) ib=namchg(1,ia)
   if (ia.ne.99999) call chkcel(ib,2,j)
  enddo
  close (22)
```

```
  if (ia.eq.99999) goto 100
  if (j.ne.0) call expire(1, 'Source','cell')
  icl=ib
!  write(iuo,FMT=*) ia
  open(22,file='spectr')
  d=1
  do while (d.lt.c)
   e=0
   do while (e.lt.24)
    e=e+1
    read(22,FMT=*) energ
   enddo
   d=d+1
  enddo
  ec=RANG()
  cnt=0
  sum=0
  d=0
  do while ((sum.lt.ec).and.(d.lt.24))
   d=d+1
   read(22,FMT=*) cnt
   sum=sum+cnt
  enddo
  if (d.eq.1) erg=0.005
  if (d.eq.2) erg=0.015
  if (d.eq.3) erg=0.035
  if (d.eq.4) erg=0.075
  if (d.eq.5) erg=0.15
  if (d.eq.6) erg=0.25
  if (d.eq.7) erg=0.35
  if (d.eq.8) erg=0.5
  if (d.eq.9) erg=0.7
  if (d.eq.10) erg=0.9
  if (d.eq.11) erg=1.11
  if (d.eq.12) erg=1.33
  if (d.eq.13) erg=1.55
  if (d.eq.14) erg=1.88
  if (d.eq.15) erg=2.25
  if (d.eq.16) erg=2.75
  if (d.eq.17) erg=3.5
  if (d.eq.18) erg=4.5
  if (d.eq.19) erg=5.75
  if (d.eq.20) erg=7.25
  if (d.eq.21) erg=9
  if (d.eq.22) erg=11
  if (d.eq.23) erg=13
  if (d.eq.24) erg=14
!  write(iuo,FMT=*) erg
  close (22)
  return
end subroutine source
```